NON QUASI-STATIC EFFECTS INVESTIGATION FOR COMPACT BIPOLAR TRANSISTOR MODELING

Arkaprava Bhattacharyya

N° d'ordre : **4294**

THESE

PRESENTEE A

L'UNIVERSITE BORDEAUX I

ECOLE DOCTORALE DE SCIENCES PHYSIQUES ET DE L'INGENIEUR

Par Arkaprava BHATTACHARYYA

POUR OBTENIR LE GRADE DE
DOCTEUR

SPECIALITE : **ELECTRONIQUE**

NON QUASI-STATIC EFFECTS INVESTIGATION FOR COMPACT BIPOLAR TRANSISTOR MODELING

Soutenue le : 18 Juillet 2011

Après avis de :

M. Peter BAUREIS	Professeur	**Rapporteur**
M. Niccolò RINALDI	Professeur	**Rapporteur**

Devant la Commission d'examen formée de :

M. Peter BAUREIS	Professeur	**Rapporteur**
M. Niccolò RINALDI	Professeur	**Rapporteur**
M. Nicolas DERRIER	Ingénieur	**Examinateur**
M. Sébastien FREGONESE	Chargé de recherche, C.N.R.S	**Examinateur**
Mme Cristell MANEUX	Maître de conférences, H. D. R	**Co-directeur de thèse**
M. Thomas ZIMMER	Professeur	**Directeur de thèse**

-- 2011 --

In the memory of my uncle Dr. Ashokanshu Bhattacharyya

To my uncle Amalanshu Bhattacharyya

To my parents Arunabha and Ritika Bhattacharyya

Acknowledgment

At the outset, I would like to gratefully acknowledge the enthusiastic supervision of my research advisor Prof. Thomas Zimmer. I would like to thank my co-advisor Prof. Cristell Manuex for her sincere guidance. I am grateful to Dr. Sebastien Fregonese for providing me the technical help and support during my PhD thesis. I thank my thesis reviewers Prof. Niccolò Rinaldi and Prof. Peter Baureis for their fruitful comments and suggestion and also Dr. Nicolas Derrier, members of my thesis committee.

Moreover, I would like to thank my colleague Compact Modeling team members: Brice Grandchamp, Montassar Najari, Si-Yu Liao, Jad Bazzi, Gilles Kone, Mario Weisz, Sudip Ghosh and Amit Kumar Sahoo and my former colleague Christian Raya and Johnny Goguet. I appreciate their help and support to fulfill my goal to obtain the Doctoral degree. In total, I feel very proud to be a part of the Compact Modeling team in IMS laboratory at Bordeaux.

Finally, I wish to thank my parents, my uncles, my brothers and sisters and all my friends for their constant support and encouragement.

Table of Contents

GLOSSARY

a) Chapter **1**

Name	Significance
I_E	Static emitter current.
I_{EN}	Normal component of emitter current
I_{EI}	Inverted component of emitter current
I_C	Static collector current
I_{CN}	Normal component of collector current
I_{CI}	Inverted component of collector current
I_B	Stacic base current
$\tilde{i}_e$	Small signal emitter current
$\tilde{i}_c$	Small signal collector current
Q_b	Charge stored in base region in normal mode
Q_I	Charge stored in base region in inverted mode
Q_i	Charge stored in a region i
τ_n	Electon life time in neutral base
τ_p	Hole lifetime in neutral emitter
τ_{tN}	Base transit time in normal mode
τ_{tR}	Base transit time in inverted mode
τ_b, τ_{ob}	Constants having the dimension of time
τ_1, τ_2	Delay times associated with the dynamic paramters
τ_{N1}, τ_{N2}	Parameters having dimension of time
τ_B	Base transit time
τ_E	Emitter transit time
τ_{BED}	Base emitter junction transit time
τ_{BCD}	Base collector junction transit time
τ_C	Collctor transit time
y_{fe}	Forward transconductance
y_{ie}	Input admittance
V_T	Thermal voltage
j_N	Electron current density
j_P	Hole current density
μ_{nB}	Electron mobility inside the neutral base

μ_{pB}	Hole mobility inside the neutral base
D_{nB}	Electron diffusion coefficeint inside the neutral base
ε	Electric field inside the base
$n(x,t)$	Total electron density
$N(x)$	Static electron density
N_0	Static electron density at the base emitter junction
$\tilde{n}(x)$	Small signal electron density
$\tilde{n}_0$	Small signal electron density at the base emitter junction
$P(x,t)$	Total hole density
$P(x)$	Static hole density
P_0	Static hole density at the base emitter junction
$\tilde{p}(x)$	Small signal hole density
$\tilde{p}_0$	Small signal e hole density at the base emitter junction
$\tilde{v}$	Small signal voltage
V_{BE}	Base emitter DC voltage
α	Common base (CB) current gain
β	Common emitter (CE) current gain
W_B	Neutral base width
W_E	Neutral emitter width
x_{bc}	Base collector junction width
N_A	Acceptor concentration inside base
η	Drift factor
A_E	Emitter area
L_p	Hole diffusion length for static operation
$\tilde{L}_p$	Hole diffusion length for small signal operation
$y_{11}^{\ b}$	Common base (CB) input admittance
$y_{21}^{\ b}$	Common base (CB) transconductance
y_{11}^{e}	Common emitter (CE) input admittance
y_{21}^{e}	Common emitter (CE) transconductance
g_{fL}	Forward conductance in low injection level
g_{fH}	Forward conductance in high injection level
g_f	Forward conductance used for any level of injection
α_{11}, α_{21}	Charge partitioning factors
v_{sat}	Carrier saturation velocity in base emitter junction

b) Chapter 2

Name	Significance
E_m	Electric field in a medium m
E_n	Electric field inside base due to the negative charge
E_p	Electric field due to the positive charge
ε_m	Permitivity of a medium m
ρ	Charge density
ρ_{trap}	Electric potential
R_{net}	Total electron hole recombination rate
ϕ	Reference electric potential
ϕ_n	Electron quasi Fermi potential
ϕ_p	Hole quasi Fermi potential
n_i	Intrinsic carrier density
m_n	Electron effective mass
m_p	Hole effective mass
N_C	Density of states in conduction band
N_V	Density of states in velence band
$E_g(0)$	Bandgap energy at 0K
$E_g(T)$	Bandgap energy at TK
$E_{gbn}(T)$	Energy reduced by band gap narrowing
ΔE_C	Shift of conduction band edge
ΔE_V	Shift of valence band edge
E_{trap}	Trap energy level
m_l	Longitudinal carrier mass
m_t	Transverse carrier mass
μ_{b1}	Bulk carrier mobility
μ_{s1}	Surface carrier mobility
δn	Excess carrier concentration

c) Chapter 3

	HICUM parameters
C_{10}	Saturation current (GICCR constant)
Q_{p0}	Zero-bias hole charge

h_{jei}	B-E depletion charge weighting factor in HBTs
h_{jci}	B-C depletion charge weighting factor in HBTs
h_{fE}	Emitter minority charge weighting factor in HBTs
h_{fC}	Collector minority charge weighting factor in HBTs
i_{BEiS}	Internal B-E saturation current
m_{BEi}	Internal B-E current ideality factor
i_{REiS}	Internal B-E recombination saturation current
m_{REi}	Internal B-E recombination current ideality factor
t_{Bhrec}	base current recombination time constant at the BC barrier for high forward injection (default is v2.1 compatible)
i_{BEpS}	Peripheral B-E saturation current
m_{BEp}	Peripheral B-E current ideality factor
i_{REpS}	Peripheral B-E recombination saturation current
m_{REp}	Peripheral B-E recombination ideality factor
i_{BCiS}	Internal B-C saturation current
m_{BCi}	Internal B-C current ideality factor
i_{BCxS}	External B-C saturation current
m_{BCx}	External B-C current ideality factor
C_{jEi0}	Internal B-E zero-bias depletion capacitance
V_{DEi}	Internal B-E built-in potential
z_{Ei}	Internal B-E grading coefficient
a_{jEi}	Ratio of maximum to zero-bias value of internal B-E capacitance

C_{jCi0}	Internal B-C zero-bias depletion capacitance
V_{DCi}	Internal B-C built-in potential
z_{Ci}	Internal B-C grading coefficient
V_{PTCi}	Internal B-C punch-through voltage
f_{BCpar}	partitioining factor of parasitic BC cap (default is v2.1 compatible)
τ_{f0}	Low-current forward transit time at VBC=0V
$\Delta\tau_{0h}$	Time constant for base and B-C space charge layer width modulation
τ_{Bfvl}	Time constant for modelling carrier jam at low VCE
r_{ci0}	Internal collector resistance at low electric field
$V_{\lim}$	Voltage separating ohmic and saturation velocity regime
v_{ceff}	Internal C-E saturation voltage
τ_{Ef0}	neutral emitter storage time
$g_{\tau E}$	Exponent factor for current dependence of neutral emitter storage time
τ_{hcs}	Saturation time constant at high current densities
r_{Bi0}	Zero-bias internal base resistance
f_{AVL}	Avalanche current factor
q_{AVL}	Exponent factor for avalanche current
Cth	Thermal capacitance
Rth	Thermal resistance
alit	Factor for additional delay time of transfer current
alqf	Factor for additional delay time of minority charge

General introduction

In this era of the communication revolution, progress of humankind is faster than ever. The whole credit goes to the invention, modification and application of various semiconductor devices that are being used in various ways. Starting from the bipolar device, today's semiconductor market consists of unipolar devices like MOSFET (metal-oxide-semiconductor field-effect transistor) or HEMT (High electron mobility transistor). The basic bipolar device had experienced vast improvements and HBT (heterojunction bipolar device) was formed. These heterostucture devices are typically consisting of SiGe or III-V materials. The improvement in SiGe HBT leads to a new technology in 1992 called BiCMOS (bipolar complementary metal oxide semiconductor) [1] which quickly adjusted in various system applications. The SiGe ICs are representing a growth rate of 42% per year [2], a remarkable figure by any economic standard. The SiGe technology is used vastly in cellular application but optical networking, storage drives and radar system implementation are also in cards.

a) SiGe HBT used in high frequency operation

To achieve higher current gain and cutoff frequency, the basic structure of bipolar transistor has to be altered. The improvement, following the band gap engineering, consists of a combination of Si (wide band gap emitter) and Ge (narrow band gap base) to form the SiGe HBT. The first results of SiGe HBT were presented by IBM in the IEDM conference in 1987 [3]. Since then, the continuous modification to obtain high operating frequency has become an important research field and binds thousands of researchers of that field. In IEDM 2010, IHP, one of the DOTFIVE [4] members, presented maximum oscillation frequency of 500GHz, which is till date, considered the highest for SiGe devices [5]. In Figure **I**, a novel device structure from the DOTFIVE project is shown. This device is said to reach a fmax value of 400GHz [4]

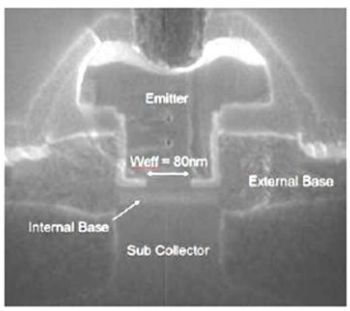

Figure **I**: SEM cross section of a new HBT device from DOTFIVE project.

In the last decade, III-V semiconductors opened a new opportunity in the arena of wireless communication. But at the time of high volume integration, SiGe replaces III-V materials due to the cost efficiency and low power consumption of group IV materials. Figure **II** points the ITRS roadmap on wireless communication [6].

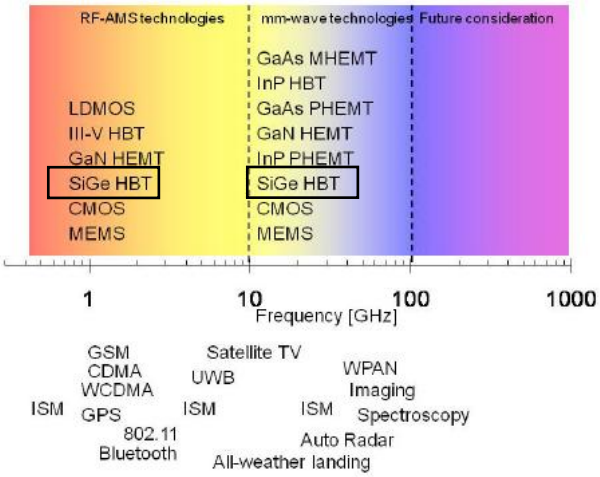

Figure **II**: Application of RF and analog/mixed signal technology [6].

THz technology is an emerging field which has demonstrated a wide-ranging potential. Extensive research in the last years has identified many attractive application areas and paved the technological path towards broadly usable THz systems. The project DOTFIVE is planned to establish the basis for fully integrated cost efficient electronic THz solutions. A schematic overview on some of the application areas identified is shown in Figure **III**

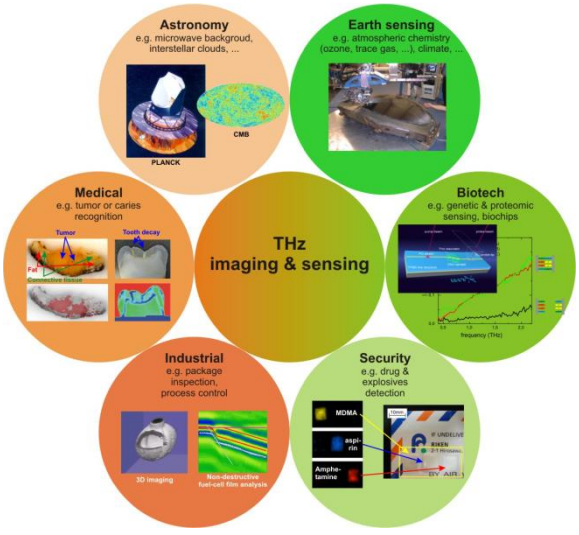

Figure **III**: Application fields considering THz frequencies.

b) Motivation of the work

- **Project description: (General goals)**

The project SIAM (Silicon analogue to millimeter wave technology) aims at the establishment of silicon technology platforms for emerging high frequency and mm-wave consumer applications like 77GHz automotive radars, 60GHz wireless networking (WLAN and WPAN) and 100Gbit/s optical data communications. The main aim of 2T206 SIAM project is to investigate and compare 130 nm SiGeC bipolar CMOS (BiCMOS) and 65 nm silicon-on-insulator (SOI) CMOS [7] on a high resistivity substrate for these applications. It is supporting the European effort towards establishing technological foundations to build the necessary infrastructure in the operating frequency range of 50-100GHz, and towards providing European citizens with a powerful communication network allowing for broadband communication everywhere and every time [8]. Next figure (Figure **IV**) represents the TEM (Transmission Electron Microscope) image of such device with SiGe:C HBT.

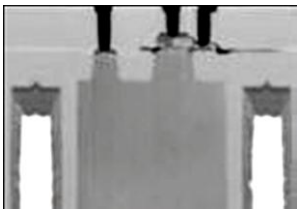

Figure **IV**: SiGe:C HBT technology BiCMOS/200mm [7]

- **PhD work**

As the operating frequency approaches near the cut off frequency of transistor, the quasi static approach does not provide the accurate phase shift of dynamic parameters. The effect is called Non Quasi Static (NQS) effect. Also the compact bipolar transistor models become often inaccurate at higher frequency. The main aim of this work is to investigate the NQS effect from the physical point of view and also investigate the compact modeling approach of this effect. The whole work is divided into five different parts.

1. First of all, literature concerning the NQS effect is studied. Starting from the basic transistor equations dynamic parameters are calculated and compared with the previously implemented models.

2. Next, a popular physics based compact model (HICUM) [9] is analyzed. The circuit implementation of NQS phenomena gives a clear understanding of compact modeling approach.

3. Measurement results are modeled at high frequency using HICUM model and the NQS circuit implementation is verified. Also, a scalable approach is investigated. The necessity of an improved model is shown and a new model is verified with these same measurements.

4. Physical device simulation (TCAD) is performed in a modern high speed device up to very high frequency (500GHz) to deeply investigate the NQS behavior. Then simulated results are then modeled using HICUM.

5. A new concept device with a SiGe spike inside emitter is fabricated and simulation has been performed in that device to show NQS behavior. After, the simulation results are modeled using HICUM model.

Reference

[1] Harame, D.L.; Crabbe, E.F.; Cressler, J.D.; Comfort, J.H.; Sun, J.Y.-C.; Stiffler, S.R.; Kobeda, E.; Burghartz, J.N.; Gilbert, M.M.; Malinowski, J.C.; Dally, A.J.; Ratanaphanyarat, S.; Saccamango, M.J.; Rausch, W.; Cotte, J.; Chu, C.; Stork, J.M.C., "A high performance epitaxial SiGe-base ECL BiCMOS technology," Electron Devices Meeting, 1992. IEDM '92. Technical Digest., International.

[2] John D. Cressler, SiGe and Si Strained-Layer Epitaxy for Silicon Heterostructure Devices.

[3] Iyer, S.S.; Patton, G.L.; Delage, S.S.; Tiwari, S.; Stork, J.M.C.;, "Silicon-germanium base heterojunction bipolar transistors by molecular beam epitaxy," Electron Devices Meeting, 1987 International.

[4] http://www.dotfive.eu, "DOTFIVE website."

[5] "DOTFIVE presents high-speed SiGe HBTs," Semiconductor Today compounds and advanced silicon, vol. 6, Mar. 2011.

[6] "RF and A/MS Technologies for Wireless Communications," ITRS 2009 chapter, .

[7] http://www2.imec.be/content/user/File/leaflet_Cmore/CMORE_bicmos2010.pdf, "CMORE_bicmos2010."

[8] http://www.catrene.org/web/downloads/profiles_medea/2T206-SIAM-profile-outMEDEA%20%2821-7-09%29.pdf, "MEDIA+ SIAM project documentation."

[9] http://www.iee.et.tu-dresden.de/iee/eb/hic_new/hic_doc.html, "HICUM L2 Documentation."

Chapter 1

[NQS THEORY]

1.1 Introduction

Steady state transistor operations were always analyzed using basic drift diffusion equations which explained junction transistor behavior fairly well. As time progressed more complicated effects were observed and introduction of new approach became prominent. The problem arises while investigating the dynamic behavior of transistors like the AC or fast switching operation. For a transient operation certain time delay was observed for both switch on and switch off cases [1]. As an example, Figure **1.1** highlights the variation of electron concentration profile inside the quasi neutral base region in transient operation

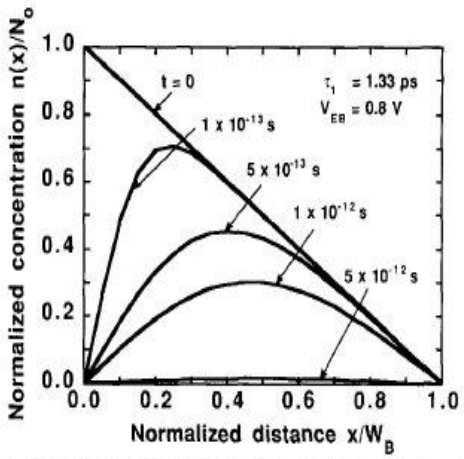

Fig. 5. Transient variation of electron concentration profile when V_{EB} decreases from the switch-on voltage to zero.

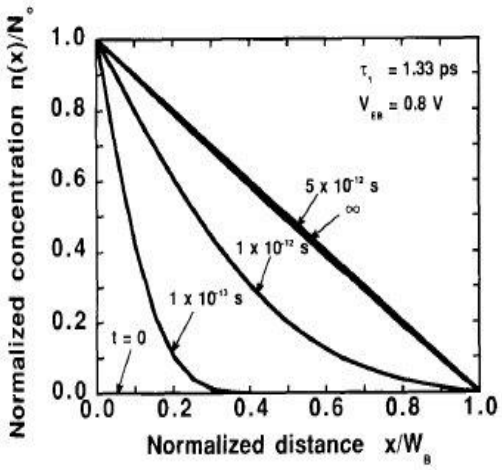

Fig. 8. Transient variation of electron concentration profile when V_{EB} increases from zero to the switch-on voltage.

Figure **1.1** : Transient phenomena in base region. (a) switch off (b) switch on [1]

Scholars were engaged to introduce new concept that would help modeling transistor at high frequency. At that time Winkel applied a time delay inside the current gain and recalculated conductance parameters [2]. This was the starting point of including time delays inside steady state calculations which afterwards we call NQS calculation. At the beginning of 90's many researchers calculated NQS related parameters following different approaches. The famous charge partitioning concept was introduced [3] [4] and reported in agreement with simulations. Afterwards Rinaldi [6] introduced a general closed form solution for all injection level and his work allowed achieving all the previously described models from a closed form solution with the help of minor approximations. In this part first we will consider the charge control approach and then recalculate NQS related parameters using basic device equations.

1.2 Classical charge control model and extension for high frequency application

To examine a junction transistor in more details we need to calculate the terminal currents at three nodes (Emitter, Base, and Collector) of a transistor. Terminal currents obviously depend on the excess electron concentration at the narrow p type base region. The calculation is very similar to that used to calculate the narrow base diode currents [7]

The charge control approach is useful for analyzing the transistor terminal currents, particularly in ac applications. Following this approach we can separate arbitrary excess electron distribution in the base into the normal and inverted distribution (Figure **1.2**)

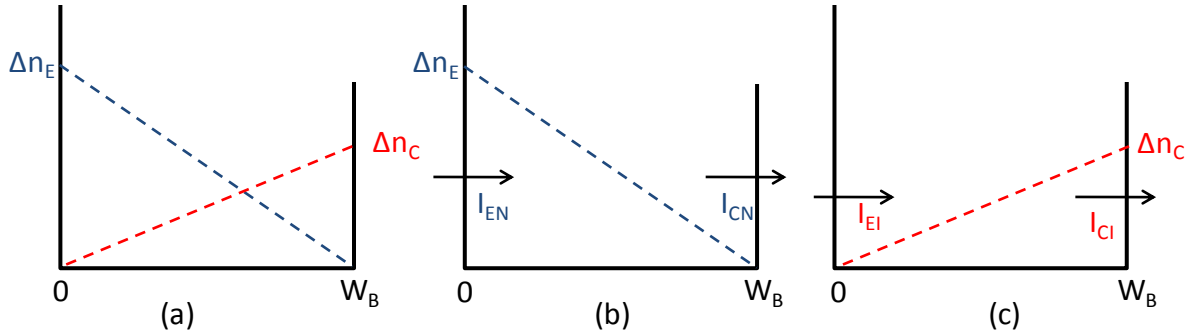

Figure 1.2 : excess electron distribution in neutral base in normal and inverted mode of operation. (a) Approximation with emitter and collector junction forward biased. (b) Emitter and collector currents in normal mode. (c) Emitter and collector currents due to inverted mode of operation.

Here I_{EN}, I_{CN} represent the normal and I_{EI}, I_{CI} represent the inverted components of currents at emitter and collector terminals respectively. The currents for the normal and inverted modes in terms of storage charges can be constructed and reads as follows,

$$I_E = I_{EN} + I_{EI} \qquad \textbf{1.1}$$

$$I_C = I_{CN} + I_{CI}$$

These equations (**1.1**) are the basic form of the Ebers-Moll equations [8]. Expressing these currents as a function of storage charge, we have,

$$I_{EN} = \frac{Q_b}{\tau_{tN}} + \frac{Q_b}{\tau_n}, I_{CN} = \frac{Q_b}{\tau_{tN}} \quad \textbf{1.2}$$
$$I_{EI} = -\frac{Q_I}{\tau_{tR}}, I_{CI} = -(\frac{Q_I}{\tau_{tR}} + \frac{Q_I}{\tau_n})$$

Where Q_b and Q_I are the storage charges in the normal and inverted modes, τ_{tN} and τ_{tR} are transit times in these two modes and τ_n is the minority carrier lifetime in the base region.

With the help of equations (**1.1**) and including the effect of time dependence of storage charge we can rewrite the equations (**1.2**) as,

$$I_E = Q_b(\frac{1}{\tau_{tN}} + \frac{1}{\tau_n}) - \frac{Q_I}{\tau_{tR}} + \frac{dQ_b}{dt} \quad \textbf{1.3}$$
$$I_C = \frac{Q_b}{\tau_{tN}} - Q_I(\frac{1}{\tau_{tR}} + \frac{1}{\tau_n}) - \frac{dQ_I}{dt}$$
$$I_B = \frac{Q_b}{\tau_n} + \frac{Q_I}{\tau_n} + \frac{dQ_b}{dt} + \frac{dQ_I}{dt}$$

These equations can be expressed in the general form,

$$I_B = \sum \frac{Q_i}{\tau_i} + \sum \frac{dQ_i}{dt} \quad \textbf{1.4}$$
$$I_C = \sum \frac{Q_i}{\tau_{oi}} + \sum \frac{dQ_i}{dt}$$
$$Q_i = f_i(V_{BE}, V_{CB}, I_C)$$

Here Q_i represents the total charge at a region i.

For a low level injection and reversely biased base-collector junction, we can neglect the time dependent contribution of i_c and equations set (**1.4**) becomes

$$I_B = \frac{Q_b}{\tau_b} + \frac{dQ_b}{dt} \quad \textbf{1.5}$$
$$I_C = \frac{Q_b}{\tau_{ob}}$$
$$Q_b = Q_0(\exp\frac{V_{BE}}{V_T} - 1)$$

τ_b, τ_{ob} are two constants having the dimension of time.

Changing the time domain into the frequency domain we get two sets of ac parameters. In the common-emitter configuration the current gain becomes,

$$\beta = \frac{\tau_b / \tau_{ob}}{1 + j\omega\tau_b} = \frac{\beta_0}{1 + j\omega/\omega_\beta} \qquad \textbf{1.6}$$

Where $\omega_\beta = \frac{1}{\tau_b}$ and $\beta_0 = \tau_b / \tau_{ob}$

Transconductance and input admittance are also calculated as,

$$y_{fe} = \frac{I_c}{V_T} = g_m \qquad \textbf{1.7}$$

$$y_{ie} = \frac{y_{fe}}{\beta} = g_m\left(\frac{1}{\beta_0} + j\frac{\omega}{\omega_T}\right)$$

With transition frequency $\omega_T = \frac{1}{\tau_{ob}}$

These small signal expressions (Equations **1.6**) display a number of well known properties correctly. The behavior of $|\beta(\omega)|$ is constant at low frequencies with a cutoff at ω_β and falling at the rate of 20dB/dec. But the main drawback is that excess phase in β is not accounted in this calculation. At that very point a correction term inside the charge control approach was introduced by Winkel [2]. A close similarity between the differential equations that govern the current flow in transistor and the equations that describe the flow of electric signal in transmission line was observed. When the carrier lifetime and electric field in the transistor are constant, the analogy will be a uniform transmission line. We can approximate the network as a summation of two networks, one with minimum phase type and another that only changes the phase of the signal. In the time domain a suitable approximation of the second network would be a constant delay.

Replacing (**1.5**) we will get a new set of equations

$$i_b(t) = \frac{Q_b(t)}{\tau_b} + \frac{dQ_b(t)}{dt} \qquad \textbf{1.8}$$

$$i_c(t) = \frac{Q_b(t-\tau_1)}{\tau_{ob}}$$

$$Q_b(t+\tau_2) = Q_0(\exp\frac{v_{be}(t)}{v_T} - 1)$$

And the small signal parameters changed accordingly [2]

$$\beta = \frac{\beta_0}{1 + j\beta_0\omega/\omega_T}\exp(-j\omega\tau_1) \qquad \textbf{1.9}$$

$$y_{fe} = g_m \exp\{-j\omega(\tau_1+\tau_2)\}$$

$$y_{ie} = g_m(\frac{1}{\beta_0} + j\frac{\omega}{\omega_T})\exp(-j\omega\tau_2)$$

Equations **1.9** represent the first attempt to include time varying phase factor inside calculations. These equations prove their significance in vast domain as one of the modern compact models HICUM [9] basically applies it to model NQS effect.

1.3 Calculation of current components in a drift transistor in small signal operation

In quasi-static approach, basic current components are calculated only using the time independent part of the drift diffusion equation [7]. For the small signal analysis where the time dependence of minority carrier becomes predominant, it is obvious to consider time variation of the excess carrier concentration.

In the following calculation an npn transistor is considered with exponential acceptor doping profile. Carrier mobility is assumed to be constant inside the base for all injection level and an average value of electron diffusion coefficient has been applied for the calculation i.e. heavy doping effect has not been considered. The classical drift diffusion equation in the quasi neutral base region for the electron and hole charge reads [10]

$$j_N(x,t) = q\mu_{nB} n(x,t)\varepsilon + qD_{nB}\frac{\partial n(x,t)}{\partial x} \qquad \textbf{1.10}$$

$$j_P(x,t) = q\mu_{pB} p(x,t)\varepsilon - qD_{pB}\frac{\partial p(x,t)}{\partial x}$$

Here, all the symbols represent their usual meaning. We consider negligible recombination inside the base region and omitting recombination term from the basic continuity equation, we get,

$$\frac{\partial n(x,t)}{\partial t} = \frac{1}{q}\frac{\partial j_N(x,t)}{\partial x} \qquad \textbf{1.11}$$

Differentiating (**1.10)** with respect to the space variable x and putting in (**1.11**) gives a second order partial differential equation in $n(x,t)$.

$$\mu_{nB} V_T \frac{\partial^2 n(x,t)}{\partial x^2} + \mu_{nB}\varepsilon\frac{\partial n(x,t)}{\partial x} - \frac{\partial n(x,t)}{\partial t} = 0 \qquad \textbf{1.12}$$

Next, assuming a small signal perturbation is introduced over the DC bias condition; all the electrical parameters can be constructed as a summation of a DC and a small signal AC component.

$$V_{BEtot} = V_{BE} + \tilde{v}e^{j\omega t} \qquad \textbf{1.13}$$

$$n(x,t) = N(x) + \tilde{n}(x)e^{j\omega t}$$

Where, N(x) is the DC component of excess carrier concentration and ñ(x) is the small signal component. At the edge of base emitter junction (x=0) equation (**1.13**) becomes,

$$n(0,t) = N_0 + \tilde{n}_0 e^{j\omega t}$$

Differentiating n(x,t) with respect to x and t and putting inside equation (**1.12**), we obtain a second order exact differential equation in $\tilde{n}(x)$.

$$\frac{d^2\tilde{n}(x)}{dx^2} + \left(\frac{\varepsilon}{V_T}\right)\frac{d\tilde{n}(x)}{dx} - \left(\frac{j\omega}{D_{nB}}\right)\tilde{n}(x) = 0 \qquad \textbf{1.14}$$

Where we have used Einstein relations, $D_{nB} = \mu_{nB} V_T$ and approximated $\frac{\partial n}{\partial t} = 0$ and $\frac{d\tilde{n}}{dx} = \frac{d^2\tilde{n}}{dx^2} = 0$ at steady state.

Equation (**1.14**) is a second order homogeneous differential equation which can be solved easily with the help of boundary conditions i.e. at x=0, ñ=ñ$_0$ and at x=W$_B$, ñ=0.

The solution of equation (**1.14**) is [10]

$$\tilde{n}(x) = \tilde{n}_0 \exp\left(\frac{A}{2}(1-u_x)\right)\frac{\sinh u_x \xi_{fl}}{\sinh \xi_{fl}} \qquad \textbf{1.15}$$

Where,

$$A = -\frac{\varepsilon W_B}{V_T} \qquad \textbf{1.16}$$

$$u_x = 1 - \frac{x}{W_B}$$

$$\xi_{fl} = \frac{\eta}{2}\sqrt{1 + \frac{4j\Omega}{A^2}}$$

$$\Omega = \omega \frac{W_B^{\ 2}}{\mu_{nB} V_T}$$

This equation (**1.15**) is admittedly rather complicated and the electron distribution described is not immediately apparent. The factor $\tilde{n}(x)$ is the sinusoidal varying reference and the expression describes the phase and the amplitude at any point with respect to the base width.

Equation (**1.15**) is a general solution for the excess carrier concentration and it is always modified depending upon the injection condition. Low and high injection are treated separately and presented below.

- **Low Injection (LI) level**

For LI we approximate ($N << N_A$, $P \approx N_A$) and the built in electric field can be calculated by setting $j_P(x,t) = 0$. (Equation **1.10**)

$$\varepsilon = \frac{1}{N_A}\frac{dN_A}{dx}V_T = \frac{-\eta}{W_B} \qquad \textbf{1.17}$$

Here we have assumed a drift transistor with an exponential base doping,

$$N_A = N_{A0}\exp(-\eta\frac{x}{W_B}) \qquad \textbf{1.18}$$

Comparing equation (**1.16**) with (**1.17**) we find A=η for low injection level.
It is customary to express Ω (equation **1.16**) in terms of the base transit time. For a drift diffusion transistor, base transit time can be calculated easily

$$\tau_B = \frac{1}{2}\frac{W_B^{\,2}}{\mu_{nB}V_T} \text{ considering diffusion transistor [7]} \qquad \textbf{1.19}$$

$$\tau_B = \frac{W_B^{\,2}}{\mu_{nB}V_T}(\frac{\eta - 1 + \exp(-\eta)}{\eta^2}) \text{ for drift transistor in low level of injection [11]}$$

$$\tau_B = \frac{1}{4}.\frac{W_B^{\,2}}{\mu_{nB}V_T} \text{ for transistor in high level of injection [11]}$$

Taking equation (**1.19**) into account ξ_{fl} can be expressed as a function of τ_B,

$$\xi_{fl} = \frac{\eta}{2}\sqrt{1 + \frac{4j\omega\tau_B}{\eta - 1 + \exp(-\eta)}} \qquad \textbf{1.20}$$

Next figure shows the magnitude of normalized carrier concentration variation over the base width. To obtain these plots, some device parameter values are assumed such as $W_B = 20nm$, $\tau_B = 0.5\times10^{-12}\,\text{sec}$. Frequency range is considered between 1GHz to 500GHz. The drift factor (η) is a positive number and attended integer values upto 8. It is notable that at high drift field ($\eta > 3$), the transistor becomes a purely drift transistor.

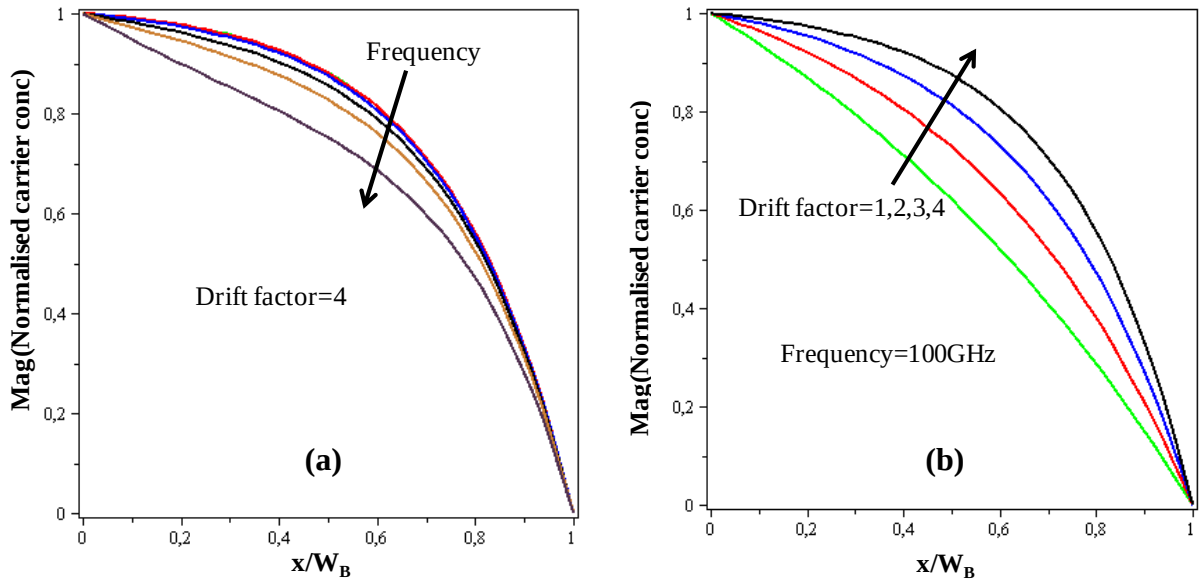

Figure 1.3 : (a) Normalised excess carrier as a function of normalised distance for different frequencies (1GHz, 10GHz, 100GHz, 200GHz, 300GHz, 500GHz). The plot shows a clear frequency dependence at high frequency. (b) Normalized excess carrier as a function of normalized distance at a constant frequency for different drift factors.

The next step is to obtain the small signal current components which can be obtained from the current density,

$$I_n\big|_{x=0} = \tilde{i}_e = qA_E D_{nB}\left[\frac{\varepsilon}{V_T}\tilde{n}\big|_{x=0} + \frac{\partial\tilde{n}}{\partial x}\Big|_{x=0}\right] \qquad \textbf{1.21}$$

$$I_n\big|_{x=W_B} = \tilde{i}_c = qA_E D_{nB}\left[\frac{\varepsilon}{V_T}\tilde{n}\big|_{x=W_B} + \frac{\partial\tilde{n}}{\partial x}\Big|_{x=W_B}\right]$$

Using equation (**1.15**) a set of small signal terminal currents can be achieved for low injection level.

$$\tilde{i}_c = -\tilde{n}_0 qD_{nB}A_E \frac{\xi_{fl}e^{\eta/2}}{W_B.\sinh\xi_{fl}} \qquad \textbf{1.22}$$

$$\tilde{i}_e = -\frac{\tilde{n}_0 qD_{nB}A_E}{W_B}\left[\xi_{fl}\coth\xi_{fl} + \frac{\eta}{2}\right]$$

For a transistor operating in common base configuration, the current gain (α) is defined as the ratio of the collector current to the emitter current. Small signal current gain can be easily formulated using equation **1.22**

$$\alpha = \frac{\xi_{fl} e^{\eta/2}}{\frac{\eta}{2}\sinh \xi_{fl} + \xi_{fl}\cosh(\xi_{fl})} \qquad \textbf{1.23}$$

Common emitter current gain (β) can be constructed from equation **1.23** as $\beta = \frac{\alpha}{1-\alpha}$. The magnitude and phase variations of current gain are shown in Figure **1.4**

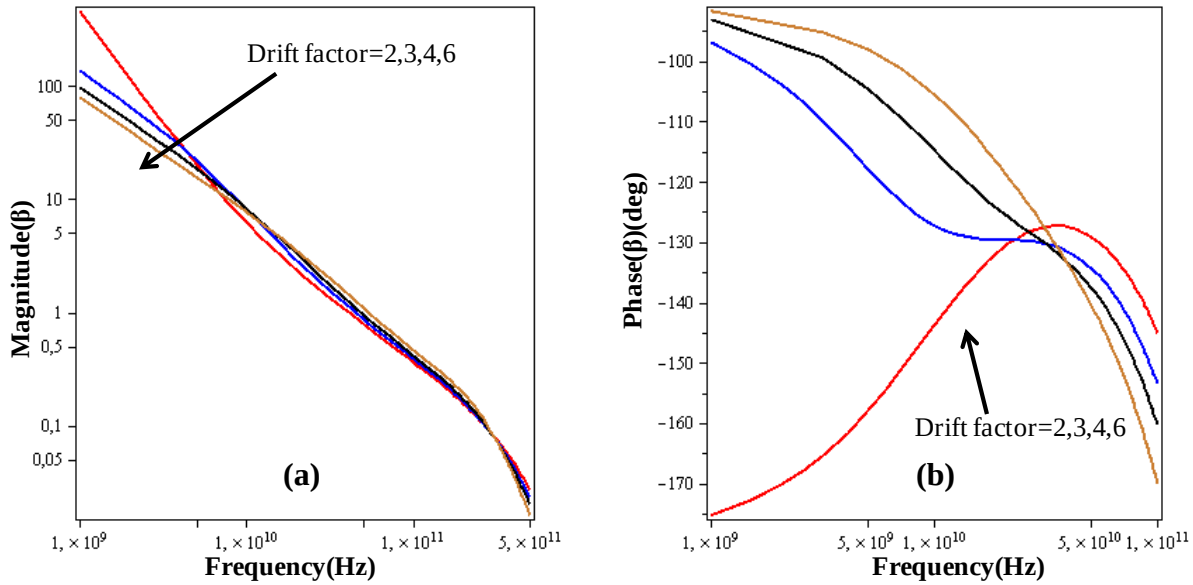

Figure **1.4** : Magnitude and phase variation of common emitter current gain for different drift factors.

Again coming back to the current calculation, we observe, at the limit of $\omega \to 0$, equation (**1.22**) changes to,

$$\tilde{i}_c\big|_{\omega=0} = -\tilde{n}_0 q D_{nB} A_E \frac{(\eta/2)e^{\eta/2}}{W_B.\sinh \eta/2} \qquad \textbf{1.24}$$

$$\tilde{i}_e\big|_{\omega=0} = -\frac{\tilde{n}_0 q D_{nB} A_E}{W_B}\frac{\eta}{2}\left[\coth\frac{\eta}{2}+1\right]$$

The ratio of frequency dependent and independent collector currents is

$$\tilde{i}_{c\_norm} = \frac{\tilde{i}_c(\omega)}{\tilde{i}_c(\omega = 0)} = \frac{\frac{\xi_{fl}}{\sinh \xi_{fl}}}{\frac{\eta/2}{\sinh \eta/2}} \qquad \textbf{1.25}$$

Equation (

1.25) is also noted in [12]

The next figure shows the variation of normalized small signal current over frequency for different drift factors.

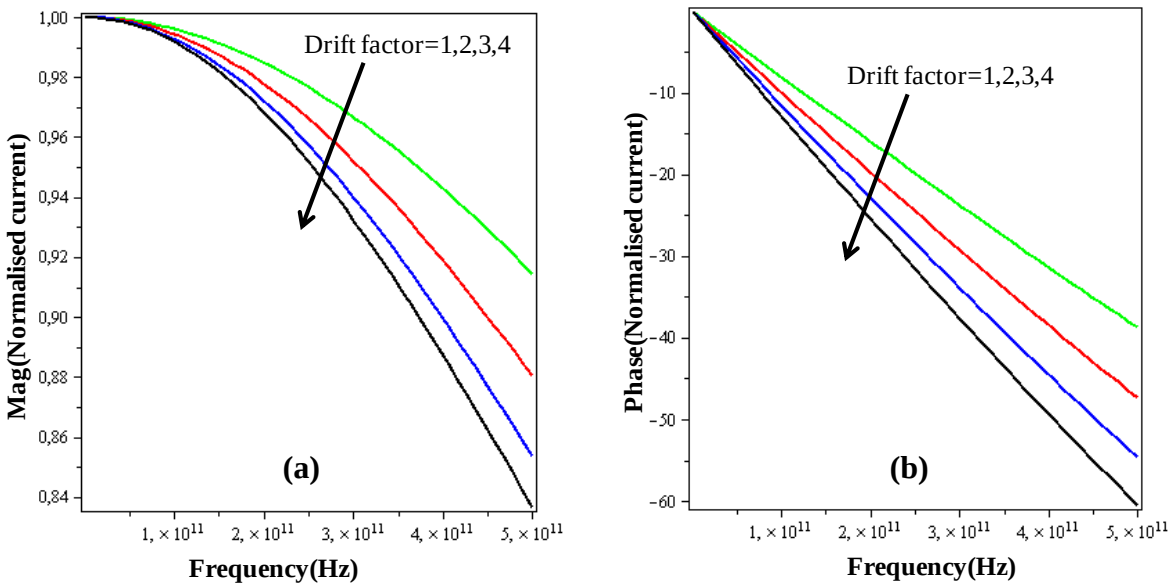

Figure **1.5 :** Magnitude and phase variation of normalized collector current at different drift factor.

To compare small signal current components with the DC current component for a drift transistor, DC transfer current can be calculated easily by following the same procedure. [1]

$$I_C = qD_{nB}A_E \frac{N_0}{W_B} \frac{\eta}{e^{-\eta} - 1} \qquad \textbf{1.26}$$

The current component is the same as in [6]. Here we have assumed that no recombination is present inside the base region, i.e. $\frac{dI_C}{dx} = 0$ inside the base. As the base width changes with the external bias variation terminal currents depend only on the external bias points.

DC excess carrier concentration is achieved simply by solving second order differential equation in $N(x)$ and is given by,

$$N(x) = \frac{N_0}{\left(1 - e^{-\eta}\right)}\left[1 - e^{-\eta u_x}\right] \qquad \textbf{1.27}$$

Where static excess carrier concentration at the edge of base emitter junction is given by,

$$N_0 = \frac{n_i^2}{N_A}\exp\left(\frac{V_{BE}}{V_T}\right)$$

Equation 1.27 presents the excess carrier concentration due to the DC bias variation in a drift transistor. Again, equation 1.15 shows the excess carrier concentration inside the neutral base region due to the small signal perturbation. It is interesting to compare two types of excess carrier concentration as we have equations for both small signal analysis and normal static operation (Figure **1.6**).

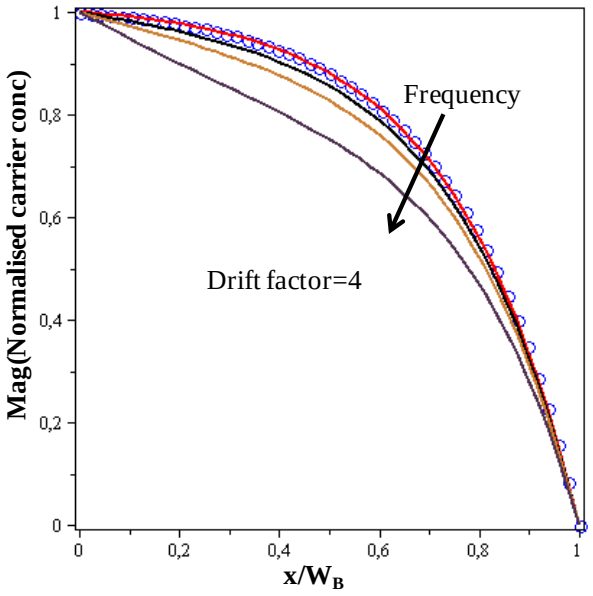

Figure **1.6** : comparison between small signal and quasi static excess carrier concentrations at a constant drift factor. Quasi static part is shown in blue circle and small signal part in line.

Figure **1.6** suggests that increasing frequency shifts the magnitude of excess carrier inside the quasi neutral base region. Difference in carrier concentration means additional small signal charge inside base region.

Up to now, we have calculated the excess carrier concentration for Small signal as well as for DC bias variation. At the base emitter junction, the relation between small signal and DC carrier concentrations can be arrived following a few steps. Considering the law of injection at the edge of the base emitter junction, we can express carrier concentration on the emitter side as,

$$(N_0 + \tilde{n}_0)P_0 \approx n_i^{\,2} \exp(\frac{V_{BEtot}}{V_T}) \qquad \textbf{1.28}$$

$$N_0 P_0 \approx n_i^{\,2} \exp(\frac{V_{BE}}{V_T})$$

From equations (**1.28**) assuming that $\tilde{v} \ll V_T$ we get directly the relation between excess carrier concentration at emitter side for LI condition.

$$\tilde{n}_0 = \frac{\tilde{v}}{V_T} N_0 \qquad \textbf{1.29}$$

With the help of equations (**1.28** and **1.25**) a relation between the small signal excess carrier concentration and forward transfer current can be established,

$$\tilde{n}_0 = \frac{I_C W_B}{q A_E D_{nB}} \frac{e^{-\eta} - 1}{\eta} \left(\frac{\tilde{v}}{V_T} \right) \qquad \textbf{1.30}$$

Keeping in mind the relation between $\tilde{n}_0$ and, I_C, the relation between small signal transfer current ($\tilde{i}_c(\omega)$) and static transfer current (I_C) becomes,

$$\frac{\tilde{i}_c(\omega)}{I_C} = \frac{\frac{\xi_{fl}}{\sinh \xi_{fl}}}{\frac{\eta/2}{\sinh \eta/2}} \frac{\tilde{v}}{V_T} \qquad \textbf{1.31}$$

This ratio of transfer currents can be readily compared with the normalized current formulation (equation

1.25). The only difference is the factor $\frac{\tilde{v}}{V_T}$ which represents the relation between the small signal and quasi static excess carrier concentration. In the limit of $\omega \to 0$ small signal current is directly proportional to the static forward current and the proportionality constant depends upon the magnitude of small signal perturbation.

$$\tilde{i}_c\big|_{\omega=0} = I_c \frac{\tilde{v}}{V_T} = qD_{nB}A_E \frac{N_0}{W_B} \frac{\eta}{(e^{-\eta}-1)} \frac{\tilde{v}}{V_T} \qquad \textbf{1.32}$$

Terminal currents are calculated and compared in different condition like the DC and small signal application. It is noted that the magnitude of applied small signal voltage plays a significant role for small signal current.

The accumulated charge due to small signal operation can be calculated just by integrating minority carrier concentration (**1.15**)

$$\tilde{Q} = \frac{2qA_E\tilde{n}_0W_B}{(\eta^2 - 4\xi^2_{fl})}\left[2\xi_{fl}\left(e^{\eta/2}\,\mathrm{cs}\,ch\xi_{fl} - \coth\xi_{fl}\right) - \eta\right] \qquad \textbf{1.33}$$

Accumulated base charge for DC bias variation is calculated by integrating equation (**1.27**) and is given by,

$$Q_{DC} = \frac{qA_EN_0W_B}{\eta}\left[\frac{\eta}{2}e^{\eta/2}\,\mathrm{cs}\,ch\frac{\eta}{2} - 1\right] \qquad \textbf{1.34}$$

The ratio of small signal base charge and DC charge is calculated and the magnitude and phase variation is shown in Figure **1.7**

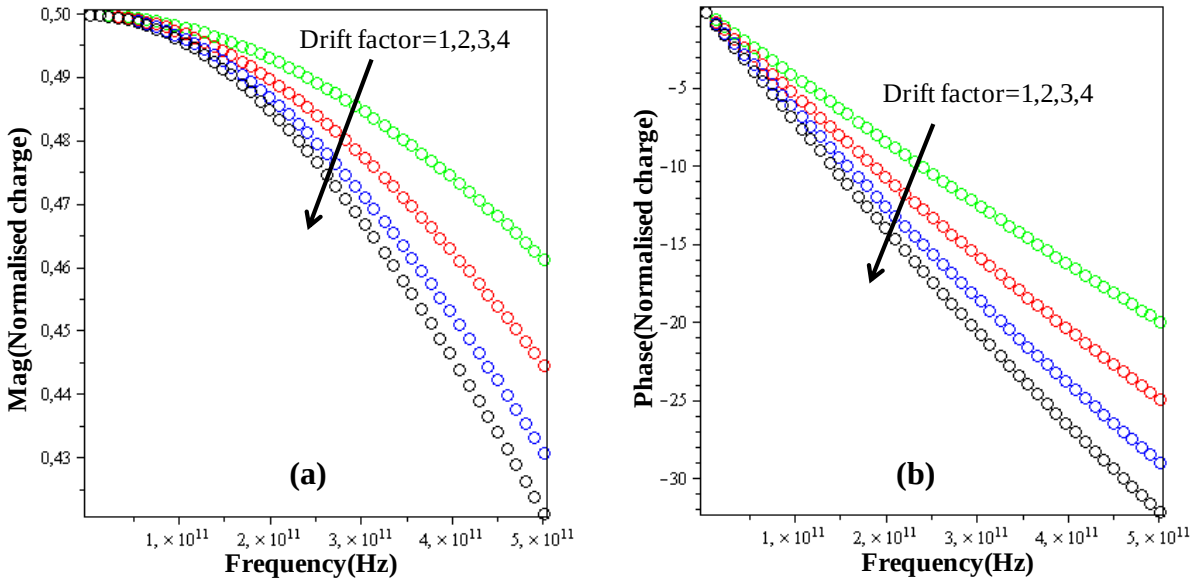

Figure 1.7 : Magnitude and phase variation of normalized charge at LI level.

Figure **1.7** typically shows the phase variation due to the charge accumulation at higher frequencies.

The above analysis provides some basic small signal equations in LI domain. These equations will be used after in admittance parameters calculation.

- **High Injection (HI) level**

In the previous part, small signal analysis in the LI condition is formulated. Next, the same analysis will be carried out in High Injection (HI) condition. The Distributive effect of parasitic resistance and capacitance are neglected (i.e ac crowding effect) [13] while considering HI level. Though it is an important factor which contributes significantly to the total delay time, it is assumed to be "extrinsic" part of the device and hence it is overlooked inside this calculation. At HI level carrier mobility is reduced due to electron-hole scattering [7] which reduces diffusion coefficient. This effect is also neglected to provide a simple calculation.

In HI, We approximate ($N \simeq P >> N_A$) and the equation (**1.10**) reduces to

$$j_n(x,t) = 2qD_{nB}\frac{\partial n(x,t)}{\partial x} \qquad \textbf{1.35}$$

The doubling of the electron diffusion coefficient is known as Webster effect.

Following the same procedure as for the LI level, a second order differential equation for the excess carrier concentration is constructed.

$$\frac{d^2\tilde{n}(x)}{dx^2} - \frac{j\omega}{2D_{nB}}\tilde{n}(x) = 0 \qquad \textbf{1.36}$$

Considering the same boundary conditions used for LI condition i.e. at x=0, ñ=ñ$_0$ and at x=W$_B$, ñ=0, solution of equation **1.36** becomes,

$$\tilde{n}(x) = \tilde{n}_0 \frac{\sinh(\xi_{fH} u_x)}{\sinh(\xi_{fH})} \qquad \textbf{1.37}$$

Where $\xi_{fH} = \sqrt{\frac{j\omega W_B^{\ 2}}{2D_{nB}}} = \sqrt{2j\omega\tau_B}$

At LI level excess carrier concentration depends vastly upon the base drift factor (η). At HI level, as there is no influence of the drift field, carrier concentration is merely a straight line for a vast range of frequencies as shown in Figure **1.8**

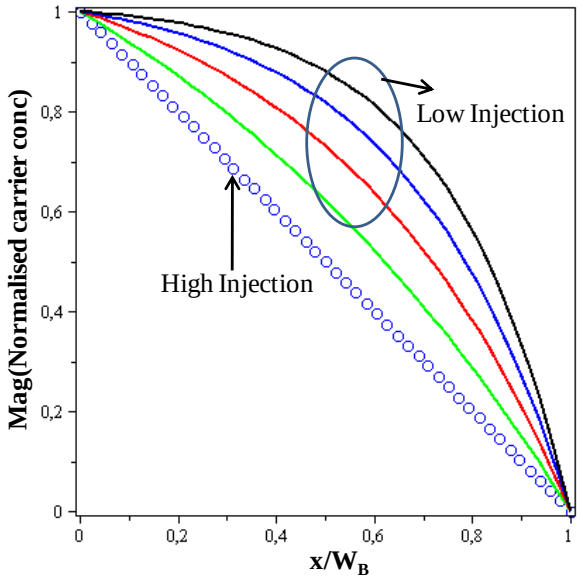

Figure **1.8** : Magnitude of normalized carrier concentration at different injection level. Different curves in LI represent different drift factors

Terminal currents for HI condition are constructed thereafter

$$\tilde{i}_e = 2qA_E D_{nB} \frac{\tilde{n}_0}{W_B} \xi_{fH} \coth \xi_{fH} \qquad \textbf{1.38}$$

$$\tilde{i}_c = 2qA_E D_{nB} \frac{\tilde{n}_0}{W_B} \frac{\xi_{fH}}{\sinh \xi_{fH}}$$

In the LI condition, small signal current gain was calculated with the help of terminal current equations. Similarly for HI condition common base current gain is calculated from equation **1.38**,

$$\alpha = \frac{1}{\cosh \xi_{fH}} \qquad \textbf{1.39}$$

Common emitter current gain (β) at HI is calculated using $\beta = \frac{\alpha}{1-\alpha}$ and plotted to compare,

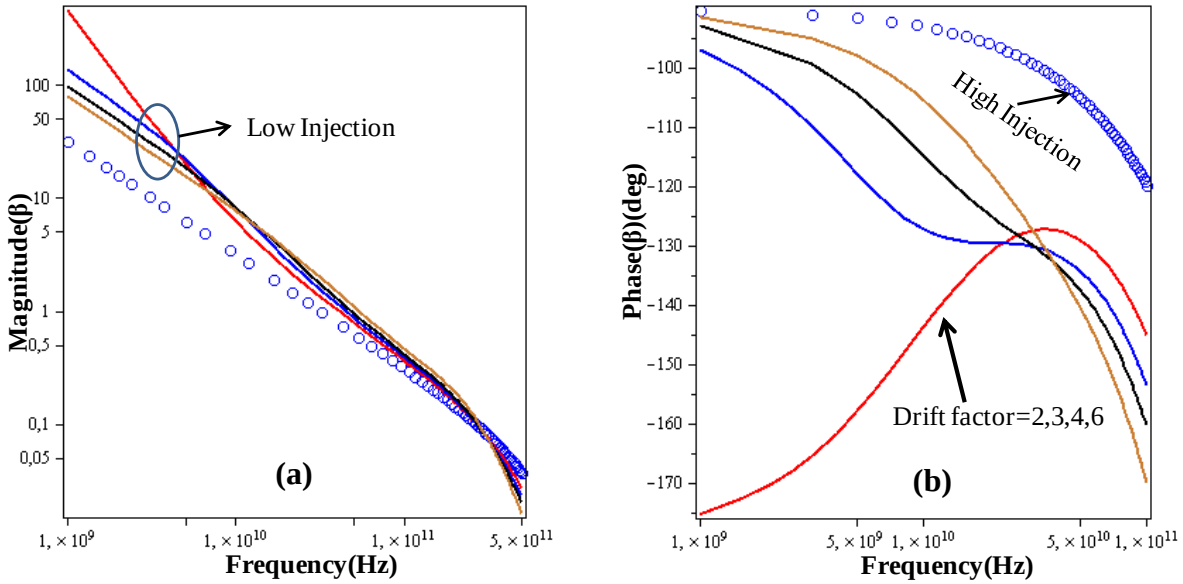

Figure **1.9 :** Comparison between small signal current gain β in LI and HI condition.

Static current for the HI level can be constructed easily following the same procedure and found to be,

$$I_C = 2qD_{nB}A_E\frac{N_0}{W_B} \qquad \textbf{1.40}$$

Equation **1.40** can be compared with the LI part (equation **1.26**). It is noticed that drift factor does not affect transistor operation at HI. Steady state excess carrier concentration also follows linear relationship with the base width.

$$N(x) = N_0\left[1-\frac{x}{W_B}\right] \qquad \textbf{1.41}$$

Equation **1.41** can be compared with the static carrier concentration of LI condition (equation **1.27**).

In the above analysis excess minority carrier concentration and terminal currents for small signal has been calculated considering both injection levels. This analysis provide frequency dependent current components which will be used in advanced calculations.

1.4 Y parameter calculation for Low injection and High injection level

The Ac characteristics of a transistor can be described in terms of two voltages and two currents. We can express input and output currents as a function of input and output voltages and define this proportionality constant as admittance (y).

In the condition of dynamic short of the collector, the y parameters are defined as [10]

$$y_{11}{}^b = \frac{\tilde{i}_e}{\tilde{v}} \qquad \textbf{1.42}$$

$$y_{21}{}^b = -\frac{\tilde{i}_c}{\tilde{v}}$$

Combining equations (**1.22**) and (**1.30**), we obtain small signal y parameters in low injection condition,

$$y_{11}^{b} = g_{fL}\frac{\eta/2+\xi_{fL}\coth\xi_{fL}}{(1+\coth\eta/2)\eta/2} \qquad \textbf{1.43}$$

$$y_{21}{}^{b} = -g_{fL}\frac{\xi_{fL}}{\sinh\xi_{fL}}\frac{\sinh(\eta/2)}{(\eta/2)}$$

Where, g_{fL} is forward conductance in low injection level. Equation (**1.43**) represents the common base y parameters at LI level for small signal operation. It is also noted in [6]. It can be noted that $y_{21}{}^{b}$ follows the same frequency dependence like $\tilde{i}_{c\_norm}$ (equation **1.25**).

These Y parameters are calculated considering the common base configuration. Common emitter small signal Y parameters are easily calculated from common base equations. The conversion of Y parameters are presented in equation

$$y_{21}^{e} = -y_{21}^{b} \qquad \textbf{1.44}$$

$$y_{11}^{e} = y_{11}^{b} + y_{21}^{b}$$

Magnitude and phase variations of small signal common emitter y parameters at LI condition are shown below,

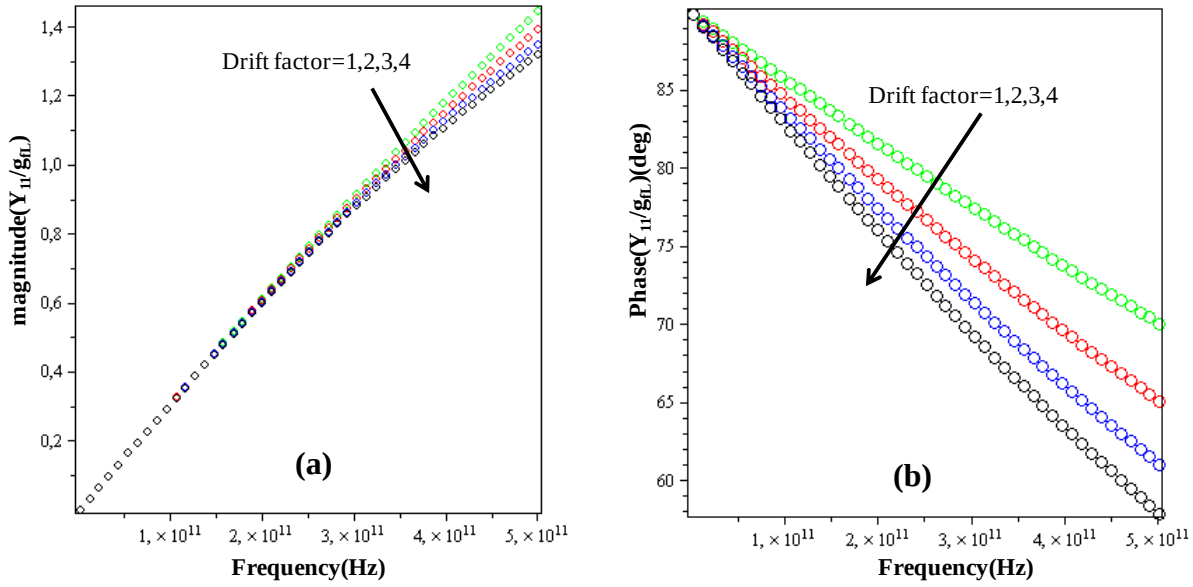

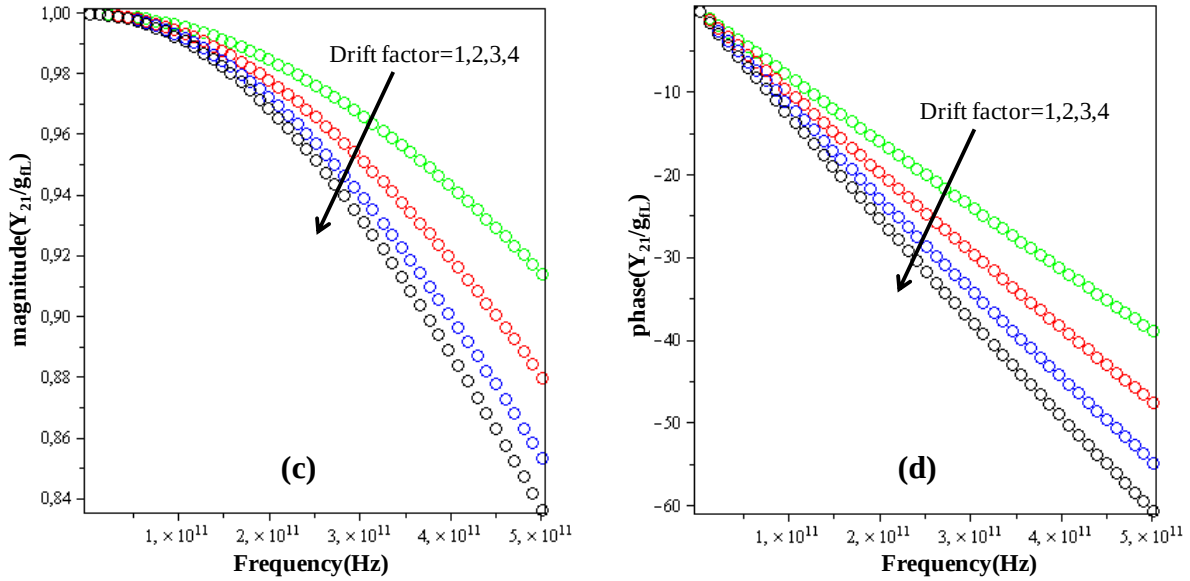

Figure **1.10 :** Calculated magnitude and phase variation of small signal common emitter Y parameters at Low Injection condition. Parameter set is the same as before.

Small signal common base Y parameters for High injection can be obtained with the help of equations (**1.38**),

$$y_{11}^{b} = g_{fH}\frac{\xi_{fH}}{\tanh(\xi_{fH})} \qquad \textbf{1.45}$$

$$y_{21}^{b} = -g_{fH}\frac{\xi_{fH}}{\sinh(\xi_{fH})}$$

Where, g_{fH} is forward conductance in high injection level. As in the HI level, terminal currents do not depend upon the drift factor, the admittance parameters in HI level are also independent of the base drift factor. Next figure (Figure **1.11**) shows the magnitude and phase variation of y parameters in HI condition.

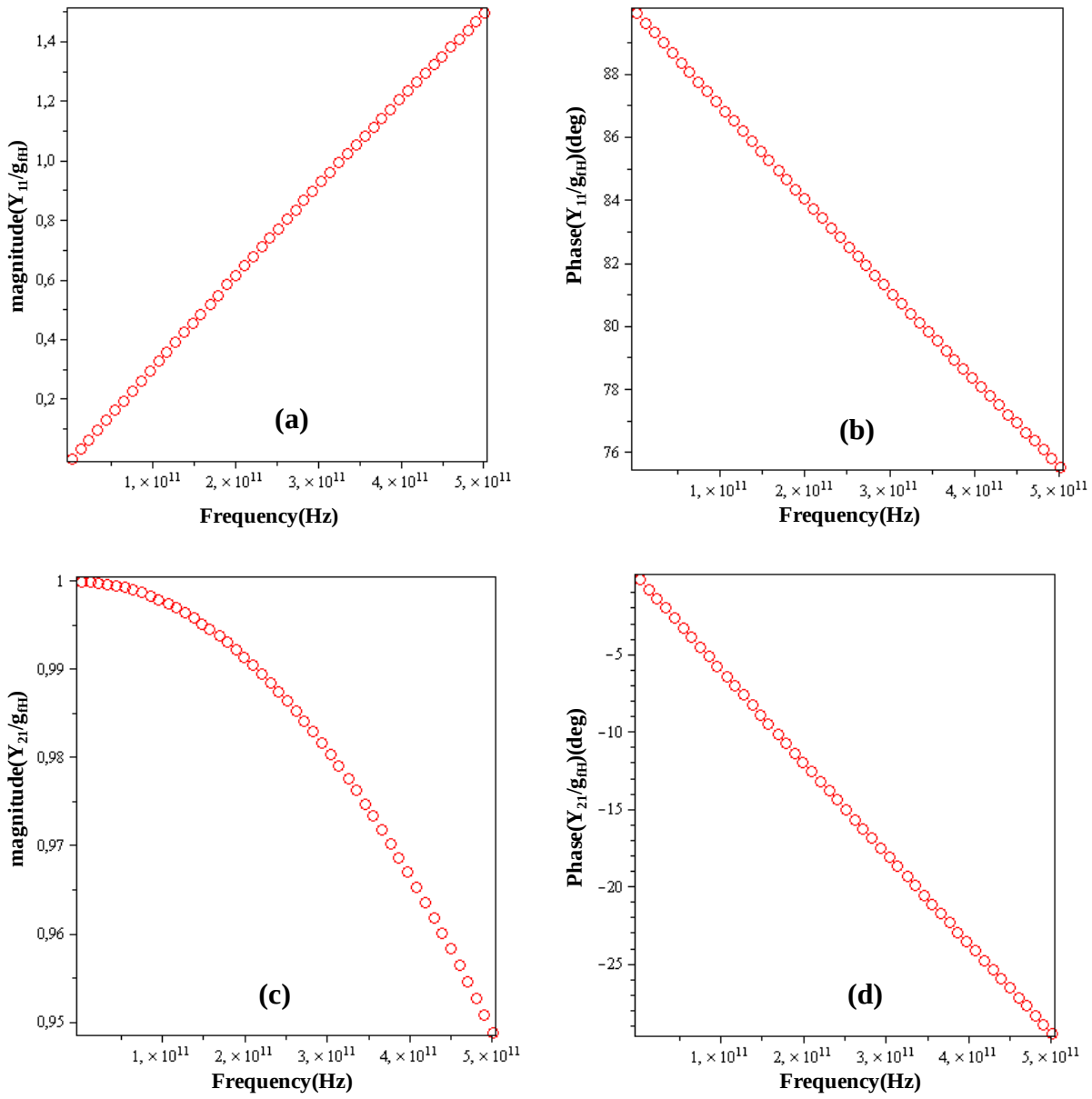

Figure **1.11** : Calculated magnitude and phase of small signal Y parameters at High Injection.

At high injection base drift factor does not affect the dynamic parameters as shown in Figure **1.11**. Comparing Figure **1.10** and Figure **1.11**, it can be said that small drift factor basically represents the HI condition where the LI condition can be represented by large drift field (η) values.

These equations of small signal Y parameters are compared with [6] and found to be the same.

The CB y parameters can be approximated in terms of polynomials of complex variable [6] [14] where different time constants are taken into account,

$$y_{11}^{b} = g_f \frac{1+s\tau_{N1}+(s\tau_{N2})^2+....}{1+s\tau_{D1}+(s\tau_{D2})^2+....} \qquad \textbf{1.46}$$

$$y_{21}^{b} = -g_f \frac{1}{1+s\tau_{D1}+(s\tau_{D2})^2+....}$$

Where g_f denotes the low frequency forward conductance, s is the complex variable and τ_{n1}, τ_{D1} are characteristic time constants. The common emitter Y parameters are given by

$$y_{21}^{e} = -y_{21}^{b} = g_f \frac{1}{1+s\tau_{D1}+(s\tau_{D2})^2+....} \qquad \textbf{1.47}$$

$$y_{11}^{e} = y_{11}^{b} + y_{21}^{b} = sg_f\tau_{N1} \frac{1+s\tau_{N2}^2/\tau_{N1}+....}{1+s\tau_{D1}+(s\tau_{D2})^2+....}$$

With suitable approximation to the general equations (**1.46**) all the previously described models in the literature can be obtained [6].

1.5 Analysis of different NQS models

Within the last decade, much interest had been devoted, to develop small signal AC and large signal transient models for bipolar transistors. The quasi static capacitance based models such as Gummel-Poon model [15] became more and more inadequate in high frequencies or under fast transient condition. A widely used method was the partitioned charge based (PCB) modeling concept which basically separated the quasi neutral base charge into emitter and collector terminals. The most popular PCB models are named after Klose and Wieder [16] and Hummel and Selvakumara [4]. Both these models deal with LI condition and calculate differently α11, the Charge Partitioning Factor (CPF). An analytical solution of LI minority carrier transport equations in the Laplace domain was given by Wu and Lindholm [17] which includes heavy doping effect and also extended upto arbitrary level of injection. The model of Seitchik [5] uses Thomas- Moll equation and exponential base doping to calculate different

time constants at LI level of operation. Rinaldi [6] [14] clearly compared all the models by developing a closed form solution of transport equations in arbitrary level of injection. The basic differences between the theoretical NQS models are shown in Table **1.1**.

Model Name	Model Type	Doping	Injection	Comments
QS model [6]	Charge Control (CC)	Constant	LI	Initial model not including time delay.
Winkel [2]	CC	Arbitrary	LI	Introduces two delay times
Klose Wieder [16]	TICCR (PCB)	Exp	LI	Calculated CPF
Hamel [4]	GTCCR (PCB)	Exp	LI	Calculate CPF α11
Wu [17]	CC	Arbitrary	LI	Calculated base transit time and delay times.
Rinaldi [6] [14]	Small signal	Exp	LI+HI	Compare all the models to provide a close form solution.

Table **1.1**: Comparison between different NQS models available in the literature.

It is a bit difficult task to compare all the previously established models because all the models use different time constants to establish admittance equation [18].

In this section different models will be analyzed and compared with the general equation that has been established previously (Equation **1.46)**.

- **Quasi Static (QS) model:**

It is the simplest model following charge control concept and does not include the base delay time inside calculation. The basic Y parameter calculation is very simple (equations **1.6**). It can be reproduced from the general equation (**1.46**) [6] while considering only the first order term in the numerator and neglecting all the frequency dependent terms in the denominator.

$$y_{11}^{b} \approx g_f(1+i\omega\tau_{N1}) \qquad \textbf{1.48}$$

$$y_{21}^{b} \approx -g_f$$

The characteristic time can be identified as the differential forward base transit time τ_f.

- **Charge partitioning model:**

The essence of charge partitioning concept relied on the fact that for a narrow diode operation only the two third of the stored charge was provided when the diode turned on applying a step voltage [10]. This idea was extended to the transistor and the ratio of the stored charge flowing to the emitter terminal to that flowing to the collector terminal was calculated to be 2:1 [1].

In the classical charge control approach the total stored charge at the quasi neutral base region was obtained while integrating the excess carrier concentration over the whole base width (W_B). If however the same integration is down in two steps i.e. first integrating up to an arbitrary distance x and then up to the base width, the reclaimable charge shows a pure partition over transistor terminals. Diffusion capacitances are then calculated considering different partitioning functions [3] [16] [4]

Taking only the first order term from the general expression (equation **1.46**), one obtain [6]

$$y_{11}^{b} \approx g_f \frac{1+i\omega\tau_{N1}}{1+i\omega\tau_{D1}} \approx g_f(1+i\omega(\tau_{N1}-\tau_{D1})) = g_f(1+i\omega\alpha_{11}\tau_f) \qquad \textbf{1.49}$$

$$y_{21}^{b} \approx -g_f \frac{1}{1+i\omega\tau_{D1}} \approx -g_f(1-i\omega\tau_{D1}) = -g_f(1-i\omega\alpha_{21}\tau_f)$$

The quantities α_{11} and α_{21} are defined as the charge partitioning factors as,

$$\alpha_{11} = (\tau_{N1}-\tau_{D1})/\tau_{N1}$$
$$\alpha_{21} = \tau_{D1}/\tau_{N1}$$

These factors describe the charge sharing at emitter and collector terminals while keeping

$$\alpha_{11}+\alpha_{21}=1$$

- **Wu-Lindholm model:**

In this model the basic drift diffusion equations were solved applying Laplace transform method considering LI level and heavy doping effects. The model can be applied inside the quasi neutral base as well as in the emitter part of the transistor [17]

Taking Laplace transform to the both sides, basic drift diffusion equations can be written,

$$\left[s + \frac{1}{\tau_n(x)} \right] L\{n(x,t)\} = \frac{1}{q} \frac{d}{dx} L\{j_n(x,t)\} \qquad \textbf{1.50}$$

$$L\{j_n(x,t)\} = qD_n \left[L\{n(x,t)\} \frac{d}{dx} (\ln N_A) + \frac{d}{dx} L\{n(x,t)\} \right]$$

A set of iterative analytical equations can be constructed using the basic equations.

$$L\{n'(x,t)\} = n_0(x) \left[1 + \frac{1}{q} \int_0^x \frac{L\{j'_n(x_1,t)\}}{D_n(x_1) n_0(x_1)} dx_1 \right] \qquad \textbf{1.51}$$

$$L\{j'_n(x,t)\} = L\{j'_n(0,t)\} + q \int_0^x \lambda^2(x_1,s).D_n(x_1).L\{n'(x_1,t)\} dx_1$$

The analytical series solution coming from equations (**1.51**) is

$$L\{n'(x,t)\} = n_0(x) \left[1 + L\{j'_n(0,t)\}. \sum_{i=1}^{\infty} A_{2i-1}(x,s). \frac{1}{q} + \sum_{i=1}^{\infty} B_{2i}(x,s) \right] \qquad \textbf{1.52}$$

Changing the integration limit to W_B instead of x and truncating the matrix elements, y parameters were constructed which can be achieved from the general equation (**1.46**) considering the first order terms only.

$$y_{11}^b \approx g_f \frac{1 + i\omega\tau_{N1}}{1 + i\omega\tau_{D1}} \qquad \textbf{1.53}$$

$$y_{21}^b \approx -g_f \frac{1}{1 + i\omega\tau_{D1}}$$

- **Seitchik model:**

Seitchik model is basically developed from the Thomas Moll model. This model [5] includes three parameters to describe the ac response of the quasi neutral base region. This small signal model can be achieved when including the second order term in the expression of y parameter (equation **1.45**) [6],

$$y_{11}^{e} = g_f \frac{i\omega\tau_f}{1+i\omega\tau_2} \qquad \textbf{1.54}$$

$$y_{21}^{e} = g_f \frac{\exp(-i\omega\tau_1)}{1+i\omega\tau_2}$$

Where, the exponential term accounts for the excess phase shift. Comparing the Taylor series expansion of y_{21}^{e} and keeping in mind the charge partitioning model, one gets [**6**]

$$\tau_1 + \tau_2 = \tau_{D1} = \alpha_{21}\tau_f \qquad \textbf{1.55}$$

This relation is also noted by Hamel [19] who approximated,

$$\tau_1 \approx \tau_2 \approx \tau_{D1}/2 \qquad \textbf{1.56}$$

From this analysis it is clear that the time constants in the Seitchik model is not only function of the first order term, but the second order term also.

Small signal gain is modelled by,

$$\beta = \beta_0 \frac{\exp(-i\omega\tau_1)}{1+i\omega\tau_f\beta_0} \qquad \textbf{1.57}$$

- **Winkel model:**

This model is analysed in the previous section in details. Equation **1.9** presents the set of necessary small signal parameters. To compare it with the general formulation (equation **1.46**), model equation coming from Winkel's analysis are,

$$y_{11}^{e} \approx g_f i\omega\tau_f \exp(-i\omega\tau_2) \qquad \textbf{1.58}$$

$$y_{21}^{e} \approx g_f \exp(-i\omega(\tau_1+\tau_2))$$

$$\beta = \beta_0 \frac{\exp(-i\omega\tau_1)}{1+i\omega\tau_f\beta_0}$$

Comparing Winkel's model with Seitchik model, it is obvious that both the model uses similar kind of formulation for the current gain and admittance parameters. The accuracy,

therefore, should be the same for these models. To compare, phase of Y_{21} parameter is plotted following Winkel and Seitchik formulations (Figure **1.12**)

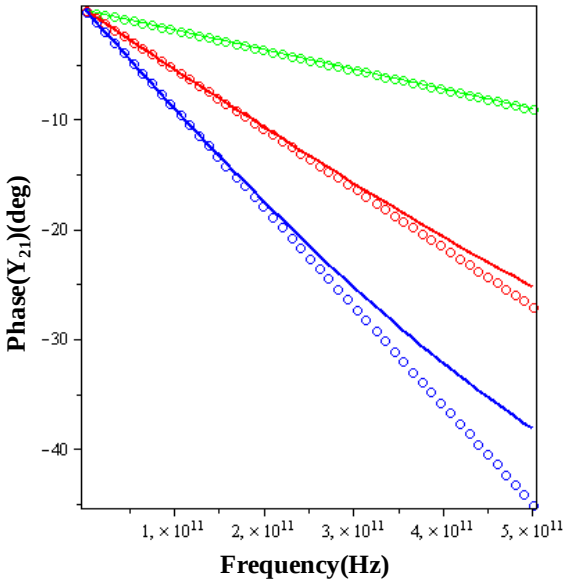

Figure **1.12** : phase of Y_{21} with different models- Winkel (in symbol), Seitchik (in line). Three different curves correspond to different values of fitting parameter alit (alit= 0.1, 0.3, 0.5) which relates delay time to the total transit time (τ_f).

Phase of Y_{21} is almost the same for these two models. It also established that Seitchik and Winkel's model are the best available formulation for high frequency operation. In practice, there is a possibility of covering NQS behaviour due to the parasitic resistances and capacitances in modern devices. However, for a practical application, simpler models like Wu-Lindholm and Hummel also provide considerable accuracy in NQS modelling.

1.6 Transit time calculation for small signal analysis

When we consider transistors at high frequency operation, there are some parameters that effect high speed transistor operations. Some of these frequency limitations are junction capacitances, the charging time associated with the capacitance and the transit time of carrier.

The total transit time can be written as a summation of transit time coming from the different parts of the structure [7]

$$\tau_f = \tau_E + \tau_{BED} + \tau_B + \tau_{BCD} + \tau_C \quad \textbf{1.59}$$

Total transit time is mainly due to the base transit time and it is well known for a drift diffusion transistor (equations **1.19**).

In the following section we will try to develop analytic expression for τ_{BCD} (BC junction transit time) and τ_E (emitter transit time) for the small signal application.

1.6.1 Base collector junction transit time

To achieve high speed performance it is essential to downscale vertical dimensions to reduce the overall delay [20]. As in the modern HBT transistor deals with graded base profile, the built in electric field reduces the base transit time significantly. As a consequence of this process, the signal delay in the BC junction has become an important factor for the total delay and hence included inside the model [21]

Base collector junction is considered as high field region where carrier travels at a constant velocity which is the saturation velocity inside this region. We assume that the excess minority carrier concentration at the base collector junction boundary is zero and no recombination takes place inside the junction. For a junction of thickness x_{bc} and carrier saturation velocity v_{sat}, the displacement current inside this junction is assumed to be [22]

$$\tilde{i}_{cc} = \frac{qv_{sat}}{x_{bc}} = \frac{q}{\tau} \quad \textbf{1.60}$$

Assuming that the transfer current encounters an exponential delay when travelling base collector junction, we calculate the current by multiplying the transfer current ($\tilde{i}_c(x)$) over the current function ($\tilde{i}_{cc}$) and integrating it over time.

$$\tilde{i}_c'(x) = \int_0^{\tau} \tilde{i}_c(x).\frac{\tilde{i}_{cc}}{q} e^{j\omega t'}.dt' \quad \textbf{1.61}$$

Integration gives the result,

$$\tilde{i}_c'(x) = \tilde{i}_c(x).\phi_c = \tilde{i}_c(x).\frac{\sin(\omega\tau_c)}{\omega\tau_c}.e^{-j\omega\tau_c} \qquad \textbf{1.62}$$

Where, the function ϕ_c represents the BC junction delay and collector transit time (τ_c) is assumed to be [23]

$$\tau_c = \frac{x_{bc}}{2v_{sat}}$$

The magnitude of $\frac{\tilde{i}_c'(x)}{\tilde{i}_c(x)}$, equals to $\frac{\sin(\omega\tau_c)}{\omega\tau_c}$, is nearly unity even at high frequencies. So the small signal transfer current only encounters an exponential delay without changing the current magnitude while passing the base collector junction. In the next figure (Figure **1.13**) the magnitude and phase variation of the function ϕ_c is shown

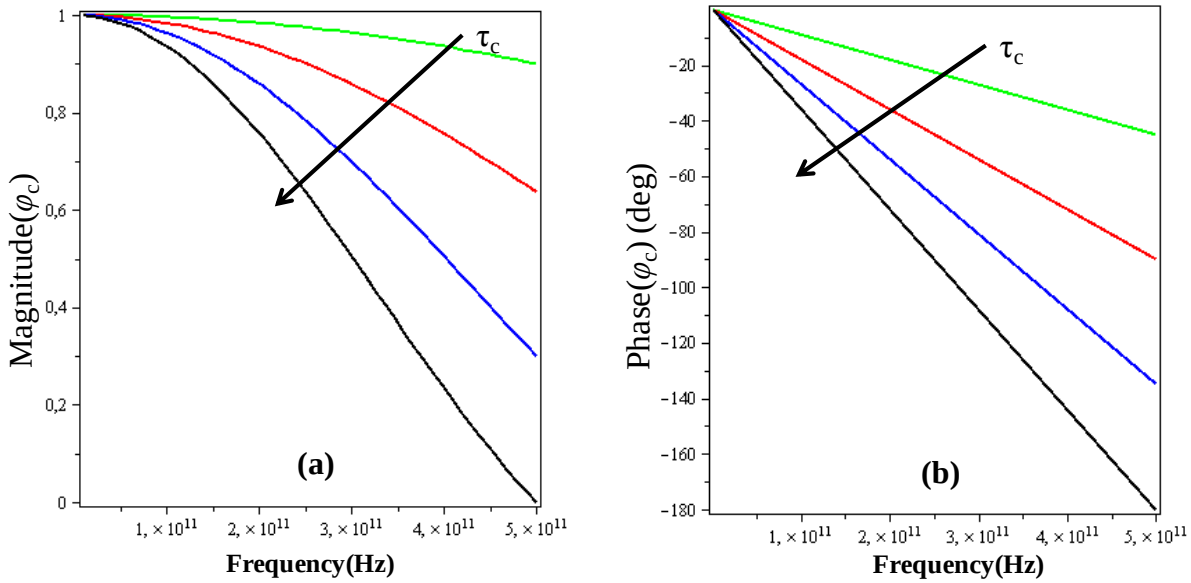

Figure **1.13** : Magnitude and phase variation of BC junction delay function for different collector transit times (τ_c =0.25ps, 0.5ps, 0.75ps, 1ps).

The results for BC junction delay will be used afterwards to model the excess phase shift of Y_{21} parameter at higher frequencies. This delay term $\frac{\sin(\omega\tau_c)}{\omega\tau_c}.e^{j\omega\tau_c}$ had also been added inside the general formulation of Y parameters as shown in [21].

1.6.2 Emitter transit time

In modern technology, heavily doped polysilicon is used inside the emitter [13]. This predominantly increases the emitter transit time (τ_E) and sometimes comparable to the base transit time (τ_B) [24]. As a consequence partitioned charge based models predict wrong results when applied to the emitter region as all the models assume negligible recombination inside the calculation. Our approach is to investigate τ_E for small signal operation considering a simple structure and applying almost the same procedure that has been presented while calculating the base dynamics for a drift transistor.

Small signal analysis has been carried out inside the quasi neutral emitter region considering constant doping profile at the emitter. Next Figure **1.14** : shows the diagrammatic representation of the transistor under consideration.

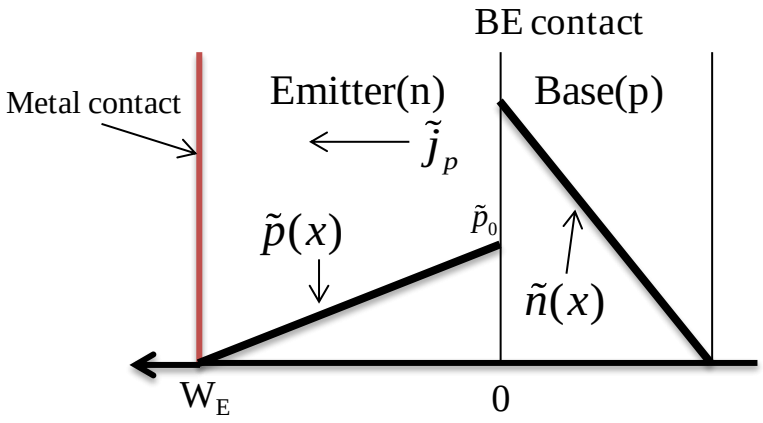

Figure **1.14 :** Small signal excess carrier concentration inside base and emitter.

Rewriting drift-diffusion equations for a n type emitter region and considering recombination inside the continuity equation, we obtain,

$$j_P = q\mu_{pE} n\varepsilon - qD_{pE}\frac{\partial p}{\partial x} \qquad \textbf{1.63}$$

$$j_N = q\mu_{nE} p\varepsilon + qD_{nE}\frac{\partial n}{\partial x}$$

$$-\frac{1}{q}\frac{\partial j_P}{\partial x} = \frac{\partial p}{\partial t} + \frac{p}{\tau_p}$$

Where τ_p stands for the hole recombination lifetime insider the emitter.

Assuming an ac perturbation over the DC bias variation all the electrical parameters can be expressed a summation of a DC and a time varying part. Expressing total minority carrier concentration as,

$$p(x,t) = P(x) + \tilde{p}(x)e^{j\omega t} \qquad \textbf{1.64}$$

Assuming the emitter doping profile is constant, equations 1.63 can be combined for low level of injection condition ($n \approx N_D$). The resulting second order equation for small signal bias variation becomes,

$$\frac{d^2\tilde{p}}{dx^2} - \frac{1}{\tilde{L}_p^2}\tilde{p} = 0 \qquad \textbf{1.65}$$

Where the effective diffusion length ($\tilde{L}_p$) is given by,

$$\frac{1}{\tilde{L}_p^2} = \frac{1}{L_p^2}(1 + j\omega\tau_p) \qquad \textbf{1.66}$$

Equation **(1.65)** is a second order homogeneous differential equation which can be solved easily with the help of boundary conditions i.e. at x=0, $\tilde{p} = \tilde{p}_0$ and at x=W_E, $\tilde{p} = 0$

The solution of equation (**1.65**) is

$$\tilde{p}(x) = \tilde{p}_0 \frac{\sinh\{u_x\Omega\}}{\sinh(\Omega)} \qquad \textbf{1.67}$$

Where, the terms are presented as,

$$\Omega = \frac{W_E}{\tilde{L}_p} = \frac{W_E}{L_p}(1 + j\omega\tau_p)^{1/2} \qquad \textbf{1.68}$$

$$u_x = 1 - \frac{x}{W_E}$$

$$\tilde{p}_0 = \frac{n_i^2}{N_D}\exp\left(\frac{V_{BE}}{V_T}\right)\frac{\tilde{v}}{V_T}$$

After differentiating $\tilde{p}(x)$, excess hole current density (equation **1.67**) at both ends of the quasi neutral emitter becomes,

$$\tilde{j}_p\Big|_{x=0} = qD_p\tilde{p}_0\tilde{L}_p \coth(\frac{W_E}{\tilde{L}_p}) \qquad \textbf{1.69}$$

$$\tilde{j}_p\Big|_{x=W_E} = qD_p\tilde{p}_0\tilde{L}_p \operatorname{csc} h(\frac{W_E}{\tilde{L}_p})$$

As the hole diffusion length (L_p) inside the emitter is much greater than the emitter length (W_E) we can approximate

$$\frac{W_E}{L_p} = \left\{\left(\frac{W_E}{L_p}\right)^2 + \frac{j\omega {W_E}^2}{D_p}\right\}^{1/2} \approx \left(\frac{j\omega}{D_p}\right)^{1/2} W_E = \frac{W_E}{L_p'}$$

The quantity $\frac{W_E}{\tilde{L}_p'}$ can also be represented as $\frac{W_E}{\tilde{L}_p'} = \left(\frac{j\omega}{D_p}\right)^{1/2} W_E = \left(\frac{j\omega}{\omega_0}\right)^{1/2}$

The total small signal charge is obtained by integrating equation (**1.67**) which is given by,

$$\tilde{Q}_{ac} = qA_E\tilde{p}_0\tilde{L}_p \tanh(\frac{W_E}{2\tilde{L}_p}) \qquad \textbf{1.70}$$

Emitter transit time for small signal operation is obtained dividing diffusion capacitance (C_D) by the transconductance (g_m).

Base emitter diffusion capacitance for the small signal operation is defined as,

$$C_D = \frac{d\tilde{Q}_{ac}}{d\tilde{v}} = \frac{qA_E n_i^2}{N_D V_T}\tilde{L}_p \tanh(\frac{W_E}{2\tilde{L}_p'})\exp(\frac{V_{BE}}{V_T}) \qquad \textbf{1.71}$$

Transconductance is also calculated from the current density,

$$g_m = \frac{A_E\ \tilde{j}_n\big|_{x=0}}{\tilde{v}} = \frac{A_E \beta\ \tilde{j}_p\big|_{x=0}}{\tilde{v}} = \frac{qA_E n_i^{\ 2} D_p}{N_D V_T \tilde{L}_p} \beta \coth(\frac{W_E}{\tilde{L}_p}) \exp(\frac{V_{BE}}{V_T}) \qquad \textbf{1.72}$$

And the emitter transit time for the small signal operation is given by,

$$\tilde{\tau}_e = \frac{C_D}{g_m} = \frac{\tilde{L}_p^{\ 2}}{\beta D_p} \tanh(\frac{W_E}{2\tilde{L}_p}) \tanh(\frac{W_E}{\tilde{L}_p}) \qquad \textbf{1.73}$$

Similarly the calculated transit time due to the DC bias variation reads,

$$\tau_e = \frac{L_p^{\ 2}}{\beta D_p} \tanh(\frac{W_E}{2L_p}) \tanh(\frac{W_E}{L_p}) \qquad \textbf{1.74}$$

At the limit of where $\omega \to 0$ and $W_E << Lp$ equation (**1.73**) and (**1.74**) reduces to the well-known equation for emitter transit time,

$$\tau_e \approx \frac{1}{\beta}\left[\frac{W_E^{\ 2}}{2D_p}\right] \qquad \textbf{1.75}$$

In this section, an attempt has been made to investigate the frequency dependence of emitter transit time when the system is exited with a small signal perturbation. Although, the calculation is fairly simple, the small signal emitter transit time (equation **1.73**) shows frequency dependence. A more detailed investigation in this subject is necessary to conclude the effect of emitter transit time in the total time delay.

1.7 Conclusion

In this chapter, the physical approach towards the high frequency dynamic parameter calculation is presented. Both the charge control concept and small signal calculations are examined in this part. Dynamic parameters (transconductance and input admittance) are calculated from the small signal analysis and compared with the popular models present in the literature.

For all the calculation of bias dependent time delay, it has been assumed that the delay time is proportional to the total transit time. The contribution in total transit time of a modern bipolar transistor comes from different transistor parts. In this chapter, base collector (BC) junction transit time and neutral emitter transit time are calculated for small signal operation and said to be an important part of the total time delay. Consequently, the results obtained from the BC junction delay will be used after to suggest a new phase shift network in the HICUM model.

Reference

[1] Suzuki, K.; Satoh, S.; Nakayama, N.; Fujitsu Labs. Ltd., Atsugi, "Transient analysis of stored charge in neutral base region," *Electron Devices, IEEE Transactions on*, May 1992, vol. 39, pp. 1164 - 1169.

[2] te Winkel, J., "Extended charge-control model for bipolar transistors," *Electron Devices, IEEE Transactions on*, April 1973, vol. 20, pp. 389 - 394.

[3] Fossum, J.G.; Veeraraghavan, S., "Partitioned-charge-based modeling of bipolar transistors for non-quasi-static circuit simulation," *Electron Device Letters, IEEE*, 1986, vol. 7, pp. 652 - 654.

[4] Hamel, J.S. Selvakumar, C.R., "The general transient charge control relation: a new charge control relation for semiconductor devices," *Electron Devices, IEEE Transactions on*, 1991, vol. 38, pp. 1467 - 1476.

[5] Seitchik, J.A. Chatterjee, A. Yang, P., "An accurate bipolar model for large signal transient and ac applications," *Electron Devices Meeting, 1987 International*, vol. 33, pp. 244 - 247.

[6] Rinaldi, N.F., "Modeling of small-signal minority-carrier transport in bipolar devices at arbitrary injection levels," *Electron Devices, IEEE Transactions on*, 1998, vol. 45, pp. 1501 - 1510.

[7] Streetman, Banerjee, *Solid State Electronic Devices*, Prentice Hall, .

[8] Ebers, J.J. Moll, J.L., "Large-Signal Behavior of Junction Transistors," *Proceedings of the IRE*, vol. 42, pp. 1761 - 1772.

[9] "HICUM Documentation."

[10] Lindmayer; Wrigley, *FUNDAMENTALS OF SEMICONDUCTOR DEVICES*, D. Van Nostrand Company (1965), .

[11] H. C. De Graaff, F. M. Klaassen, *Compact Transistor Modelling for Circuit Design (Computational Microelectronics)*, Springer-Verlag, .

[12] Jacob, J. DasGupta, A. Schroter, M. Chakravorty, A. Dept. of Electr. Eng., Indian Inst. of Technol. Madras, Chennai, India, "Modeling Nonquasi-Static Effects in SiGe HBTs," July. 2010.

[13] Wu, B.S.; Lindholm, F.A., "Non-quasi-static models including all injection levels and DC, AC, and transient emitter crowding in bipolar transistors," *Electron Devices, IEEE Transactions on*, 1989, vol. 38, pp. 167 - 177.

[14] Rinaldi, N.F., "Non-quasi-static modeling of bipolar transistors for CAD applications,"

Microelectronics, 1997. Proceedings., 1997 21st International Conference on, pp. 261 - 264 vol.1.

[15] H. K. Gummel and H. C. Poon, "An integral charge control model of bipolar transistors," *Bell Syst. Tech. J,* vol. 49, pp. 827–852.

[16] Klose, H.; Wieder, A.W, "The transient integral charge control relation—A novel formulation of the currents in a bipolar transistor," *Electron Devices, IEEE Transactions on*, 1987, vol. 34, pp. 1090 - 1099.

[17] Wu, B.S.; Lindholm, F.A., "One-dimensional non-quasi-static models for arbitrarily and heavily doped quasi-neutral layers in bipolar transistors," *Electron Devices, IEEE Transactions on*, 1989, vol. 36.

[18] Rinaldi, N.F., "Reply to comments on "Modeling of small-signal minority-carrier transport in bipolar devices at arbitrary injection levels"," *Electron Devices, IEEE Transactions on*, 2002, vol. 49, pp. 2371 - 2373.

[19] Hamel, J.S., "An accurate charge control approach for modeling excess phase shift in the base region of bipolar transistors," *Electron Devices, IEEE Transactions on*, 1996, vol. 43, pp. 1092 - 1098.

[20] A. van der Ziel1 and T.G.M. Kleinpenning2, "High-frequency response of microwave transistors," *Solid-State Electronics*, vol. 30, pp. 771-772.

[21] Rinaldi, N.F., "Modelling of collector signal delay effects in bipolar transistors," *Solid-State Electronics*, 1998, vol. 43, pp. 359-365.

[22] Liu, *Fundamentals of III-V Devices: HBTs, MESFETs, and HFETs/HEMTs*, Wiley-Interscience.

[23] Meyer, R.G. Muller, R.S, "Charge-control analysis of the collector-base space-charge-region contribution to bipolar-transistor time constant τT," *Electron Devices, IEEE Transactions on*, vol. 34, pp. 450 - 452.

[24] Hamel, J.S., "Compact modeling of the influence of emitter stored charge on the high frequency small signal AC response of bipolar transistors using quasi-static parameters," *Solid-State Circuits, IEEE Journal of*, 1996, vol. 31, pp. 106 - 113.

Chapter 2

[TCAD SIMULATION AND DEVICE PHYSICS]

2.1 Introduction

Communication and information system frequently undergoes rapid and sophisticated changes. Nowadays, Heterojunction Bipolar Transistor (HBT) and High Electron Mobility Transistor (HEMT) serve mostly as the building blocks of the communication system [1]. The advancement of downscaling of Si heterostructure devices have improved the circuit performance and also reduced the cost per function. Another intelligent way that reduced the time and cost of technology development was the vast use of Technology Computer Aided Design (TCAD). TCAD is used in the fabrication of process design, semiconductor device design, technology characterization of circuit design and also in the computer integrated manufacturing [2] [1]. It is not only useful to predict the device behavior or the product cost, but also significantly reduces the product cycle time. Next Figure **2.1** points the relationship between TCAD, process development and circuit implementation [1].

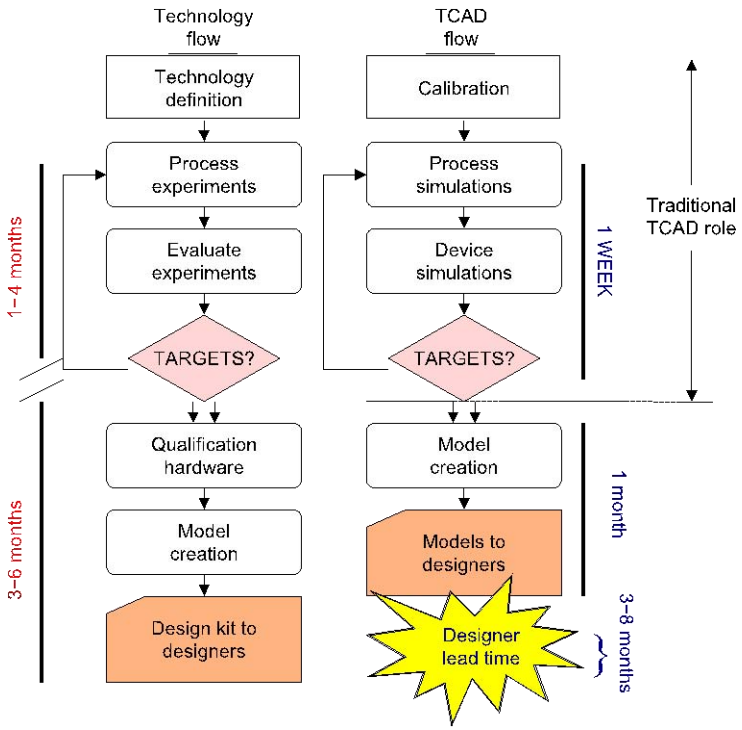

Figure **2.1:** product cycle for technology development [1]

Maintaining the TCAD flow the initial step was to virtually fabricate the transistor structure by applying step by step process simulation. Generation and orientation of suitable mesh is a valuable point of consideration at that step. Once the process simulation is completed the device is simulated using the known physical models to calibrate the structure i.e. to obtain the similar result as from measurements. In this chapter we shall mainly focus on the various physical models necessary for device simulation [3].

2.2 Process simulation

The main goal of process simulation is to model a virtual device with geometry and properties identical to the real structure. Sentaurus TCAD process [4] is an advanced, complete, and highly flexible multi-dimensional process simulator for developing and optimizing silicon and compound semiconductor process technologies. It offers unique predictive capabilities for modern silicon and non-silicon technologies, which is calibrated to a wide range of the latest experimental data using proven calibration methodology. It is powerful numerical algorithms simulate process steps like implantation, diffusion and dopant activation, etching, deposition, oxidation, and epitaxial growth in different semiconductor material with efficient meshing for robust and stable calculation. The fabrication of integrated circuit devices requires a series of processing steps called a process flow. A process flow is simulated by issuing a sequence of commands that corresponds to the individual process steps. In addition to a several control commands allows selecting physical models and parameters, grid strategies, and graphical output preferences. Also process conditions like the ambient chemical composition, temperature, pressure, etc. during individual fabrication steps can be controlled. The final output is a 2D or 3D device structure which can be used for device simulation. The major processing steps involved in the manufacturing of integrated circuit devices are shown in Figure **2.2** . Each of these steps containing numerous possible variations in process controls, and may take several weeks to complete [5]

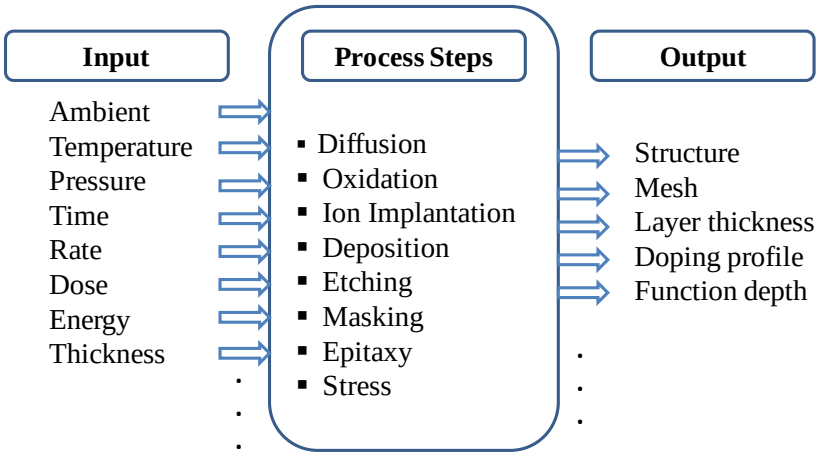

Figure **2.2:** Major process steps involved in the manufacturing of integrated circuit devices [2]

2.3 Device simulation (physical model)

Device simulation is important part in TCAD simulation because it gives insights into complex phenomena that cannot be obtained separately through experimentation. Many of these phenomena involved in semiconductor can be described by partial differential equations (PDEs): as a result, much of the TCAD software is based on the solution of PDEs [2] [6]. To solve the PDEs approximate methods like finite element or the finite difference methods are used by the simulator.

The main governing models of semiconductor devices are discussed below,

2.3.1 Transport equation

- **Poisson and continuity equation**

Poisson equation is one of the three governing equations in the semiconductor device physics [7]. In mathematics Poisson equation, a partial differential equation with vast application in electrostatics, theoretical physics and mechanical engineering, is named after the French mathematician Poisson [8].

Assuming $\vec{E}_m$ is the electric field in a medium where the permittivity is ε_m, Poisson equations relates the electric field and charge density ρ as,

$$\nabla.\overrightarrow{E_m} = \frac{\rho}{\varepsilon_m} \qquad \textbf{2.1}$$

Electric field vector can be represented as gradient of potential function. As vector calculus predicts that curl of $\vec{E}$ is zero, Poisson equation can be written as a function of electrostatic potential,

$$\nabla.(\nabla\phi) = \nabla^2\phi = -\frac{\rho}{\varepsilon_m} \qquad \textbf{2.2}$$

In device simulation, charge density is the summation of total ionized and mobile charge and total trap charge,

$$\rho = q(p - n + N_D - N_A) + \rho_{trap} \qquad \textbf{2.3}$$

So the Poisson equation becomes,

$$\nabla^2\phi = -\frac{q}{\varepsilon_m}(p - n + N_D - N_A) - \rho_{trap} \qquad \textbf{2.4}$$

Including the total recombination, charge continuity equation reads,

$$\nabla.\vec{J}_N = q\frac{\partial n(x,t)}{\partial t} + qR_{net} \qquad \textbf{2.5}$$

$$-\nabla.\vec{J}_P = q\frac{\partial p(x,t)}{\partial t} + qR_{net}$$

Where R_{net} is the total electron hole recombination rate and $\vec{J}_N$, $\vec{J}_P$ are electron and hole current density respectively.

- **Drift diffusion model**

The drift diffusion model can be derived from the Boltzmann transport equation [9] by applying the basic principle of irreversible thermodynamics [10]. This model uses Poisson and continuity equation in addition to the current density caused by the drift field of immobile ionized charge.

$$\vec{J}_N = nq\mu_n \vec{E}_n = -nq\mu_n \nabla \phi_n \qquad \textbf{2.6}$$

$$\vec{J}_P = pq\mu_p \vec{E}_p = -pq\mu_p \nabla \phi_p$$

Where μ_n and μ_p are electron and hole nobilities, and ϕ_n, ϕ_p are electron and hole quasi Fermi potentials. Quasi Fermi potential helps to calculate electron and hole concentration inside an intrinsic or a compound semiconductor. Electron and hole concentration can be written as, [2]

$$n = n_i \exp\left(\frac{\varphi - \phi_n}{V_T}\right) \qquad \textbf{2.7}$$

$$p = n_i \exp\left(\frac{\phi_p - \varphi}{V_T}\right)$$

Here, n_i is the effective intrinsic density. φ, the potential which is above the quasi Fermi level for n type and below the quasi Fermi level for the p type semiconductor. This potential is calculated from the reference potential which is set equal to Fermi potential for intrinsic semiconductor like Si [10]

Combining equation **2.6** and **2.7** we arrive to the basic drift diffusion equations [2]

$$\vec{J}_N = q\mu_n n \vec{E}_{ntot} + qD_n \nabla n \qquad \textbf{2.8}$$

$$\vec{J}_P = q\mu_p p \vec{E}_{ptot} + qD_p \nabla p$$

Where $\vec{E}_{ntot}$ the total electric field is represented by,

$$\vec{E}_{ntot} = -\left(\nabla\phi + V_T \ln n_i\right) \qquad \textbf{2.9}$$

$$\vec{E}_{ptot} = -\left(\nabla\phi - V_T \ln n_i\right)$$

Equations **2.8** represent current magnitude as well as the direction which indicates a steady flow of carrier in the direction of concentration gradient. Overall, drift diffusion model is a simple model which assumes full impurity ionization and non degenerate statistics. It cannot encounter the non local effects since the electron gas is assumed to be in thermal equilibrium with the lattice temperature [7]. Drift diffusion model can be extended to thermodynamic model just by including lattice heat flow equation (temperature gradient) inside the formulation. Assuming a lattice is in thermal equilibrium with the carrier at temperature T, the thermodynamic model reads,[7]

$$\vec{J}_N = -nq\mu_n\left(\nabla\phi_n + P_n\nabla T\right) \qquad \textbf{2.10}$$

$$\vec{J}_P = -pq\mu_p\left(\nabla\phi_p + P_p\nabla T\right)$$

Where P_n and P_p are the absolute thermoelectric power.

- **Hydrodynamic model**

The downscaling of modern semiconductor devices assisted to achieve high speed transistors. Meanwhile non local effects which are neglected in the drift diffusion model are prominent in these sophisticated transistors. Both the internal and external device characteristics are found to be incorrect as it cannot predict the velocity overshoot in III-V semiconductors [7]. In hydrodynamic transport model carrier temperature is considered different from the lattice temperature. In general hydrodynamic model contains Poisson and continuity equation and energy conservation equation for electron, hole and lattice.

$$\vec{J}_N = -q\mu_n\left(n\nabla E_C + KT_n\nabla n + f_n^{td}Kn\nabla T_n - 1.5nKT_n\nabla \ln m_n\right) \quad \textbf{2.11}$$

$$\vec{J}_P = q\mu_p\left(p\nabla E_V - KT_p\nabla p - f_n^{td}Kp\nabla T_p - 1.5pKT_p\nabla \ln m_p\right)$$

The first term takes into account the contribution due to the spatial variations of electrostatic potential, electron affinity, and the band gap [7]. The three remaining terms in take into account the contribution due to the gradient of concentration, the carrier temperature gradients, and the spatial variation of the effective masses m_n and m_p.

2.3.2 Band structure

Band structure plays the most important role in device simulation [10]. Realistic band structure is rather complex and hence are fully applied only inside the Monte Carlo simulation. For the general use the effective mass for the electrons and holes and effective density of states in intrinsic and compound semiconductors are mainly analyzed.

- **Intrinsic density**

For an intrinsic semiconductor the intrinsic carrier density can be represented as a function of band gap energy [7]

$$n_i(T) = \sqrt{N_C(T)N_V(T)}\exp(\frac{-E_g}{2KT}) \quad \textbf{2.12}$$

Where N_C and N_V represent the density of states at conduction and valence band respectively.

For a doped semiconductor, intrinsic carrier density changes due to doping dependent bandgap narrowing. It can be represented by,

$$n_{i,eff}(T) = n_i\exp(\frac{E_{bng}}{2KT}) \quad \textbf{2.13}$$

- **Bandgap energy**

Various models define the temperature dependence of bandgap energy in semiconductor. For the basic semiconductor material temperature dependence of band gap is calculated as,

$$E_g = E_g(0) - \frac{\alpha_T T_L^2}{\beta_T + T_L} \quad \textbf{2.14}$$

α_T and β_T are material parameters and $E_g(0)$ is the bandgap energy at 0K. As Sentaurus device uses different bandgap models, $E_g(0)$ is assumed to be a summation of common term and a variable term (equation 2.15)

$$E_g(0) = E_{g,0} + \delta E_{g,0} \quad \textbf{2.15}$$

The effective band gap is constructed by reducing the amount of energy reduced by band gap narrowing.

$$E_{g,eff}(T) = E_g(T) - E_{gbn}(T) \quad \textbf{2.16}$$

- **Bandgap narrowing**

Band gap narrowing (BGN) is one of the most crucial heavy doping effects observed in modern semiconductors. Increased doping of the semiconductor affects the periodic property of the crystal lattice and hence band widening, band tailing and electron electron interaction occur [10]. Band gap narrowing has a great impact on transistor behavior as it changes the bandgap difference between the emitter and base. For a highly doped base region, BGN increases the emitter injection efficiency and reduces turn on voltage. In HBTs BGN effects the alignment at the base emitter heterointerface which influences the tunneling and thermionic emission current across the junction [10][7]

Sentaurus Device provides different bandgap models namely BennettWilson, delAlamo,OldSlotboom, and Slotboom (the same model with different default parameters),JainRoulston and TableBGN [7].

The model of Slotboom [11] is the most popular BGN model in Silicon [10]. This model reads,

$$\Delta E_g = E_{ref}\left[\ln\left(\frac{N_{tot}}{N_{ref}}\right)+\sqrt{\ln^2\left(\frac{N_{tot}}{N_{ref}}\right)+0.5}\right] \qquad \textbf{2.17}$$

The shift of the conduction band and valence band edges are calculated as [10]

$$\Delta E_C = \left(\frac{\Delta E_C}{\Delta E_g}\right)\Delta E_g \qquad \textbf{2.18}$$

$$\Delta E_V = \Delta E_g - \Delta E_C$$

The Slotboom model is based on experimental measurements of $\mu_n n^2$ in n-p-n transistor and $\mu_p p^2$ for p-n-p transistor with different base doping concentrations and a 1D model for the collector current.

- **Effective carrier mass and Effective density of states**

Considering parabolic conduction and valence band, density of states (DOS) can be calculated from the calculation of the effective mass [10]. The effective DOS masses scaled by electron mass represent relative carrier mass. For the direct band gap semiconductor Γ value gives the value of the relative mass. For indirect band gap semiconductor like Si, Ge, the transverse and the longitudinal mass from the X valley (L for Ge) are taken into account [10].

In Sentaurus device lattice temperature dependent electron mass is described by [7]

$$m_n = 6^{2/3}\left(m_t^2 m_l\right)^{1/3} + m_m \qquad \textbf{2.19}$$

Where the temperature dependence for Si is described by [12]

$$\frac{m_t(T)}{m_0} = a\frac{E_g(0)}{E_g(T)} \qquad \textbf{2.20}$$

Parameters are defined inside the parameter file for the device. DOS for the conduction band follows,

$$N_C(m_n, T_n) = 2.54099\times10^{19}\left(\frac{m_n}{m_0}\right)^{3/2}\left(\frac{T_n}{300K}\right)^{3/2} cm^{-3} \qquad \textbf{2.21}$$

Similarly, the relative carrier mass for the holes are represented by [7]

$$\frac{m_p(T)}{m_0} = \left(\frac{a+bT+cT^2+dT^3+eT^4}{1+fT+gT^2+hT^3+iT^4}\right)^{2/3} + m_m \qquad \textbf{2.22}$$

The effective DOS for N_V is represented by,

$$N_V(m_p, T_p) = 2.54099\times10^{19}\left(\frac{m_p}{m_0}\right)^{3/2}\left(\frac{T_p}{300K}\right)^{3/2} cm^{-3} \qquad \textbf{2.23}$$

2.3.3 Carrier mobility

Electron and hole mobility are the basic carrier transport parameter that influence the electrical behavior. It is supposed to be constant for undoped materials and decay in compound semiconductor due to high electric filed or the interaction between lattice vibration, impurity or surface. Different mobility (bulk and surface) combine following the Mathiessen's rule [7].

$$\frac{1}{\mu} = \frac{1}{\mu_{b1}} + \frac{1}{\mu_{b2}} + \cdots + \frac{1}{\mu_{s1}} + \frac{1}{\mu_{s2}} + \cdots \qquad \textbf{2.24}$$

- **Philips unified mobility model**

The Philips unified mobility model proposed by Klaassen [13] provides unified description of the majority and minority carrier bulk mobilities. In addition to describing the temperature dependence of the mobility, the model includes the effect of electron–hole scattering, screening of ionized impurities by charge carriers, and clustering of impurities. Because the carrier mobility is given as an analytical function of the donor, acceptor, electron and hole concentrations, and the temperature, this model is well suited for simulation proposes, and excellent agreement is obtained with published experimental data on Si [10].

In the Philips unified mobility model carrier mobility is considered to be composed of two parts, first part representes the phonon scattering and another part accounts for all other bulk scattering mechanisms.
The partial mobility of each carrier is given by,

$$\frac{1}{\mu_{i,b}} = \frac{1}{\mu_{i,L}} + \frac{1}{\mu_{i,DAeh}} \qquad \textbf{2.25}$$

The index i takes the value e for electron and h for holes. First part in the equation 2.25 is due to interaction with lattice vibration which is represented by,

$$\frac{1}{\mu_{i,L}} = \mu_{i,\max}\left(\frac{T}{300K}\right)^{-\theta_i} \qquad \textbf{2.26}$$

The second contribution has the form,

$$\frac{1}{\mu_{i,DAeh}} = \mu_{i,N}\left(\frac{N_{i,sc}}{N_{i,sc.eff}}\right)\left(\frac{N_{i,ref}}{N_{i,sc}}\right)^{\alpha_i} + \mu_{i,c}\left(\frac{n+p}{N_{i,sc.eff}}\right) \qquad \textbf{2.27}$$

Effective donor or acceptor concentrations are calculated by introducing some clustering function and then approximated by some analytical functions in Sentaurus device [7].

- **High field mobility models**

At high electric field, carrier velocity becomes no longer proportional to the electric field as it saturates to the saturation velocity. In Sentaurus device high field saturation model is composed of actual mobility model, velocity saturation model and drivind force model. In the Canali [14] model carrier mobility is represented by,

$$\mu(F) = \frac{(a+1)\mu_{low}}{a + \left[1 + \left(\frac{(a+1)\mu_{low} F_{hf}\, s}{v_{sat}}\right)^{\beta}\right]^{1/\beta}} \qquad \textbf{2.28}$$

Where, μ_{low} denotes the low field mobility, F_{hf} is the deriving field and v_{sat} represents the carrier saturation velocity.

2.3.4 Energy and momentum relaxation

Energy relaxation time models are used in the relaxation time terms in Hydrodynamic equations. A constant energy relaxation times or a quadratic dependence on the electron temperature are usually assumed. Using non constant term for energy relaxation inside mobility models provides better modeling characteristics at high field region (i.e. velocity overshoot). It also improves the bias dependent and small signal simulation [10]

- **Relaxation time model**

There are mainly two procedures to model the energy relaxation time. The direct method assumes an average of electron energy and uses MC simulation result. From the interpolation of MC results for different electric fields, relaxation time is obtained directly as a function of electron temperature.

In Sentaurus device energy dependent energy relaxation time is applied as a table function and it can be accessible from the parameter file.

2.3.5 Generation and recombination

Carrier generation and recombination process is a very important phenomenon particularly for bipolar devices. For a typical device total carrier lifetime is assumed to be composed of contribution from the different recombination processes by an inverse law,

$$\frac{1}{\tau_{tot}} = \frac{1}{\tau_{SRH}} + \frac{1}{\tau_{AUG}} + \frac{1}{\tau_{DIR}} + \frac{1}{\tau_{SURF}} \qquad \textbf{2.29}$$

This includes doping dependent Shockley-Read-Hall (SRH), Auger recombination, direct recombination and surface SRH recombination.

- **Shockley-Read-Hall (SRH) recombination**

Electron transition between the bands passes through a new energy state created by the impurity of lattice. The impurity state can absorb the difference between the momentums of two carriers and hence recombine. For indirect band gap semiconductors like Si, SRH recombination is dominant [10].

In Sentaurus device the net SRH recombination is defined as,

$$R_{net}^{SRH} = \frac{np - n_{i,eff}^2}{\tau_p(n + n_1) + \tau_n(p + p_1)} \qquad \textbf{2.30}$$

With,

$$n_1 = n_{i,eff} \exp(\frac{E_{trap}}{KT}) \qquad \textbf{2.31}$$

$$p_1 = n_{i,eff} \exp(\frac{-E_{trap}}{KT})$$

E_{trap} is the difference between the defect level and intrinsic level. For Si devices the default value of E_{trap} is set to zero. Minority carrier lifetime (τ_n) are modeled as a product of doping dependent, field dependent and temperature dependent factor.

➢ SRH doping dependence

Doping dependence is modeled using the Scharfetter relation inside Sentaurus device,

$$\tau_{dop} = \tau_{\min} + \frac{\tau_{\max} - \tau_{\min}}{1 + \left(\frac{N_{A,0} + N_{D,0}}{N_{ref}} \right)^{\gamma}} \quad \textbf{2.32}$$

Such dependence arises from the experimental data [15]. These parameters are accessible from the parameter file for the Scharfetter relation inside the simulator.

➢ SRH temperature dependence

To date there is no correspondence of temperature dependence of carrier lifetime [7]. This appears due to a different understanding of recombination lifetime as [16]

$$\tau = \frac{\delta n}{R_{net}} \quad \textbf{2.33}$$

Where, δn stands for excess carrier concentration. For a power device it is calculated that lifetime increases with increasing temperature [16]. This is modeled in Sentaurus device by power law or by exponential law,

$$\tau(T) = \tau_0 \left(\frac{T}{300K} \right)^{\alpha} \quad \textbf{2.34}$$

$$\tau(T) = \tau_0 \exp C \left(\frac{T}{300K} - 1 \right)$$

➢ **SRH field enhancement**

At a high electric field ($>3\times10^{5}V/m$) field enhancement reduces the recombination lifetime by field enhancement factors. This is due to the Trap Assisted Tunneling (TAT) which is an important mechanism for the indirect band gap semiconductors. There are two types of field enhancement available in Sentaurus device simulator, Hurkx TAT [17] and Shenk TAT model.

- **Auger recombination**

Auger recombination is very important for the high doping regions inside the device. The band to band Auger recombination is modeled as,

$$R_{net}^{A}=\left(C_n n+C_p p\right)\left(np-n_{i,eff}^{2}\right) \qquad \textbf{2.35}$$

Where C_n and C_p are the Auger parameters. Comparing different direct band gap III-V semiconductor materials it is established that Auger co efficient increases with decreasing bandgap [7].

Temperature dependence of Auger coefficient is modeled by simple power law (for Si) or by polynomial expansion.

$$C_{\gamma}^{AUG}(T)=C_{\gamma,300K}^{AUG}\left(\frac{T}{300K}\right)^{\alpha} \qquad \textbf{2.36}$$

$$C_{\gamma}^{AUG}(T)=C_{\gamma,300K}^{AUG}+K_1\left(\frac{T}{300K}\right)+K_2\left(\frac{T}{300K}\right)^{2}$$

2.4 Conclusion

The main aim of this chapter is to understand the physics behind TCAD device simulation. It is fairly well established that in modern days, TCAD tools are an integral part of semiconductor device industry. Starting from the process simulation, there exist numerous tools for device simulation or parameter extraction. In this chapter, the different physical models used in TCAD device simulations are analyzed. This analysis helps to build a physical understanding behind different electrical behaviors of real time measurements. Again, for the calibration process, the understanding of different physical models is important. In calibration, only a few parameters are tuned to achieve the desired output results and will be shown in the last chapter.

Reference

[1] John D. Cressler, *Measurement and Modeling of Silicon Heterostructure Devices*.

[2] G. A. Armstrong,C. K. Maiti, *TCAD for Si, SiGe and GaAs integrated circuits*.

[3] Dragica Vasileska, Stephen M. Goodnick, *Computational Electronics Synthesis Lectures on Computational Electromagnetics*, Morgan & Claypool, .

[4] Synopsys, *Sentaurus Process UserGuide*.

[5] Thesis Mahmoud Al-Sa'di, "TCAD Based SiGe HBT Advanced Architecture Exploration," 2011, Bordeaux 1.

[6] J. Vobecky, J. Voves, P. Hazdra, I. Adamcik, *TCAD - A Progressive Tool for Engineers (1993)*.

[7] Synopsys, *Sentaurus Device UserGuide*.

[8] L.C. Evans, *Partial Differential Equations*, American Mathematical Society.

[9] Arkeryd, Leif, *On the Boltzmann equation*, Arch. Rational Mech.

[10] Vassil Palankovski,Rüdiger Quay, *Analysis and Simulation of Heterostructure Devices*, Springer; 1 edition (February 17, 2004), .

[11] Slotboom, J.W.; de Graaff, H.C, "Bandgap narrowing in silicon bipolar transistors," *Electron Devices, IEEE Transactions on*, vol. 24.

[12] Green, Martin A., "Intrinsic concentration, effective densities of states, and effective mass in silicon," *Journal of Applied Physics*.

[13] D.B.M. Klaassen, "A unified mobility model for device simulation—I. Model equations and concentration dependence," *Solid-State Electronics*, vol. 35.

[14] Canali, C. Majni, G. Minder, R. Ottaviani, G., "Electron and hole drift velocity measurements in silicon and their empirical relation to electric field and temperature," *Electron Devices, IEEE Transactions on*.

[15] Roulston, D.J. Arora, N.D. Chamberlain, S.G., "Modeling and measurement of minority-carrier lifetime versus doping in diffused layers of n+-p silicon diodes," *Electron Devices, IEEE Transactions on*.

[16] Tyagi, M. S.; van Overstraeten, R., "Minority carrier recombination in heavily-doped silicon," *Solid-State Electronics*.

[17] Hurkx, G.A.M.; Klaassen, D.B.M.; Knuvers, M.P.G., "A new recombination model for device simulation including tunneling," *Electron Devices, IEEE Transactions on*.

Chapter 3

[NQS IMPLEMENTATION INSIDE COMPACT MODEL]

3.1 Introduction: HICUM model overview

HICUM is a semi physical compact bipolar transistor model for arbitrary transistor configuration [1]. The name HICUM was derived from HIgh CUrrent Model, indicating the operating region at high current densities, a very important region for high speed transistor applications. The model is based on an extended and Generalized Integral Charge Control Relation (GICCR) and GICCR concept is applied consistently without inadequate simplifications in HICUM. Next figure (Figure **3.1**) shows a schematic cross section of SiGe bipolar transistor fabricated with non selective epitaxial growth process and circuit diagram of HICUML2 model representation of the different parts of the transistor [2].

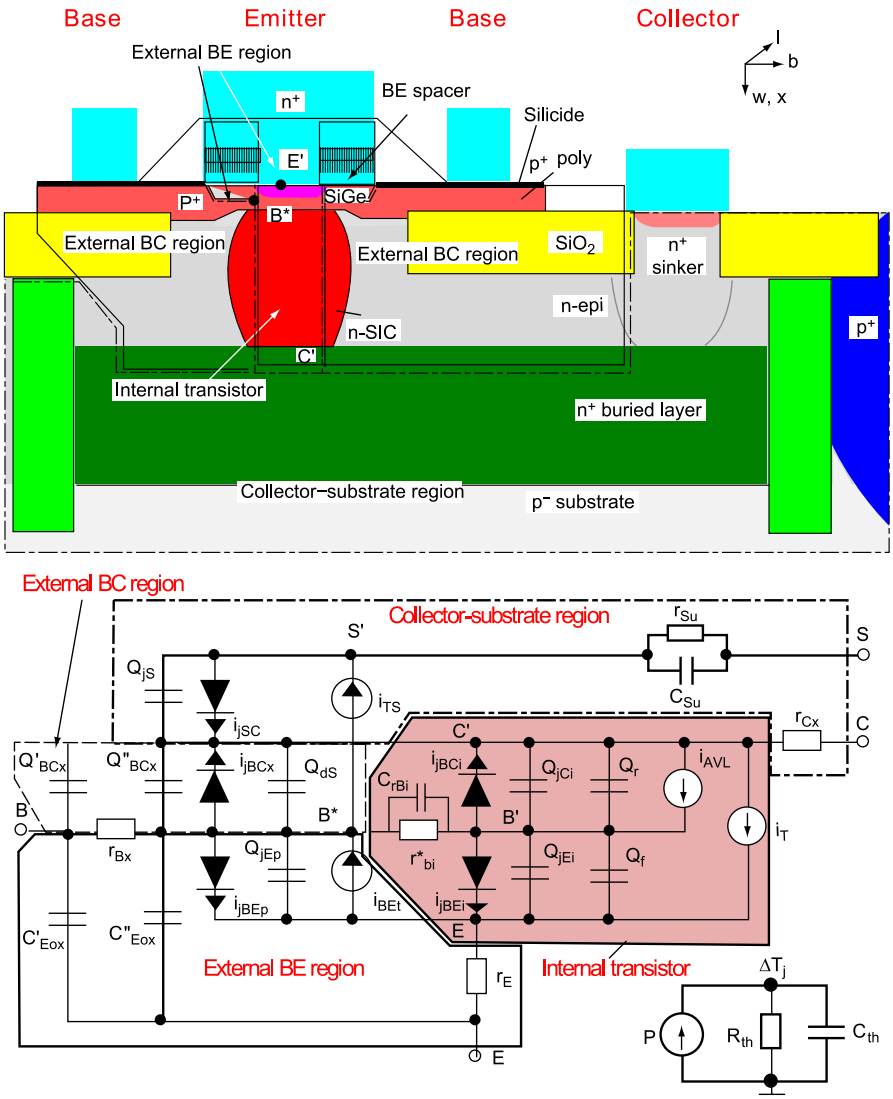

Figure **3.1**: Upper figure: Schematic deep trench isolated SiGe HBT. Lower figure: large signal circuit diagram (HICUM L2) with the self heating network [2]. The internal transistor is shown with different color.

Comparing to SGPM, HICUM contains two additional nodes namely B* and S'. The node B* separates the bias dependent internal base resistance from the bias independent external one and it helps to model the emitter periphery effect in modern transistors. In HICUM model bias dependent depletion capacitance and current dependent diffusion capacitance are assumed. GICCR is applied inside the model to calculate charge contribution due to different regions of the transistor. The most important part of the HICUM model is the transit time modeling which is totally different from the other compact models. Total transit time is separated into low and high injection component and modeled applying a step by step procedure. Overall the model provides a scalable approach that helps to build a single parameter list for a certain technology.

In the next part, the main physical equations inside the HICUM model are discussed with some details.

3.1.1 HICUM model equations

- **Transfer current**

The 1D GICCR result for transfer current is described in HICUM [3] as,

$$I_T \cong I_C = \frac{C_{10}}{Q_{pT}}[\exp(\frac{V_{B'E'}}{V_T}) - \exp(\frac{V_{B'C'}}{V_T})] \quad \textbf{3.1}$$

Where, C_{10} is a model parameter which is calculated from the Generalized Integral Charge Control Relation (GICCR) relation.

$$C_{10} = \left(qA_E\right)^2 V_T \overline{\mu_{nB} n_i^2} \quad \textbf{3.2}$$

In HICUM model, total base charge (Q_{pT}) is considered as an important internal variable. Total base charge (Q_{pT}) is composed of zero bias hole charge (Q_{p0}), weighted sum of depletion charges and weighted sum of forward and reverse minority charges as,

$$Q_{p,T} = Q_{p0} + h_{jei}Q_{jEi} + h_{jci}Q_{jCi} + Q_{f,T} + Q_{r,T} \qquad \textbf{3.3}$$

Here, Q_{p0} is the zero bias hole charge inside base. Depletion charges due to the BE junction and BC junction are Q_{jEi} and Q_{jCi} which are modeled using two HICUM parameters (h_{jei}, h_{jci}). Other two parts represent the forward and reverse component respectively. The forward component of base charge ($Q_{f,T}$) can be summed as,

$$Q_{f,T} = Q_{f0} + h_{fE}\Delta Q_{Ef} + \Delta Q_{Bf} + h_{fC}\Delta Q_{Cf} \qquad \textbf{3.4}$$

Hare, Q_{f0} is the low current charge component, ΔQ_{Ef} ΔQ_{Bf} ΔQ_{Cf} are minority charge at neutral emitter, base and collector regions. The weighting factors like h_{fE} h_{fC} depend upon the grading and bandgap of various transistor regions in HBT. The next figure (Figure **3.2**) shows the different charge component inside the transistor.

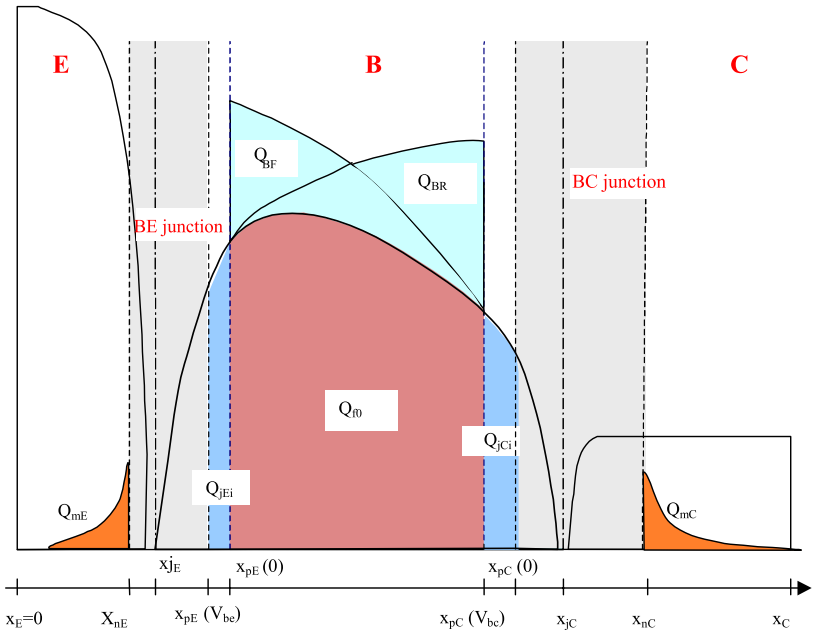

Figure **3.2**: HICUM formulation of different parts of base charge inside HBT in both forward and reverse operation [4].

- **Quasi static base current**

Quasi static base current is composed of bottom and peripheral components. These current factors include contribution from physical mechanism like volume recombination (SRH and Auger), surface recombination and tunneling [3]. The bottom component which represents the injection from the effective emitter area is modeled in HICUM as,

$$i_{jBEi} = i_{BEiS}\left[\exp\left(\frac{V_{B'E'}}{m_{BEi}V_T}\right)-1\right] + i_{REiS}\left[\exp\left(\frac{V_{B'E'}}{m_{REi}V_T}\right)-1\right] + I_{Bhrec} \qquad \textbf{3.5}$$

Saturation currents i_{BEiS}, i_{REiS} with non ideality coefficients m_{BEi} m_{REi} are model parameters. I_{Bhrec} is the recombination current due to the BC barrier effect [5] at high current densities. This quasi static assumption works well also in high frequencies. Similarly the quasi-static base current injected across the emitter periphery is given by,

$$i_{jBEp} = i_{BEpS}\left[\exp\left(\frac{V_{B*E'}}{m_{BEp}V_T}\right)-1\right] + i_{REpS}\left[\exp\left(\frac{V_{B*E'}}{m_{REp}V_T}\right)-1\right] \qquad \textbf{3.6}$$

In hard saturation current component at the base collector junction becomes prominent which is modeled as,

$$i_{jBCi} = i_{BCiS}\left[\exp\left(\frac{V_{B'C'}}{m_{BCi}V_T}\right)-1\right] \qquad \textbf{3.7}$$

Similarly for the external base collector junction,

$$i_{jBCx} = i_{BCxS}\left[\exp\left(\frac{V_{B*C'}}{m_{BCx}V_T}\right)-1\right] \qquad \textbf{3.8}$$

- **Depletion capacitance**

In HICUM depletion charge and capacitance are assumed to follow the classical formulation,

$$C_j = \frac{C_{j0}}{(1 - V/V_D)^{Z_j}} \qquad \textbf{3.9}$$

$$Q_j = \int_0^V C_j dV'$$

Here, V_D is the built in potential and C_{j0} is the zero bias capacitance. $V = V_D$ is a pole of equation **3.9** which is not suitable for the compact model formulation. Moreover simple theoretical expression does not predict the behavior of depletion capacitance at high reverse bias (punch through). HICUM capacitance parameters are discussed below,

Base-emitter junction

With the classical model parameters V_{DEi} Zei and an additional parameter a_{jEi} which is defined as the ratio of maximum capacitance to the zero bias capacitance, the expression for the base emitter junction capacitance reads,

$$C_{jEi} = \frac{C_{jEi0}}{(1 - V_j/V_{DEi})^{Zei}} \cdot \frac{dv_j}{dv_{B'E'}} + a_{jEi} C_{jEi0} \left(1 - \frac{dv_j}{dv_{B'E'}}\right) \qquad \textbf{3.10}$$

Where the auxiliary voltage v_j uses a hyperbolic smoothing expression,

$$V_f = V_{DEi}(1 - a_{jEi}^{-1/Z_{Ei}}) \qquad \textbf{3.11}$$

$$v_j = V_f - V_T \frac{x + \sqrt{x^2 + a_{fj}}}{2}$$

$$x = \frac{V_f - V_{B'E'}}{V_T}$$

The corresponding charge equation becomes,

$$Q_{jEi} = \frac{C_{jEi0} V_{DEi}}{1 - Z_{Ei}} \left[1 - \left(1 - \frac{v_j}{V_{DEi}} \right)^{(1 - Z_{Ei})} \right] + a_{jEi} C_{jEi0} \left(V_{B'E'} - v_j \right) \quad \textbf{3.12}$$

Internal base collector junction

The BC junction is usually operated by reverse bias. If the internal voltage (vcb) becomes greater than the effective punch through voltage the epitaxial collector becomes fully depleted. The effective punch through voltage is given by

$$V_{jPCi} = V_{PTCi} - V_{DCi} \quad \textbf{3.13}$$

For large forward bias the parameter V_{DCi} becomes,

$$V_{fCi} = V_{DCi}(1 - a_{jCi}^{-1/z_{Ci}}) \quad \textbf{3.14}$$

Large reverse bias starts from the voltage,

$$V_r = 0.1 V_{PTCi} + 4 V_T \quad \textbf{3.15}$$

The total base collector depletion capacitance is modeled as a summation of three bias dependent components, large reverse bias, medium bias and high forward bias.
At medium bias,

$$C_{jCi,cl} = \frac{C_{jCi0}}{(1 - \frac{V_{jm}}{V_{DCi}})^{Z_{Ci}}} \frac{e_{j,r}}{(1 + e_{j,r})} \frac{e_{j,m}}{(1 + e_{j,m})} \quad \textbf{3.16}$$

Equation **3.16** contains classical capacitance part on the first term and also the smoothing function at the end.

At high forward bias and high reverse bias the capacitance equation looks like,

$$C_{jCi,fb} = a_{jci} C_{jCi0} \frac{1}{1+e_{j,r}} \qquad \textbf{3.17}$$

$$C_{jCi,PT} = \frac{C_{jci0,r}}{(1-\frac{V_{j,r}}{V_{DCi}})^{z_{Ci,r}}} \frac{1}{(1+e_{j,m})}$$

External base collector capacitance

The external base collector capacitance consists of a bias dependent base collector external depletion capacitance (C_{jCx}) and a bias dependent external parasitic capacitance (C_{BCpar}).

$$C_{BCx} = C_{jCx} + C_{BCpar} \qquad \textbf{3.18}$$

The total capacitance C_{BCx} is partitioned across Rbx (external base resistance) and this partition requires an additional parameter,

$$f_{BCpar} = \frac{C_{BCx2}}{C_{BCx}} \qquad \textbf{3.19}$$

The factor f_{BCpar} is geometry and technology specific parameter. The capacitance splitting is described inside HICUM as,

$$C_{BCx} = C_{BCx1} + C_{BCx2} = (1 - f_{BCpar})C_{BCx} + f_{BC}C_{BCx} \qquad \textbf{3.20}$$

- **Transit time**

The extraction of transit time parameters is a crucial point for precise modeling of bipolar transistors using the HICUM model. The transit time formulation used in HICUM model [3] is much more complex and more precise than that used within the Gummel-Poon model [6], which requires an accurate and rigorous method of parameter extraction. The transit time is

defined from the transition frequency f_T (the frequency for which the gain becomes unity for small signal current) by the relation,

$$\tau_F = \frac{1}{2\pi f_T} - (C_{je} + C_{jc})\frac{V_T}{I_C} - (R_{CX} + R_E)C_{jc} \qquad \textbf{3.21}$$

Where C_{je} and C_{jc} are the total base emitter and base collector junction capacitance, R_E and R_{CX} are emitter series resistance and extrinsic collector resistance. In HICUM the expression of total transit time (τ_f) is associated with charges in each region of transistor.

$$\tau_f = \tau_E + \tau_{BED} + \tau_B + \tau_{BCD} + \tau_C \qquad \textbf{3.22}$$

Where, the different parts represent the different regions inside the transistor.

The current and voltage dependence of the total transit time is modeled inside HICUM by two components.

$$\tau_f(v_{C'E'}, i_{Tf}) = \tau_{f0}(v_{B'C'}) + \Delta\tau_f(v_{C'E'}, i_{Tf}) \qquad \textbf{3.23}$$

Where, τ_{f0} represents the low current transit time and $\Delta\tau_f$ is the increase of transit time at high current densities.

Low current density

The BC voltage dependence of τ_{f0} is described by,

$$\tau_{f0} = \tau_0 + \Delta\tau_{0h}(C-1) + \tau_{Bfvl}\left(\frac{1}{c} - 1\right) \qquad \textbf{3.24}$$

The first term τ_0 represents the total transit time at V_{BC}=0V. The second term models the net change caused by the Early effect with the help of normalized internal BC depletion

capacitance C. The third term takes into account the carrier jam at BC space charge region at low V_{CE}. The HICUM transit time parameters for low current density are $\Delta\tau_{0h}$ and τ_{Bfvl}.

Medium and high current densities

At high current density a sudden rise of transit time occurs due to the Kirk effect. In HICUM the onset of high current effect is characterized by critical current (I_{Ck}).

$$I_{CK} = \frac{v_{ceff}}{r_{ci0}} \frac{1}{\sqrt{1+\left(\frac{v_{cef}}{V_{\lim}}\right)^2}} \left[1+\frac{x+\sqrt{x^2+a_{ickpt}}}{2}\right] \qquad \textbf{3.25}$$

With x connects the high and low electric field inside the collector. v_{ceff} r_{ci0} And $V_{\lim}$ are model parameters.

At high current density the increase of the transit time is represented by,

$$\Delta\tau = \Delta\tau_{fh}(i_{Tf}, V_{C'E'}) + \Delta\tau_{Ef}(i_{Tf}, V_{C'E'}) \qquad \textbf{3.26}$$

$\Delta\tau_{Ef}$ is the change in the emitter transit time component and is modeled with emitter transit time parameters τ_{Ef0}

$$\Delta\tau_{Ef} = \tau_{Ef0}\left(\frac{i_{Tf}}{I_{Ck}}\right)^{g_{\tau E}} \qquad \textbf{3.27}$$

Assuming negligible collector spreading increase of the base and the collector transit time can be lumped together and represented by,

$$\Delta\tau_{fh} = \tau_{hcs} w^2 \left(1+\frac{2}{\frac{i_{Tf}}{I_{Ck}}\sqrt{i^2+a_{hc}}}\right) \qquad \textbf{3.28}$$

τ_{hcs} And a_{hc} are model parameters. Normalized injection width (w) and the variable i are correlated as,

$$w = \frac{w_i}{w_c} = \frac{i + \sqrt{i^2 + a_{hc}}}{1 + \sqrt{1 + a_{hc}}} \qquad \textbf{3.29}$$

$$\Delta\tau_{Ef} = 1 - \frac{I_{Ck}}{i_{Tf}}$$

High current increase of transit time store an additional charge (ΔQ) which is represented by the sum of excess emitter charge ΔQ_{Ef} and excess base and collector charges.

$$\Delta Q = \Delta Q_{Ef} + \Delta Q_{fh} = \Delta\tau_{Ef}\frac{i_{Tf}}{1 + g_{\tau E}} + \tau_{hcs} i_{Tf} w^2 \qquad \textbf{3.30}$$

- **Base resistance**

In HICUM internal base resistance and the external base resistance are treated separately. The internal base resistance depends on the operating point, temperature and the transistor operation condition. The dc internal base resistance is modeled by,

$$r_{Bi} = r_i \psi(\eta) \qquad \textbf{3.31}$$

And it is described by the function,

$$r_i = r_{Bi0}\frac{Q_0}{Q_0 + \Delta Q_p} \qquad \textbf{3.32}$$

Q_0 is very close to the model parameter Qp_0 and is given by,

$$Q_0 = (1 + f_{DQr0})Qp_0 \qquad \textbf{3.33}$$

- **Breakdown**

In HICUM weak avalanche effect at the base collector junction is modeled by avalanche current,

$$i_{AVL} = i_{Tf}\, f_{AVL}(V_{DCi} - v_{B'C'}) \exp(-\frac{q_{AVL}}{C_{jCi}(V_{DCi} - v_{B'C'})^{1/Z_{Ci}}}) \qquad \textbf{3.34}$$

f_{AVL} , q_{AVL} Are the model parameters.

- **Self heating**

HICUM uses a thermal network (Figure 3.1) to model the rise of junction temperature due to the self heating. The sub circuit requires a thermal resistance R_{TH} and a thermal capacitance C_{TH} as model parameters and a current source to dissipate power of the device. Node voltage corresponds to the junction temperature. This thermal circuit is solved together with the transistor model.

3.1.2 NQS implementation inside HICUM

For fast transient or at high frequency operations, the quasi static approach becomes inadequate and an excess phase shift is necessarily included inside compact models. In some BJT models NQS phase is included inside gm which indeed predicts inconsistency between ac and transient modeling. The bias dependent delay should only introduce an excess phase shift without affecting the magnitude of electrical parameters. In a popular bipolar model VBIC [7] excess phase is introduced by an excess phase network. In HICUM the approach is similar and the excess phase network introduces an phase shift in transfer current as well as in minority charge.

The approach of Winkel [8] is implemented inside the HICUM model. In this approach, time delay is assumed to be proportional of the total transit time. As the total transit time is a function of V_{BE} and V_{CE}, delay time also becomes bias dependent. The starting equation with the transfer current and excess charge is presented below,

$$\underline{Q}_f = \underline{Q}_{f0} \exp(-j\omega\tau_2) \qquad \textbf{3.35}$$

$$\underline{I}_{Ci} = \underline{I}_{Ci0} \exp(-j\omega\tau_m)$$

With $\underline{Q}_f$ and $\underline{I}_{Ci}$ the quasi-static values and t_2 and t_m are corresponding additional delay times. In the first order approximation t_2 and t_m are associated with the total transit time t_f^* by two operating point independent parameters,

$$\alpha_2 = \frac{\tau_2}{\tau_f^*} \; and \; \alpha_m = \frac{\tau_m}{\tau_f^*} \qquad \textbf{3.36}$$

Where α_2 and α_m are charge partitioning factors used as NQS model parameters in the HICUM model.

Figure **3.3** shows the rough assumption of α parameters extracted as a function of collector current density from 1D device simulation.

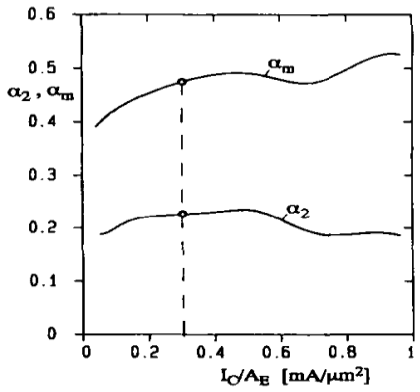

Figure **3.3**: HICUM time delay parameters as a function of current density [1]

However these relations are valid for lower frequency range. Beside, they are derived using the linear case of small signal analysis.

In HICUM model time delay is introduced in the transfer current and also in the excess charge. That is why in the HICUM model NQS circuit, we find two independent excess phase

networks- one for the transfer current and another for the excess charge. In the next part, NQS networks in the HICUM model are analyzed separately.

Bias independent phase shift in transfer current is implemented in compact model via Weil-McNamee formulation as the equivalent circuit represents. This approach is suitable for all kind of circuit analysis like ac or transient.

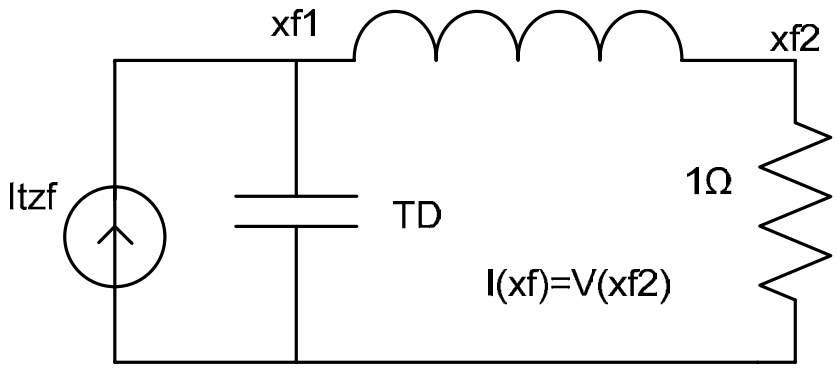

Figure **3.4:** Weil-McNamee implementation of excess phase circuit.

It includes two additional circuit nodes xf1 and xf2. As the resistor across the output terminal is 1ohm the current across it simply equals the voltage across that node. Computing the branch equations and noting the NQS current is the voltage across the 1ohm resistor, the final expression for the NQS transfer current becomes (after changing the domain by substituting $s \equiv j\omega$),

$$I_{txf} = \frac{I_{tzf}}{1 + sT_D + (sT_D^{'})^2} \qquad \textbf{3.37}$$

The implementation of this network (Figure **3.4**) is difficult as it introduces some undesired derivative to the solutions. To overcome the problem an inductor free implementation has been formulated by L. Lemaitre. The gyrator equivalent network first appeared in the VBIC update and afterwards implemented in the HICUM model.

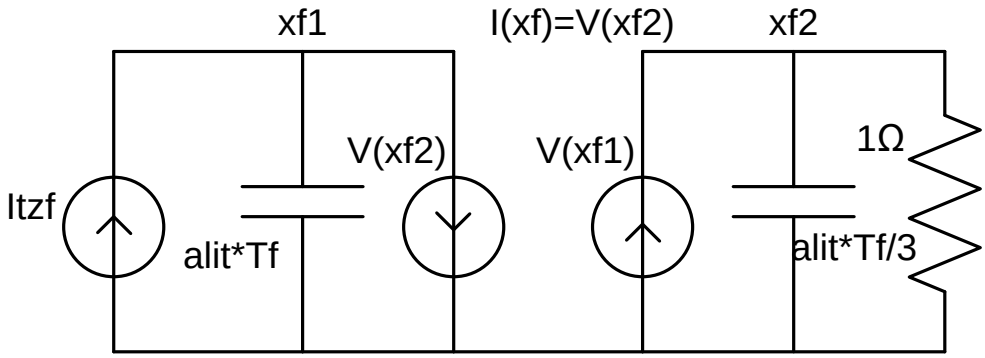

Figure **3.5**: Inductor free equivalent circuit for excess phase.

Corresponding equations are

$$I_{tzf} = \frac{d}{dt}(Q_{xf1}) + V(xf2) = \frac{d}{dt}(\alpha_{it} * T_D * V(xf1)) + V(xf2) \quad \textbf{3.38}$$

$$V(xf1) = \frac{d}{dt}(Q_{xf2}) + V(xf2) = \frac{d}{dt}(\alpha_{it} * T_D / 3 * V(xf2)) + V(xf2)$$

And,

$$I_{txf} = V(xf2) \quad \textbf{3.39}$$

With the help of equations **3.38** and **3.39**, a second order differential equation in time domain can be constructed,

$$I_{tzf} = A_2 \frac{d^2}{dt^2} I_{xf} + A_1 \frac{d}{dt} I_{xf} + I_{xf} \quad \textbf{3.40}$$

And mapping ddt to s, the corresponding expression in frequency domain for itxf becomes,

$$I_{txf} = \frac{I_{tzf}}{1 + sT_D + (sT_D^{'})^2} \quad \textbf{3.41}$$

So, the gyrator equivalent network implements the same equation as the previous model implements.

The excess charge phase shift network is similar to the transfer current network (Figure **3.5**) in HICUM L2V23 model. The only different is that the input current (I_{tzf}) is replaced by the excess charge (Q_{dei}). In the new version of HICUM model (L2V24), a simple RC network is implemented which is presented in figure **3.6**.

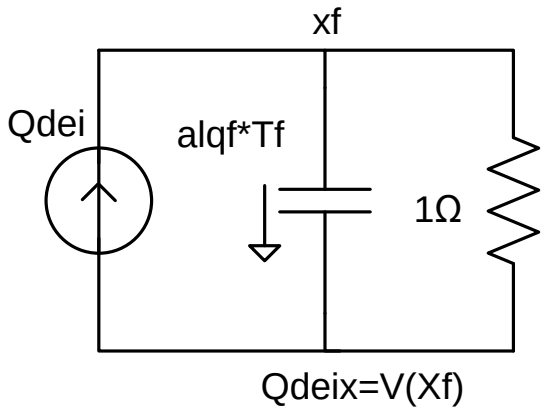

Figure **3.6**: excess charge phase network in HICUM L2V24

The NQS charge is represented by the next equation,

$$Q_{deix} = \frac{Q_{dei}}{1 + sT_D} \qquad \textbf{3.42}$$

Last of all, HICUM L2V24 NQS modeling code in VerilogA is presented for the transfer current and excess charge.

Transfer current	Excess charge
electrical xf1,xf2; Vxf1 = V(br_bxf1); Vxf2 = V(br_bxf2); Ixf1 = (Vxf2-itf)/Tf*t0; Ixf2 = (Vxf2-Vxf1)/Tf*t0; Qxf1 = alit*Vxf1*t0; Qxf2 = alit*Vxf2/3*t0; Itxf = Vxf2; I(br_bxf1) <+ Ixf1; I(br_cxf1) <+ ddt(Qxf1); I(br_bxf2) <+ Ixf2; I(br_cxf2) <+ ddt(Qxf2);	electrical xf; Vxf = V(br_bxf); fact = t0/Tf; Ixf = (Vxf - Qdei)*fact; Qxf = alqf*Vxf*t0; Qdeix = Vxf; I(br_bxf) <+ Ixf; I(br_cxf) <+ ddt(Qxf);

Table **3.1**: VerilogA code for excess phase circuit of transfer current and excess charge in HICUM L2 V24 model.

3.2 HICUM modeling in BiCMOS7RF

BiCMOS7RF, a SiGe-C technology which is widely used inside oscillator for wireless communications, is developed by ST microelectronics. In the next figure, the roadmap of ST process technologies is shown indicating the BiCMOS7RF layout [9].

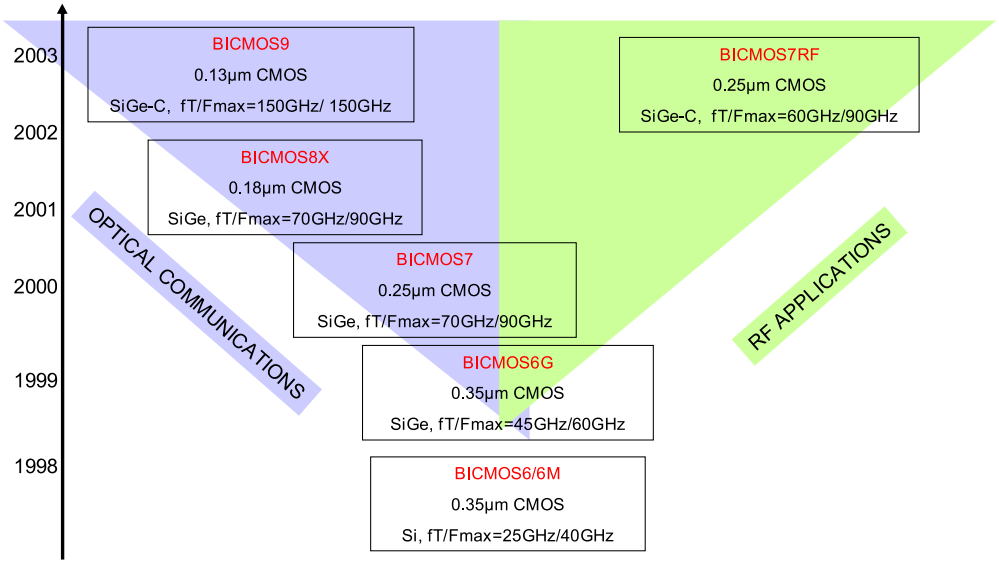

Figure **3.7**: Different Si process technologies developed by ST microelectronics [9].

The addition of C affects increasing the speed of the transistor while reducing the noise associated with the base resistance. Process technology limits the cut off frequency of this technology at 60 GHz and maximum cut off frequency at 90GHz. But to observe high frequency NQS effects, ac measurements are carried out beyond to the cut off frequency (up to 110GHz).

The transistor used for modeling contains emitter length of 12.8µm and emitter width of 0.4µm.

3.2.1 Extraction strategy using HICUM model

Single transistor parameter extraction was performed following the extraction procedure mentioned below [10]. The main intention of this parameter extraction is to verify the NQS related parameters when the transistor works beyond its cut off frequency.

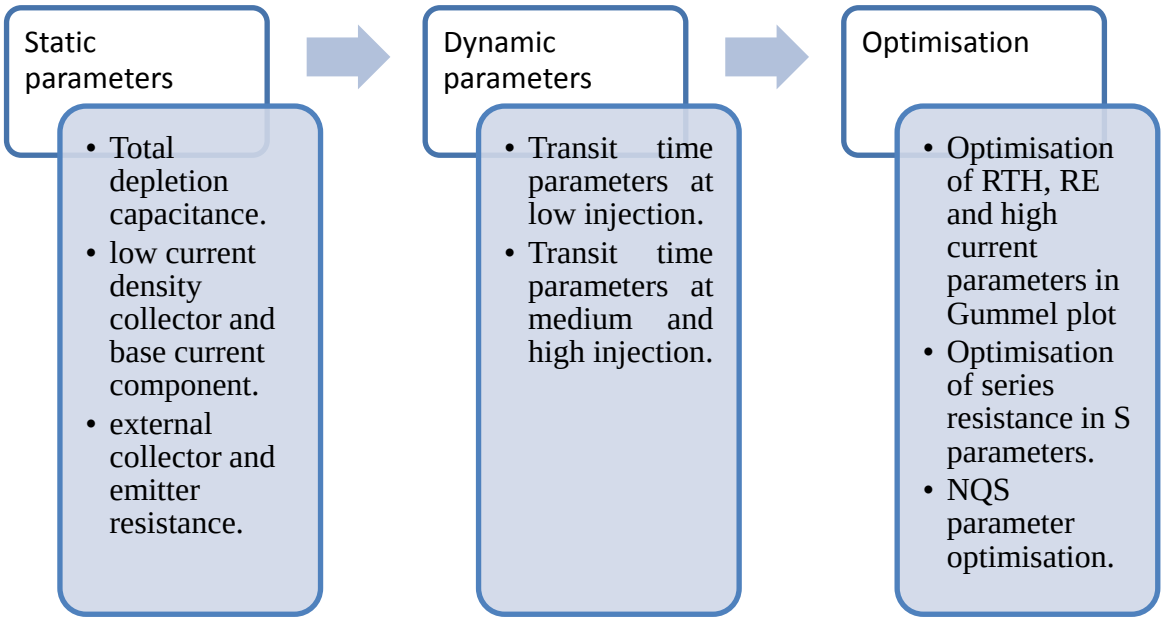

Figure **3.8**: single transistor parameter extraction methodology [10]

The parameter set obtained by single transistor parameter extraction can't assume to be accurate. In this first step extraction temperature parameters were ignored. Also the external resistances are very difficult to extract from a single geometry. However, global optimization ensures the best possible fit for measurements.

3.2.2 Modeling results

- **Gummel plot:**

Static measurement is performed setting V_{BC}=0V and varying V_{BE} from 0.5V to 0.98V which contains both the low and high injection regions. The modeling results are presented below which represent modeling of Gummel plot and Beta. Both these are modeled properly as shown in the Figure **3.9**.

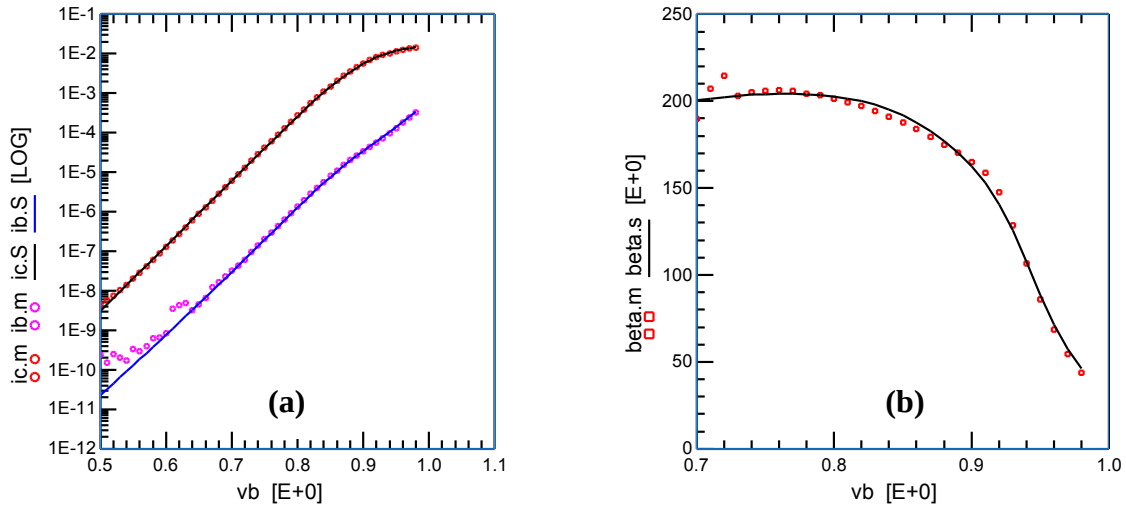

Figure **3.9**: (a) Ic and Ib (measured and simulated) as a function of V_{BE} (Gummel plot) at V_{CB}=0V (b) Beta Vs V_{BE} plot for the same configuration.

- **Output characteristics**

Output graphs are presented in Figure **3.10** showing I_C as a function of V_{CE} considering different V_{BE}s. The maximum base emitter voltage is chosen beyond peak f_T at high current region. Base collector breakdown is not reached in the measurement. Also the effect of self heating is not predominant in output characteristics.

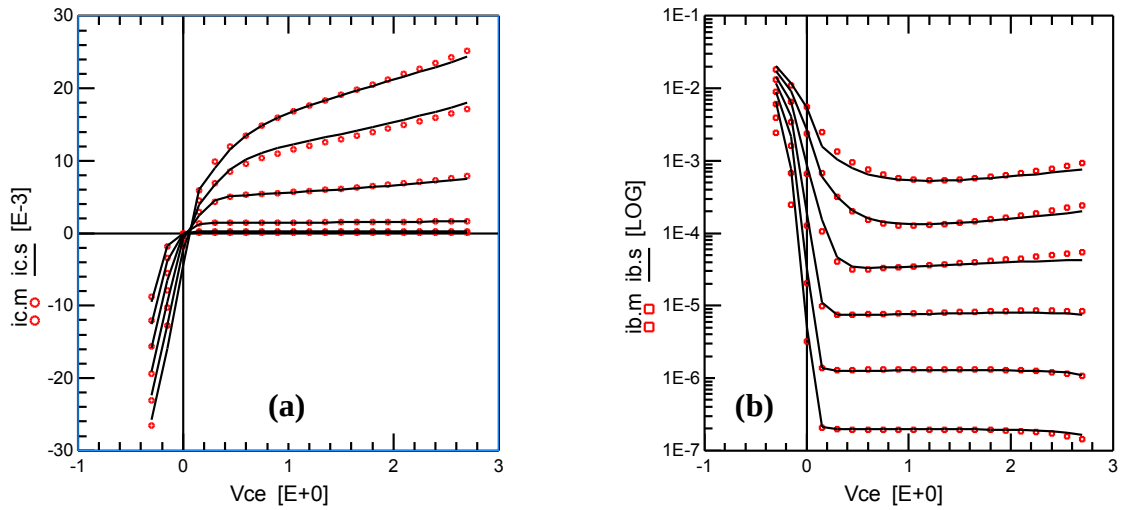

Figure **3.10**: (a) Ic-V_{CE} for different V_{BE} = 0.75V, 0.8V, 0.85V, 0.9V, 0.95 V, (b) Ib V_{CE} for the same configuration.

- **Dynamic characteristics**

Figure **3.11** shows cut off frequency as a function of VBE and Ic. The cut off frequency is calculated at 7 GHz where the magnitude of small signal current gain shows a perfect 20dB/dec slope. Modeling results show a fairly well accuracy as both the transit time and critical current is well modeled.

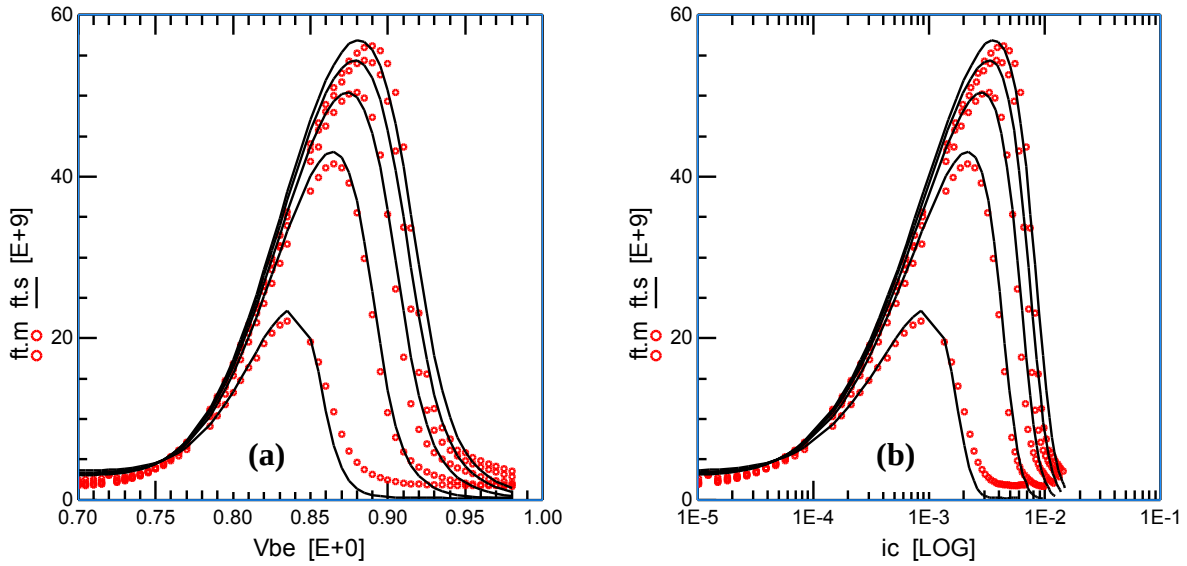

Figure **3.11**: f_T vs V_{BE} and f_T vs Ic characteristics for different V_{CE}.

- **NQS parameters**

In HICUM model NQS specific parameters are alit and alqf [3] which represent the delay time associated with the forward transfer current and excess minority charge. To activate these model parameters inside the VerilogA code one need to set the flag parameter flnqs to 1. The extraction procedure is to extract alit from Imaginary part of Y_{21} and alqf from real part of Y_{11} both at high frequency and below f_T. Practically it is far easier to optimize these parameters from the phase of h_{21}. Looking at the previous modeling results, it can be concluded that the transit time and axis resistance parameters are modeled properly. So, the NQS modeling can be performed with the help of this extracted parameter list.

Frequency sweep AC measurement is performed varying the terminal voltages up to high frequency (110GHz) in IMS laboratory.

FLNQS=0

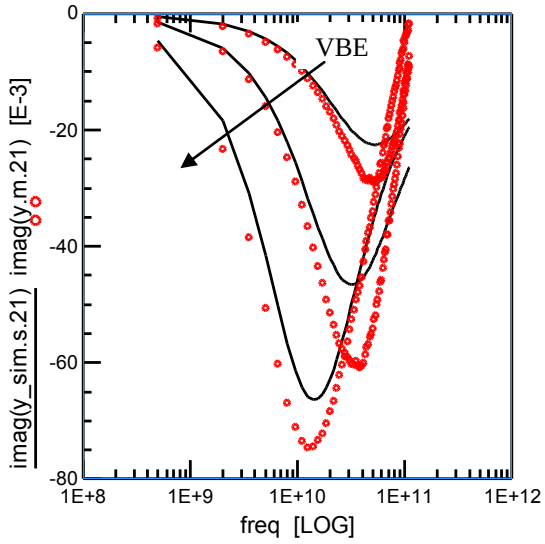

(a)

FLNQS=1

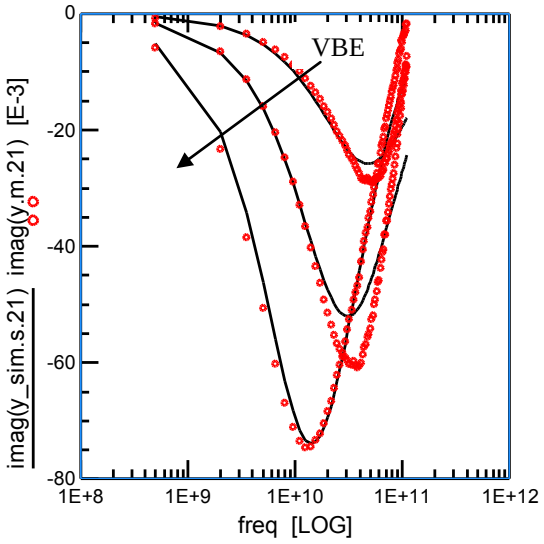

(b)

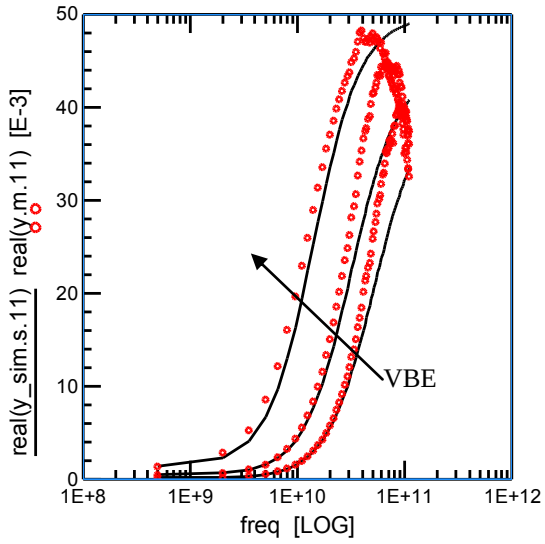

(c)

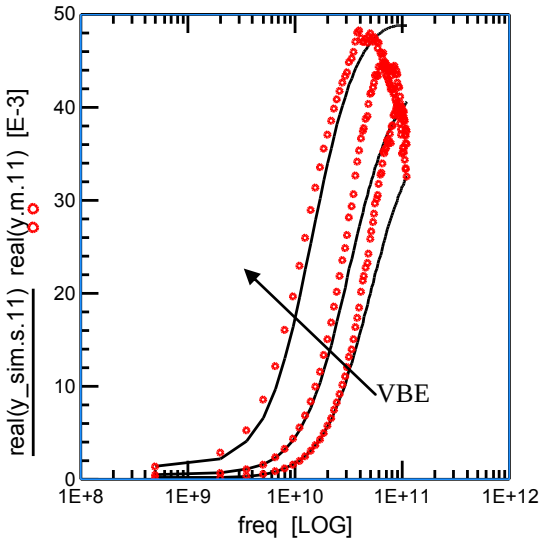

(d)

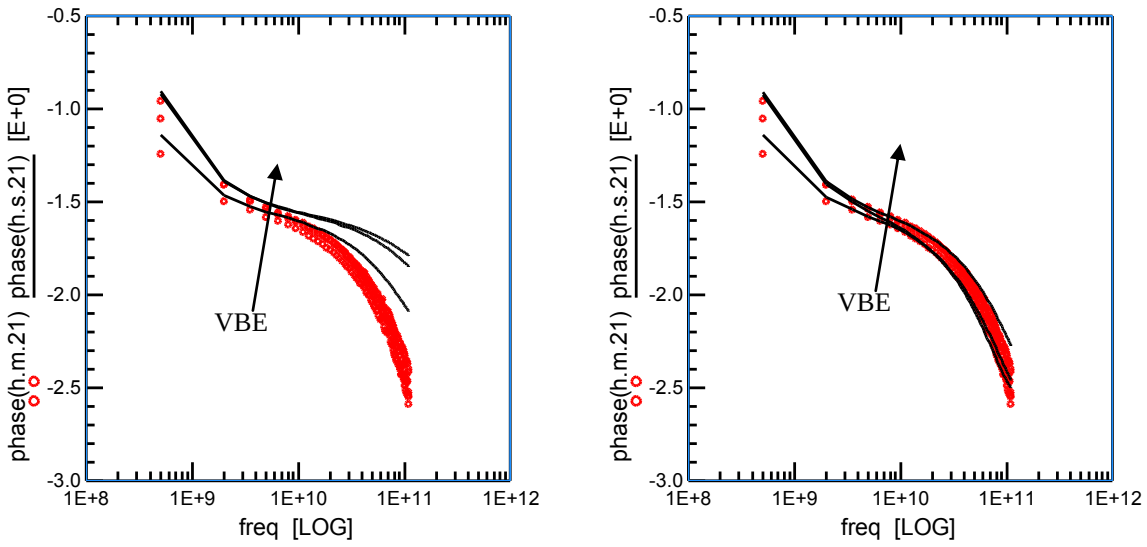

(e) **(f)**

Figure **3.12: (a, b)** Modeling results of Imaginary Y_{21} before and after NQS parameters optimization showing Non Quasi Static effect at high frequency for different V_{BE} = 0.84V, 0.88V, 0.92V at a V_{CE}= 1.6V. **(c, d)** Modeling results of Real Y_{11} before and after NQS parameters optimization for different V_{BE} = 0.84V, 0.88V, 0.92V at a V_{CE}= 1.6V. **(e, f)** Modeling results of Phase h_{21} before and after NQS parameters optimization showing Non Quasi Static effect at high frequency for different V_{BE} = 0.84V, 0.88V, 0.92V at a V_{CE}= 1.6V.

From the previous figure **3.12**, it can be readily observed that the high frequency NQS effect can be modeled by the existing HICUM excess phase network by adjusting two parameters namely alit and alqf. Though the results are quite satisfactory, there is still a scope of improvement at very high frequency (>60GHz). For example, the modeling of imaginary part of Y_{21} can be improved at high frequency.

Magnitude and phase of Y_{11} and Y_{21} are also affected by NQS delay. Figure **3.13** shows y parameters after NQS parameters optimization.

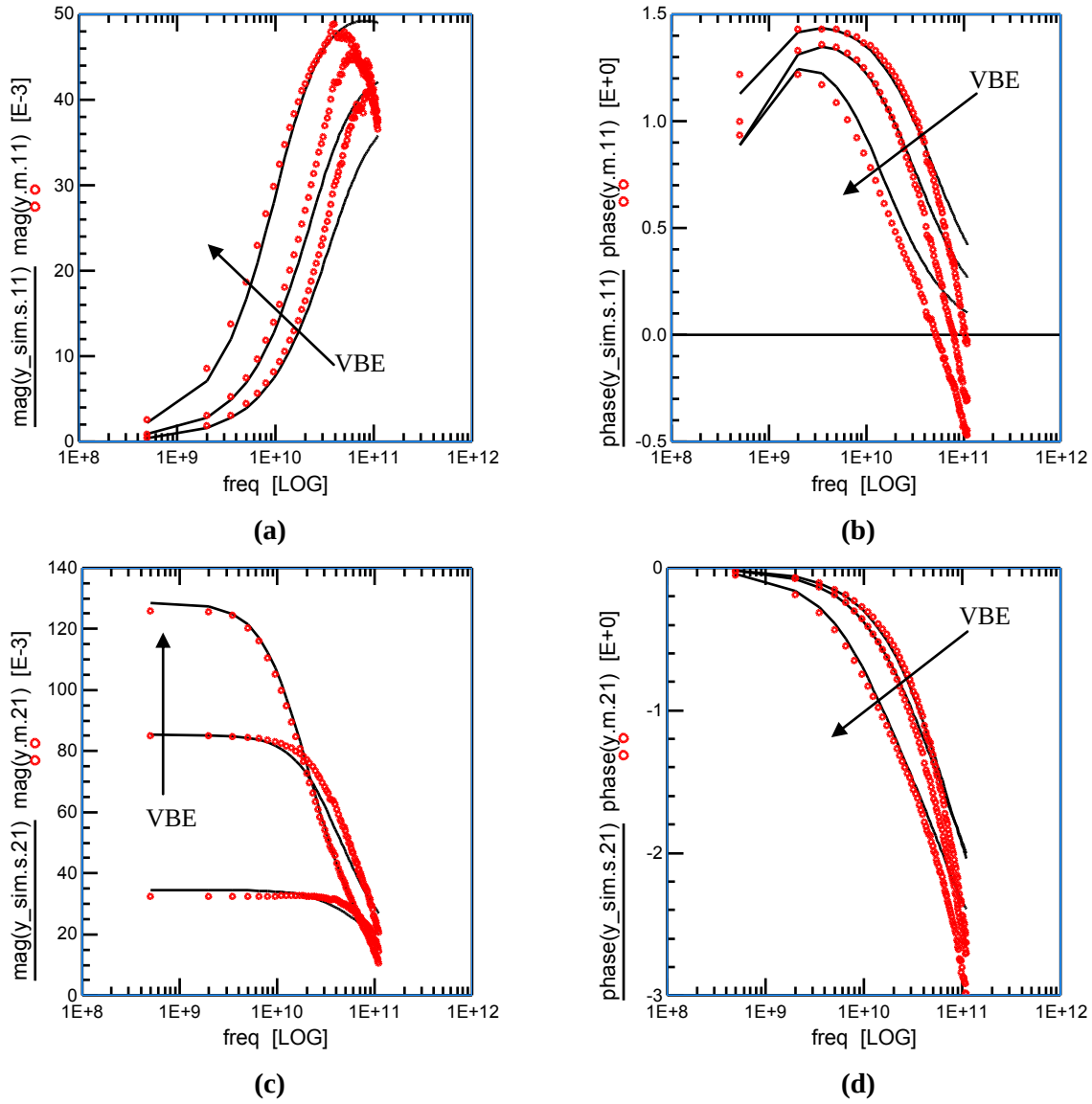

Figure **3.13**: Magnitude and Phase of Y_{11}, and Y_{21} showing Non Quasi Static effect at high frequency for different V_{BE} = 0.84V, 0.88V, 0.92V at V_{CE}= 1.6V.

Modeling results of magnitude and phase of Y_{11} and Y_{21} parameters show a acceptable fitting at high frequencies. It can be observed that the phase of Y_{11} is not properly modeled at high frequency.

Previous modeling results show an acceptable result for both the Y and h parameters at high frequency. It is also pointed that at very high frequencies, the NQS modeling is not always perfect while considering the imaginary part of Y_{21} or phase of Y_{11} parameters.

Though the measurements were performed beyond the transistors maximum cut off frequency (60GHz) there was no significant effect observed in y parameters except that there is a sudden decrease of y_{11} magnitude at higher frequency (Figure **3.13**).

3.3 NQS modeling ST B3T process withB9MW layout

Now, we consider a very modern transistor which is having a high cut off frequency (fTpeak= 240GHz). The transistor is fabricated by ST microelectronics in B9MW layout and corresponds to B3T technology. A TEM photograph of the device with a schematic is presented below [11],

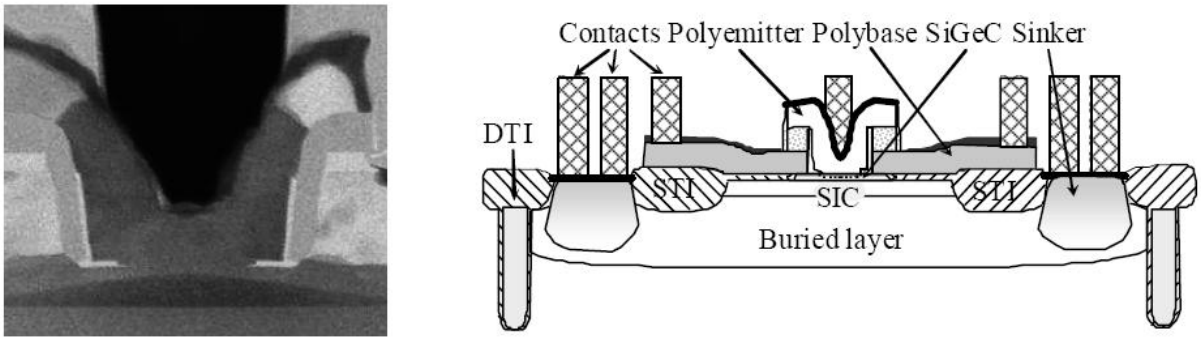

Figure **3.14**: ST BiCMOS9MW layout. Left figure shows the TEM picture and on the right hand side the device structure [11].

3.3.1 Modeling with HICUM model

Without going to the further details of step by step modeling, we directly concentrate to the NQS behavior observed in this technology. For the static and dynamic set of parameters a scalable model card is used throughout this investigation. The scalable model card (without NQS modeling) was provided by Xmod technology. As the capacitance, transit time and series resistance parameters are properly modeled inside this model card, NQS parameter optimization can be performed for a wide range of transistors. The transistors under this investigation contain different emitter lengths (L_E= 3, 5, 10µm) as well as different emitter widths (W_E=0.27, 0.54, 0.84, 1.08µm) while all having 1 emitter, 1 base and 1 collector contact respectively. NQS related parameters (alit, alqf) are optimized from phase of h_{21} from frequency sweep ac measurement considering a constant V_{CE} (V_{CE}= 1.2V) and different V_{BE} (V_{BE}=0.76V, 0.80V, 0.84V, 0.88V, 0.92V). The next figure (Figure **3.15**) indicates the modeling of h_{21} parameter for transistor with different emitter lengths but the same emitter width (0.27µm) and having one emitter, one base and one collector contact respectively.

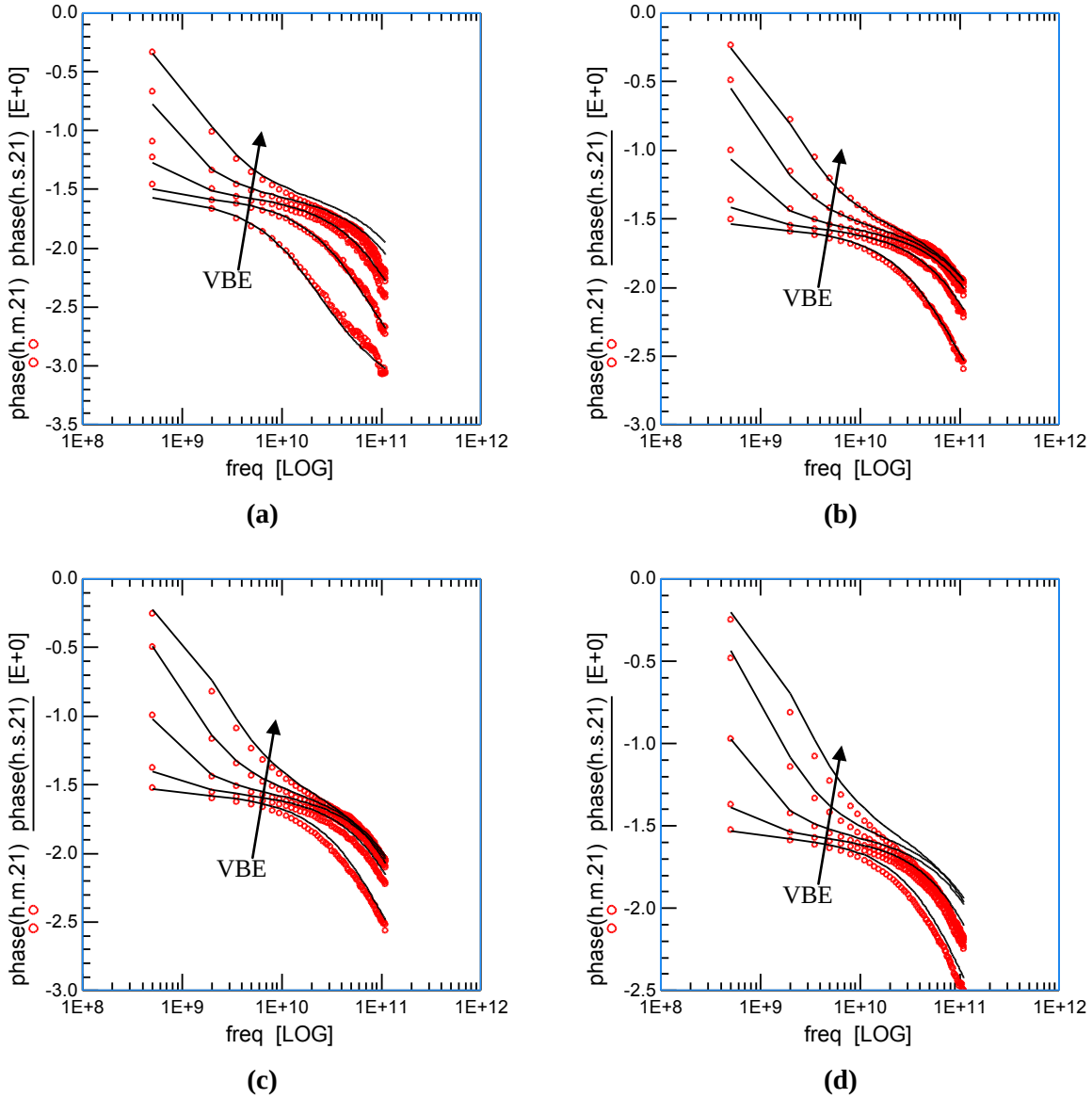

Figure **3.15**: Modeled phase h_{21} for different emitter lengths (L_E= 0.6, 3, 5, 10 µm) at an emitter width W_E= 0.27µm at V_{CE}= 1.2V and V_{BE}=0.76V, 0.8V, 0.84V, 0.88V, 0.92V. All these transistors are having one base one emitter and one collector contact respectively. Emitter lengths are (a) L_E= 0.6µm, (b) L_E= 3 µm, (c) L_E= 5 µm, (d) L_E= 10 µm.

Previous figure (Figure **3.15**) compares the phase of h_{21} parameter between different transistors. The NQS modeling provides a good global fitting up to high frequency. But, it is also noted that for the transistor having a large emitter length (L_E= 10µm), the modeling is not so satisfactory. It is shown in the next figure by plotting phase of h_{21} separately for different V_{BE}.

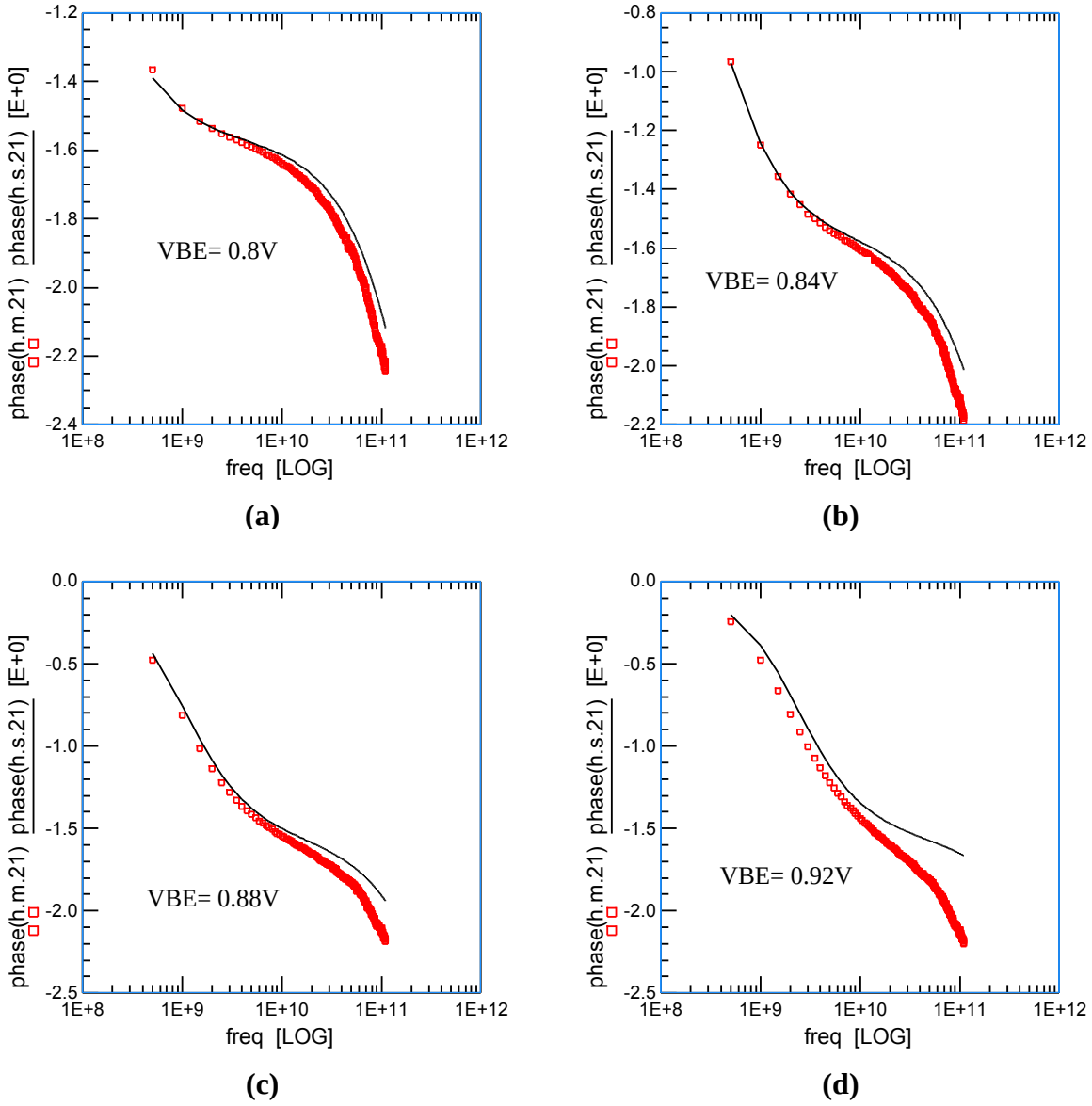

Figure **3.16**: Phase h_{21} for a single transistor with emitter length L_E= 10 µm and emitter width W_E= 0.27µm at V_{CE}= 1.2V and different V_{BE}= 0.8V, 0.84V, 0.88V, 0.92V.

It is quite clear from the previous figure (Figure **3.16**) that the high frequency modeling of small signal current gain needs to be improved. Now, the modeling results of Magnitude and Phase of Y_{11} and Y_{21} is shown for the same measurement configuration in the same transistor.

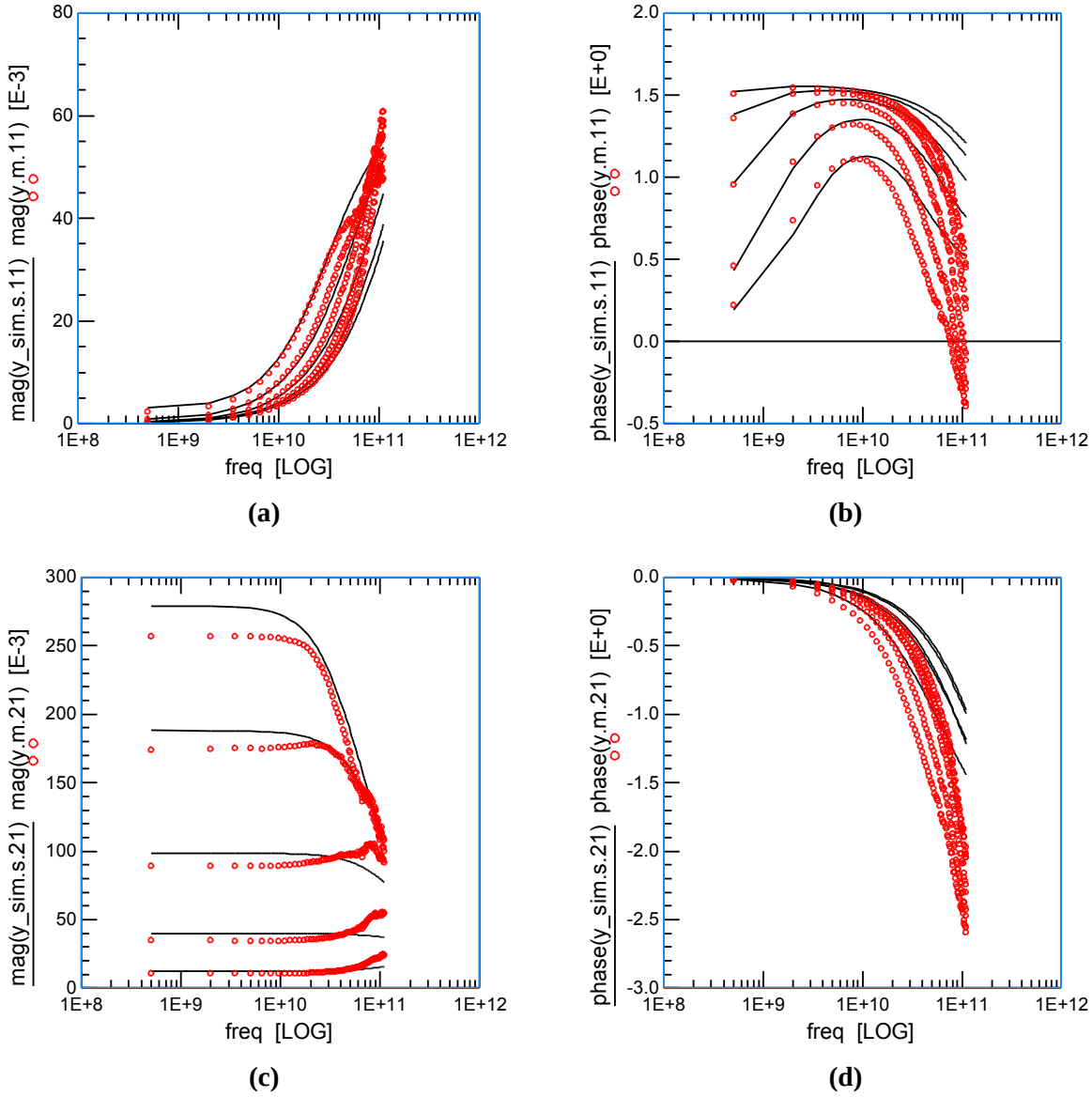

Figure **3.17**: (a, b) Magnitude and Phase of Y_{11} parameter for a single transistor at V_{CE}= 1.2V and V_{BE}=0.76V, 0.8V, 0.84V, 0.88V, 0.92V. (c, d) Magnitude and Phase of Y_{21} parameter for a single transistor at V_{CE}= 1.2V and V_{BE}=0.76V, 0.8V, 0.84V, 0.88V, 0.92V.

Again, from the Figure **3.17** the modeling inconsistency at high frequency is clearly observed. The phase of input admittance (Y_{11}) and phase of transconductance (Y_{21}) parameters are not properly modeled at higher frequencies by the existing HICUM model.

For transistors with different emitter widths (W_E=0.54, 0.84, 1.08µm) measurement shows sudden phase increase at high base emitter voltage. Modeling results of h_{21} parameters for transistors with large emitter area are presented in figure **3.18**. It can be noted that the h_{21} parameter shows a kink at high base emitter voltage for transistors with large emitter widths (0.54µm, 0.84µm, 1.08µm).

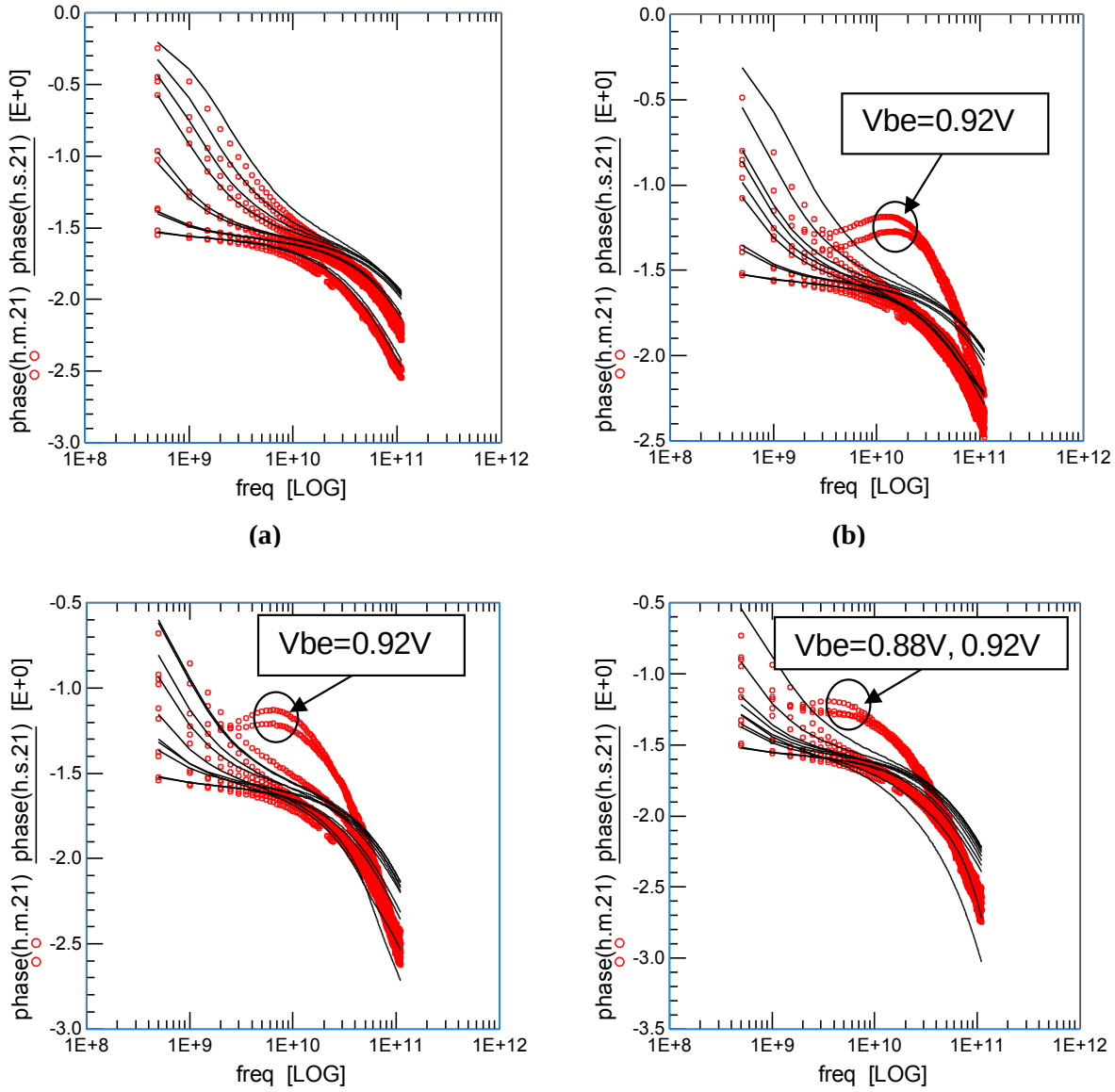

Figure **3.18**: Phase h_{21} for different emitter widths (W_E= 0.27µm, 0.54 µm 0.84 µm, 1.08µm) at an emitter length L_E= 10µm at V_{CE}=0.8, 1.2V and V_{BE}=0.76, 0.8, 0.84, 0.88, 0.92V. Emitter widths are (a) W_E= 0.27µm, (b) W_E= 0.54µm, (c) W_E= 0.84µm, (d) W_E= 1.08µm respectively.

It is difficult to optimize NQS parameters at high injection as phase h_{21} shows a kink for transistors having higher emitter widths (Figure **3.18**). Phase of h_{21} parameter is compared for a single V_{BE} for different transistors (W_E= 0.27µm, 0.54 µm 0.84 µm, 1.08µm) and shown below,

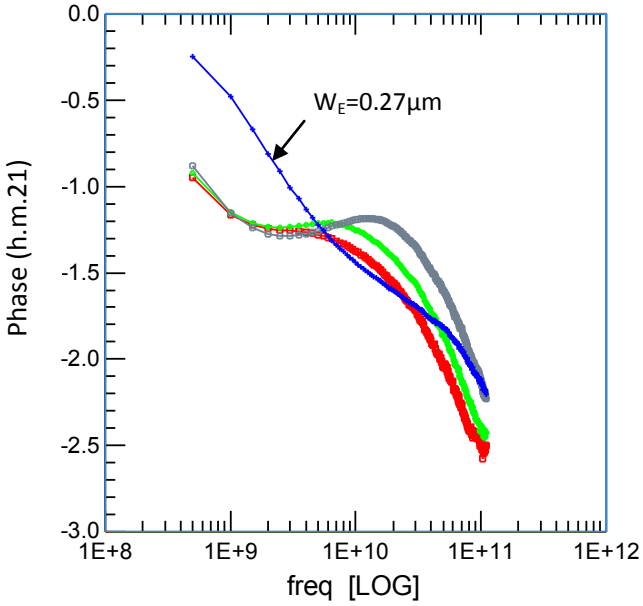

Figure **3.19**: Comparison of measured h_{21} phase of different transistors of emitter widths W_E=0.27, 0.54, 0.84, 1.08µm at V_{CE}=1.2V and V_{BE}=0.92V.

The inconsistency which is observed in phase of h_{21} is also present in Y parameters at high injection condition. Magnitude and phase of Y_{11} and Y_{21} are compare for different transistors at high injection (V_{BE}= 0.92V) and presented in the next figure,

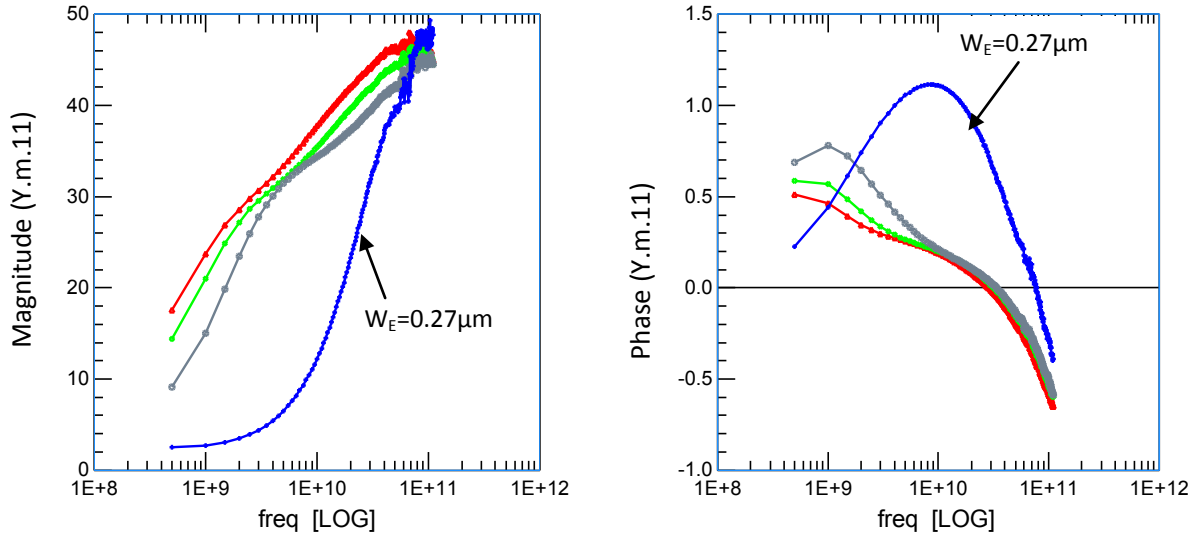

(a) **(b)**

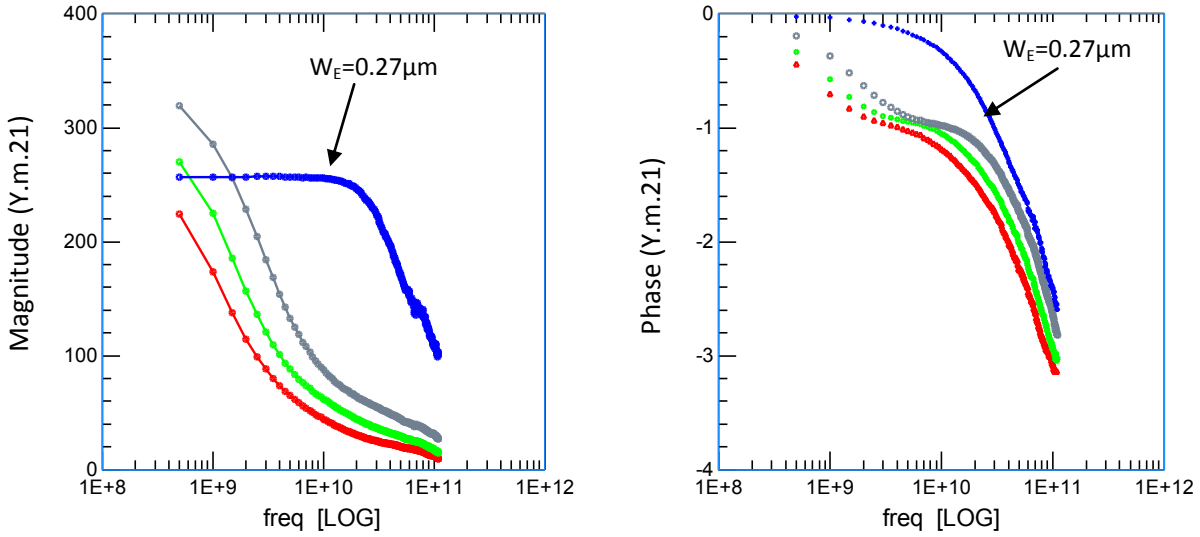

(c) **(d)**

Figure **3.20**: Comparison of measured $Y_{11}$and Y_{21} magnitude and phase of different transistors having emitter widths W_E=0.27, 0.54, 0.84, 1.08µm at V_{CE}=1.2V and V_{BE}=0.92V.

3.3.2 Scaling of NQS related parameters with HICUM model

In the previous part, NQS modeling results with HICUM L2V24 are shown for different transistors for a wide range of bias points. Next, the optimized NQS related parameters (alit, alqf) are tabulated and scaling issues are examined

- **Low injection**

As it is difficult to optimize NQS parameters for a wide bias range, the modeling was done splitting the bias range into medium and high injection region and parameters are extracted at medium injection condition. The problem of high injection is shown in previous figures (Figure **3.19, 3.20**) where the h_{21} phase shows some kink at higher injections.

Next figure (Figure **3.21**) presents NQS parameters in a transistor where the emitter length is 3µm and width is 0.27µm.

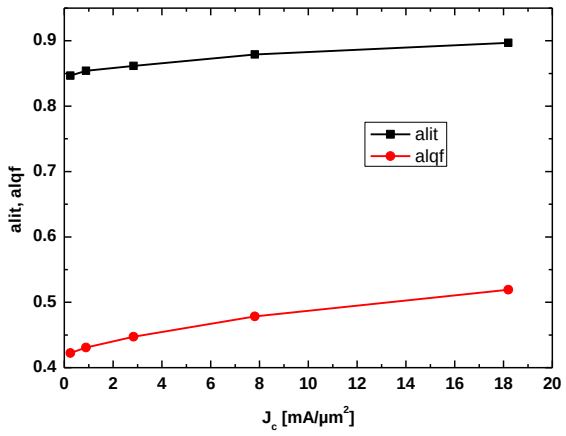

Figure **3.21**: HICUM NQS related parameters as a function of collector current density in a transistor where L_E= 3µm, W_E= 0.27µm at V_{CE}= 1.2V and V_{BE}=0.76V, 0.8V, 0.84V, 0.88V, 0.92V.

From the Figure **3.21**, it can be observed that the NQS related parameters are almost constant at high current density. The scenario is quite different for the transistors having higher emitter area (low current density).

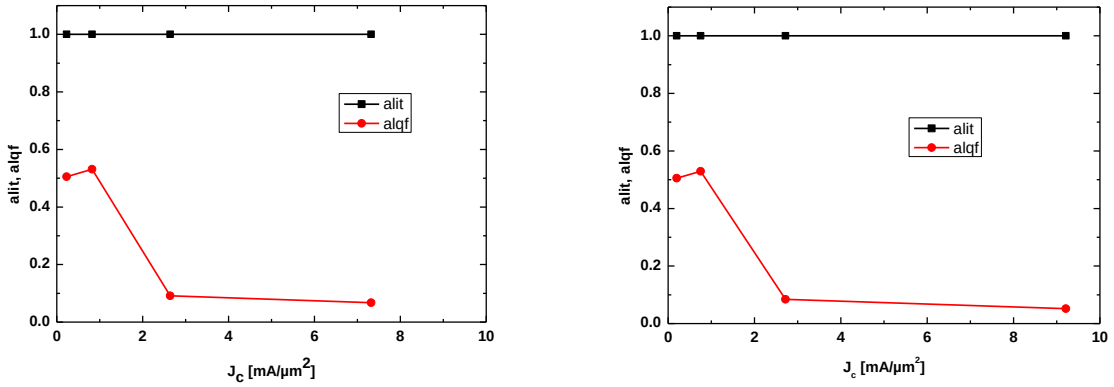

(a) **(b)**

Figure **3.22**: HICUM NQS parameters in two different transistors (a) L_E= 10µm, W_E= 0.27µm and (b) L_E= 10µm, WE= 0.54µm at V_{CE}= 1.2V and V_{BE}=0.76V, 0.8V, 0.84V, 0.88V.

The nature of the parameters as shown in Figure **3.21** is not totally followed when the transistors with higher emitter widths are considered. The difference is clearly observed in the high current density region, where the alqf parameter undergoes a sharp fall from the average value.

To compare the extracted parameters as a function of real emitter area, only two bias points below f_T are considered (V_{BE}=0.76V, 0.8V) because the high injection parameters are not consistent for large devices. The real emitter area is calculated after subtracting the spacer width of 55nm at both sides.

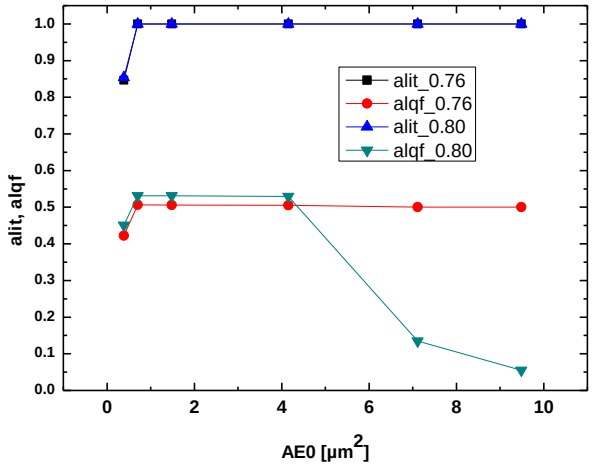

Figure **3.23**: alit and alqf as function of emitter area at V_{CE}= 1.2V and V_{BE}=0.76V, 0.8V.

While the alit parameter is almost constant at 1, alqf suddenly decrease at high emitter area transistors at V_{BE}= 0.8V. Last of all, variation of these parameters along emitter length is shown considering two bias points.

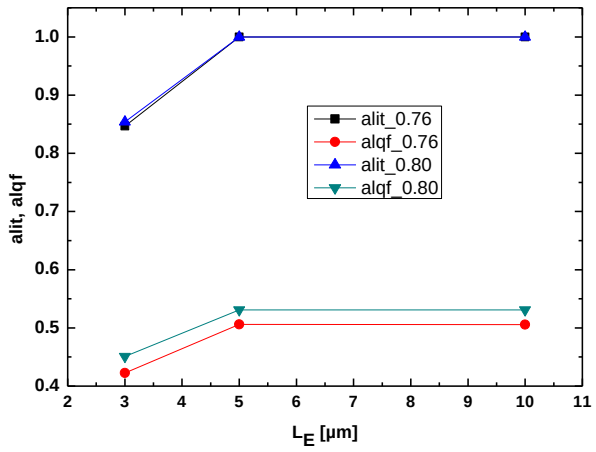

Figure **3.24**: alit and alqf as function of emitter length at V_{CE}= 1.2V and V_{BE}=0.76V, 0.8V.

From the previous analysis it is clear that the NQS parameters (alit, alqf) are very close to have constant values over emitter length but alqf decreases rapidly over real emitter area It is, therefore, possible to fix the parameters value (alit=1, alqf=0.5) inside the model code to have an overall fit over dynamic parameters without losing the accuracy of NQS modeling.

3.3.3 HICUM model with an extended phase network

It is shown in the previous part that at high frequency, the phase of h_{21} cannot be modeled properly with the existing HICUM model. As the phase network comes from a physical understanding of NQS behavior, the improvement should also contain physical basis. In this work, the effect of base collector (BC) junction delay, which was not previously included inside this model, is investigated. A new excess phase circuit is proposed including the BC junction delay. The modeling results show improvement in h_{21} phase at higher frequencies.

3.3.3.1 Model calculation

In a modern HBT transistor, with graded base profile, the built-in electric field reduces the base transit time significantly. As a consequence of this process, the signal delay due to the BC junction has become an important contributing factor in the total delay. Base-collector junction (BC) is considered as high field region where carrier travels at a constant velocity which is the saturation velocity inside that region. Assuming that the excess minority carrier concentration at the base collector junction boundary is zero and no recombination takes place inside the junction, it has been shown in the chapter 1 (equation **1.61** and equation **1.62**) that the BC junction introduces a delay which is proportional to the collector transit time. Quoting equation **1.62** of chapter 1 that assumes a small signal transfer current, entering the BC junction, the resultant current leaving the junction is described by,

$$\tilde{i}_c'(x) = \tilde{i}_c(x).\frac{\sin(\omega\tau_c)}{\omega\tau_c}.e^{-j\omega\tau_c} \qquad \textbf{3.43}$$

Where, τ_c is the collector transit time which depends upon the BC junction width and on the carrier saturation velocity in the junction and x is the length dimension in the device. The magnitude of, equals to, is nearly unity even at higher frequencies. So the small signal transfer current only encounters an exponential delay without changing the current magnitude while passing the base collector junction

Recalling Winkel's formulation of common emitter (CE) transconductance parameter, one gets,

$$y_{21}^{e} \approx g_f \exp(-j\omega\tau_1^*) \qquad \textbf{3.44}$$

Here, g_f represents the low frequency forward conductance and τ_1^* includes the bias dependent time delay. Including the BC junction delay inside the admittance parameter calculation of Winkel [8], Equation **3.44** becomes,

$$y_{21}^{e} \approx g_f \exp(-j\omega\tau_1^*)\frac{\sin(\omega\tau_c)}{\omega\tau_c}.e^{-j\omega\tau_c} \qquad \textbf{3.45}$$

Equation **3.45** can be simplified after expanding the BC junction time delay function in Taylor's series and considering up to the second term,

$$y_{21}^{e} \approx g_f \exp\left(-j\omega\tau_1^*\right)*(1-j\omega\tau_c) \qquad \textbf{3.46}$$

Equation **3.46** shows the final form of transconductance where τ_c represents the collector transit time. The first part of this equation is the same as before (Equation **3.44**) and the multiplicative constant represents an additional part due to the BC junction delay.

3.3.3.2 Implementation inside HICUM

To include the new formulation inside HICUM L2V24, equation **3.35** is restructured to give a simple form,

$$\underline{I}_{Ci} = \underline{I}_{Ci0} \frac{(1 - j\omega(altc * \tau_f))}{(1 + j\omega(alit * \tau_f))} \qquad \textbf{3.47}$$

altc is a new parameter representing the BC junction delay. Again, changing the domain by putting $s \equiv j\omega$ in equation **3.47** and with a suitable approximation [12], we get the final form of transfer current which will be implemented inside HICUM via VerilogA code

$$I_{txf} \approx \frac{I_{tzf}}{1 + sT_D} * \frac{(1 - sT_c/2)}{(1 + sT_c/2)} \qquad \textbf{3.48}$$

Next, an excess phase circuit is constructed and shown in Figure **3.25**. This circuit contains two extra nodes (xf1 and xf2) similar to the HICUM model.

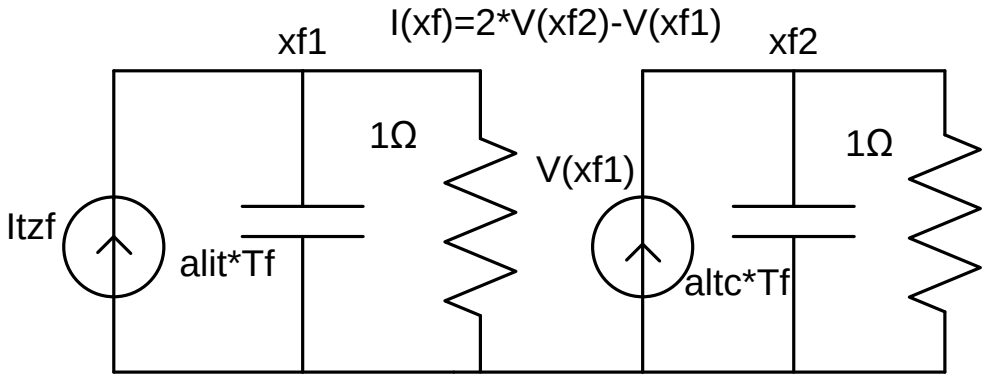

Figure **3.25**: Modified excess phase network for transfer current.

In NQS equivalent networks, 1Ω resistors are commonly used at the output node. Doing so, the current through the resistor is equal to the voltage over its nodes. When writing the circuit node equations, the 1Ω multiplication factor is omitted resulting in a mix-up of current and

voltages but the aim of the NQS network is only the mimic of a mathematical relationship. In the improved excess phase circuit, output current of the first branch is taken as an input of the second branch (Figure **3.25**). The circuit equations are formulated below.

$$I_{tzf} = \frac{d}{dt}(\alpha_{lit} * T_f * V(xf1)) + V(xf1) \qquad \textbf{3.49}$$

$$V(xf1) = \frac{d}{dt}(\alpha_{ltc} * T_f * V(xf2)) + V(xf2)$$

And the transfer function [12] which gives the final branch current (Equation **3.48**) is,

$$I_{txf} = 2 * V(xf2) - V(xf1) \qquad \textbf{3.50}$$

3.3.3.3 Modeling result with the extended model

The improved circuit equation (Equation **3.48**) is implemented inside the HICUM model via the VerilogA code. The improved model requires an extra parameter (altc) along with the previous parameters alit and alqf. The new parameter altc is considered as BC junction delay factor and it can attain a maximum value of 1. The same model card is used with the improved excess phase circuit where only the new parameter altc is optimized. The results are shown below for two different bias points.

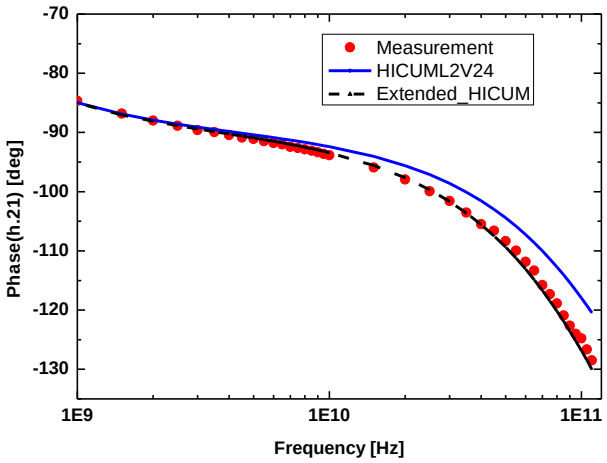

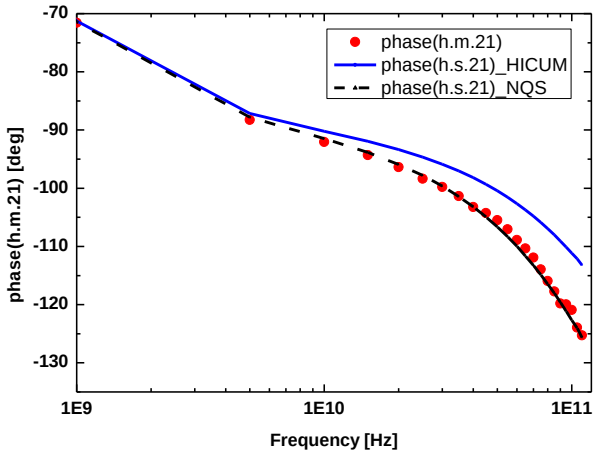

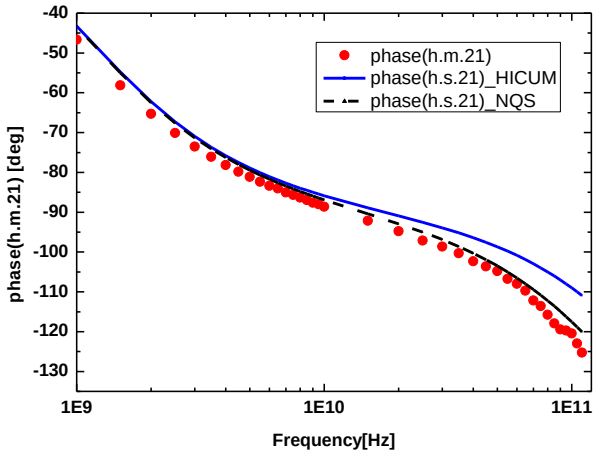

Figure **3.26**: h_{21}: phase with extended HICUM with L_E=10µm, W_E=0.27µm at a constant V_{CE}=1.2V and V_{BE} =0.8V, 0.84V, 0.88V.

3.4 Conclusion

In this chapter, compact modeling implementation of NQS effect is discussed while showing some modeling results. Two types of transistors with different technologies are chosen for modeling. The first technology is BiCMOS7RF, which provides a cut off frequency of 60GHz. In this transistor, a step by step modeling and HICUM specific parameter extraction was performed before proceeding to the NQS modeling. High frequency modeling was performed and the modeling results show a considerable fitting of dynamic parameters up to high frequency. It is also shown from the input admittance modeling that there is a scope to further improve the excess phase network.

In the next step, transistor with a very modern technology is considered to perform the NQS modeling. There a scalable model card is used and NQS modeling is performed in a vast range of transistors with different emitter lengths and widths. Modeling of high frequency phase of small signal current gain, input admittance and transconductance are presented. From the modeling results it is clear that the existing HICUM excess phase network does not provide an exact fitting in transistors having higher emitter dimension. To overcome the inconsistency, an improved network is proposed which accomplish a time delay due to the base collector junction. The implementation of the new model is done by VerilogA code in the HICUM model. After that, the modeling results compare these two models and clearly establish that the new model works better than the previous one.

Reference

[1] http://www.iee.et.tu-dresden.de/iee/eb/hic_new/hic_doc.html, "HICUM L2 Documentation."

[2] John D. Cressler, *Measurement and Modeling of Silicon Heterostructure Devices*.

[3] Michael Schroter, Anjan Chakravorty, *Compact Hierarchical Bipolar Transistor Modeling With Hicum*, World Scientific Publishing Company, Oct 2010

[4] Thesis Bertrand ARDOUIN, "CONTRIBUTION A LA MODELISATION ET A LA CARACTERISATION EN HAUTES FREQUENCES DES TRANSISTORS BIPOLAIRES A HETEROJONCTION Si/SiGe," BORDEAUX I.

[5] Fregonese, S.; Zimmer, T.; Maneux, C.; Sulima, P.Y., "Barrier effects in SiGe HBT: Modeling of high-injection base current increase," *Proceedings of the 2004 IEEE Bipolar/BiCMOS Circuits and Technology Meeting*.

[6] H. K. Gummel and H. C. Poon, "An integral charge control model of bipolar transistors," *Bell Syst. Tech. J*, vol. 49, pp. 827–852.

[7] http://www.designers-guide.org/VBIC/, "VBIC model."

[8] te Winkel, J., "Extended charge-control model for bipolar transistors," *Electron Devices, IEEE Transactions on*, 1973, vol. 20, pp. 389 - 394.

[9] STMicroelectronics, "STMicroelectronics Deep Sub-Micron Processes 120nm, 90nm, 65 nm, 45nm CMOS," Jan. 2008.

[10] Thesis Dominique Berger, "ETUDE ET VALIDATION D'UN MODELE DE TRANSISTOR BIPOLAIRE DEDIE AUX APPLICATIONS HAUTES FREQUENCES," BORDEAUX I.

[11] Thesis Christian RAYA, "MODELISATION ET OPTIMISATION DE TRANSISTORS BIPOLAIRES A HETEROJONCTION Si/SiGeC ULTRA POUR APPLICATIONS MILLIMETRIQUES," L'UNIVERSITE BORDEAUX I.

[12] MCANDREW Colin C.; HUSZKA Zoltan; CORAM Geoffrey J., "Bipolar Transistor Excess Phase Modeling in Verilog-A," *THE 2008 BIPOLAR/BICMOS CIRCUITS AND TECHNOLOGY MEETING*.

Chapter 4

[DEVICE SIMULATION RESUTLS]

4.1. Introduction

In this chapter, physical device simulation results are presented for SiGe HBT devices. Here, two kinds of device are considered- a conventional high speed HBT and a new type of HBT device with a SiGe spike incorporated inside emitter. The working device is first calibrated with measurements and then DC and AC simulations are performed with the calibrated parameter file. As all the simulations are performed in a calibrated structure, the simulation results can be treated as measured data with the real device. The simulated data are then exported to ICCAP to perform compact modeling. For compact modeling purpose, HICUM model is chosen due to its ability to model high injection operation properly. A systematic modeling was performed and the results are shown in this chapter.

In the device simulation, very high frequency simulation (500GHz) was performed and simulated data were modeled using HICUM model. The aim is to verify the HICUM excess phase circuit at very high frequencies. The modeling results of high frequency phase shift of dynamic parameters, shown in this chapter, provide a better understanding of the NQS phenomena. The next table (Table **4.1**) indicates the basic schematic of the overall process.

	STEP	Input	output
1	**Measurement**	Real transistor on wafer	Electrical measurement data
2	**Device Simulation**	Device structure	Device simulated data
3	**Calibration**	Device structure	Electrical measurement ≈ Device simulation
4	**Compact model**	Device simulation	• Model parameter file • NQS modeling result

Table **4.1**: A step by step procedure to obtain NQS related compact modeling parameters from device simulation results.

4.2. Simulation of IMEC structure

The device used for physical simulation is incorporated in 130 nm SiGe BiCMOS process technology by IMEC [1]. This advances HBT has a high cut off frequency (fTpeak= 240GHz) and it is widely used for high speed application [2]. Keeping in mind the symmetry of transistor structure only half the whole transistor is used in device simulation. Next figure (Figure **4.1**) indicates the 2D device structure used in the simulation. In this device the SiGe poly emitter is doped using Arsenic, the SiGe base is doped using Boron and the substrate and collector regions are doped using phosphorus and Arsenic. These graded Ge profile and doping profiles are identical to the profiles used for HBT structure as shown in figure **4.1**.

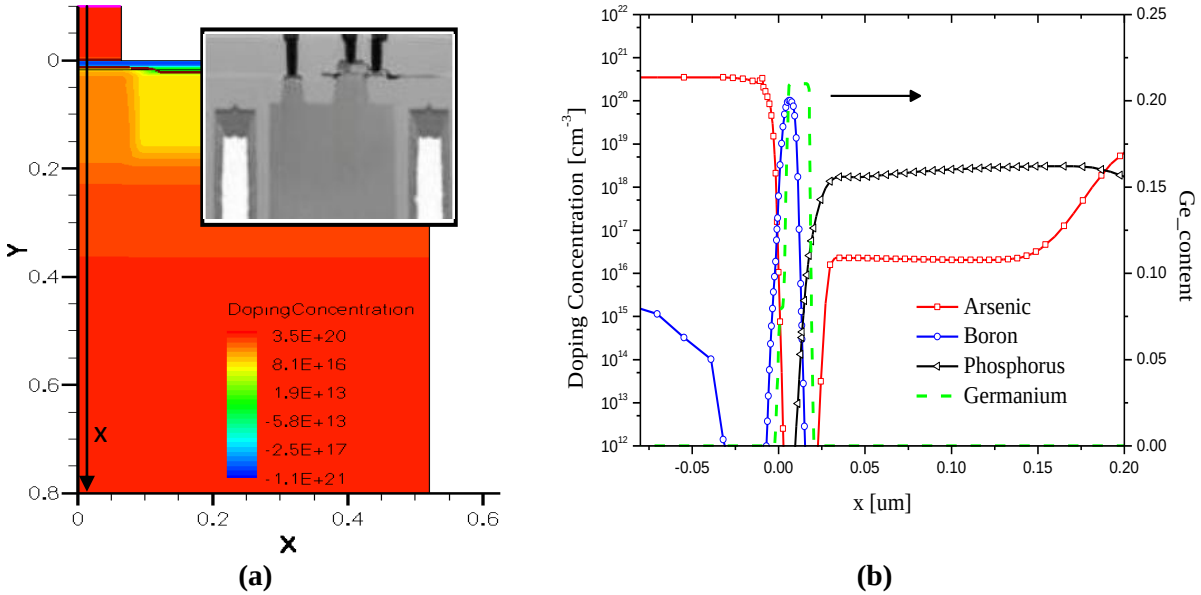

(a) **(b)**

Figure **4.1**: (a) IMEC HBT device showing the vertical cut at the middle of the base (inset: IMEC 130nm process TEM picture.) (b) The doping profiles in the emitter, base and collector regions.

4.2.1. Calibration

To use the device as a substitute for the real transistor, first the device has to be calibrated with measurements. TCAD Sentaurus [3] software tools have been used to perform the 2D device simulations using hydrodynamic model (HD) equations with a set of suitable physical models. The physics of semiconductor device is discussed in chapter 2. In this simulation, the carrier temperature equation for the dominant carriers is solved together with the electrostatic Poisson equation and the carrier continuity equations. The carrier mobility's have been calculated using Philips unified mobility model, the high field saturation was calculated

through the Canali model by using carrier temperatures as the driving force. Also, doping-induced bandgap narrowing model has been employed. The carrier generation-recombination models used are the Shockley–Read–Hall recombination model including the band to band tunneling by Hurkx model and Auger recombination model. Different calibration results for DC and AC calibration are shown below.

- **Gummel plot:**

Figure **4.2** shows measured and simulated collector (Ic) and base (Ib) currents at V_{CB}=0V (Gummel plot). To adjust the collector current at high current region some lumped resistances (R_E, R_C) have been added. Self heating is included by adjusting the thermal resistance. For the base current, simulation is performed with surface and volume recombination models. SRH recombination parameters are slightly optimized to fit the measurement at low and medium injection. Figure **4.2** indicates that the simulated collector current (Ic) shows an optimistic fitting with the measurement in the forward operating region of the device. For the base current (Ib), the calibration is perfect at low and medium injection but slightly below at very high injection.

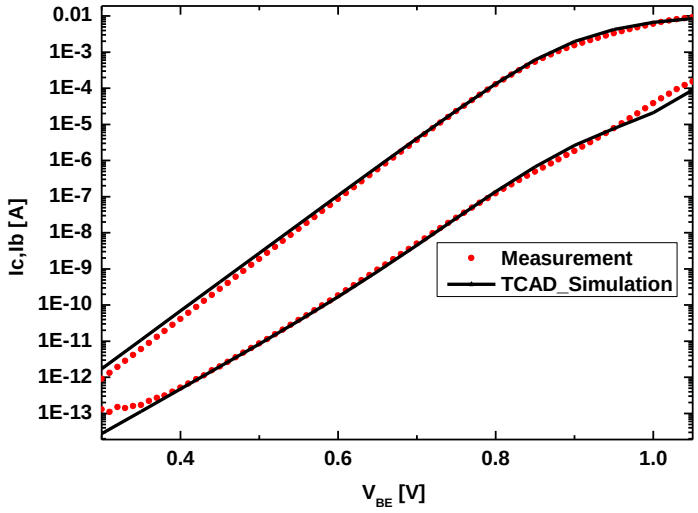

Figure **4.2**: Gummel plot comparison between measurement and TCAD simulation at V_{CB}=0V

- **Junction capacitances:**

The base-collector junction capacitance (C_{BC}), and the base-emitter capacitance (C_{BE}) are extracted from device simulation results and plotted comparing measurements and simulation

as shown in Figure **4.3**. Good agreement between measurements data and simulation results, verifying the validity of the physical models and parameters used in the TCAD simulations.

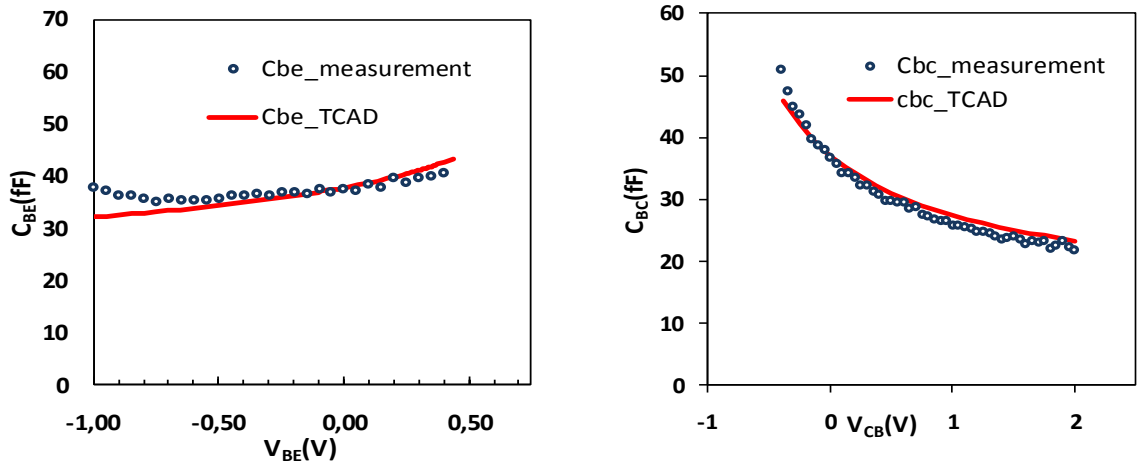

(a) **(b)**

Figure **4.3**: Junction capacitances (a) C_{BE} (b) C_{BC}. Showing both measurement and TCAD simulation.

- **Transit frequency:**

Calibrated structure is used to simulate transit frequency of the device (Figure **4.4**). The frequency sweep ac simulation is performed while keeping V_{BC} fixed at 0V and cut off frequency is extracted at 25GHz. Additional parasitic capacitances are added to fit measurement at low bias.

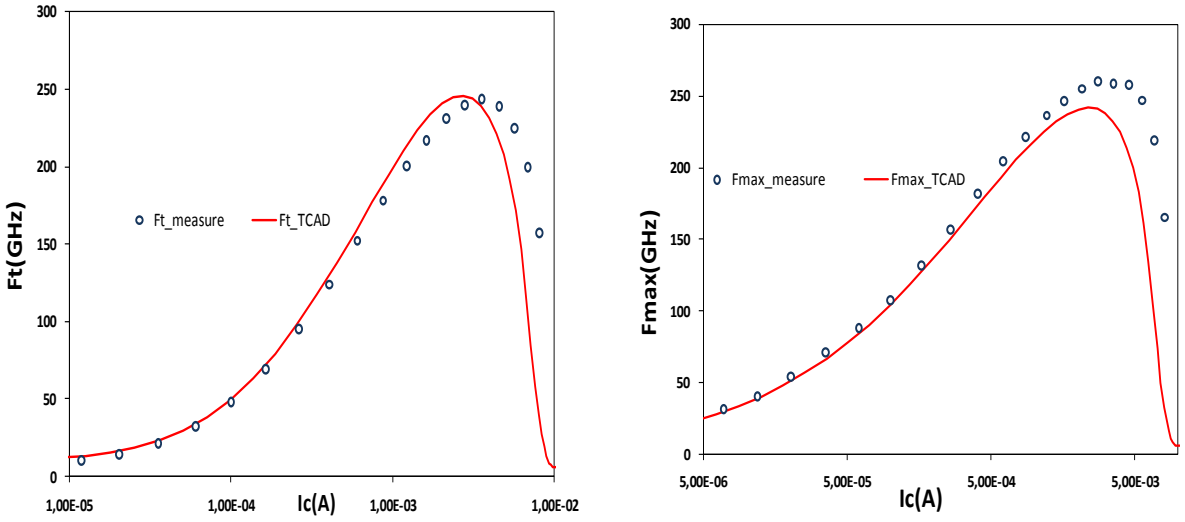

(a) **(b)**

Figure **4.4**: Measurement and TCAD simulation Ft and Fmax at V_{CB}=0V

Above figures represent the calibration of the HBT device. These plots confirm that simulated curves follow the measurement quite well. The structure is said to be calibrated and can be used to perform high frequency simulations.

4.2.2. DC and AC simulation modeling with HICUM

Device simulation results are exported to ICCAP to perform HICUM [4] modeling. Both DC and AC simulations results are exported and modeled with HICUM L2.24 model. As previously described that the device structure is calibrated with measurement, all these device simulation results can be considered as measured data. Parameter extraction is performed while following the standard extraction procedure which is described in chapter 3. Some of these extraction results are presented below.

Figure **4.5** shows the forward Gummel plot where the symbol represents the TCAD device simulated result and line represents HICUM model simulation. The modeled curve shows an exact fit at low, medium and high injection regions.

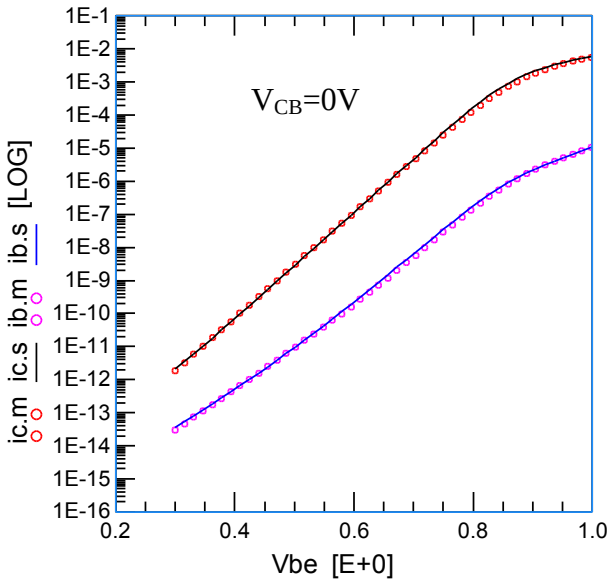

Figure **4.5**: Measured and simulated ic, ib as a function of V_{be} (Forward Gummel plot).

In the Figure **4.6**, the calibration of cut off frequency is shown for V_{CB}=0V. To obtain the Ft_Ic characteristics, AC simulation at a single frequency is performed at different V_{CE}S.

Chosen frequency for this simulation is 25GHz where unilateral gain shows a 20dB/decade slope. Peak Ft is calculated 260GHz which is true for this technology. HICUM modeling results are presented in Figure **4.6** and that confirms an acceptable modeling accuracy.

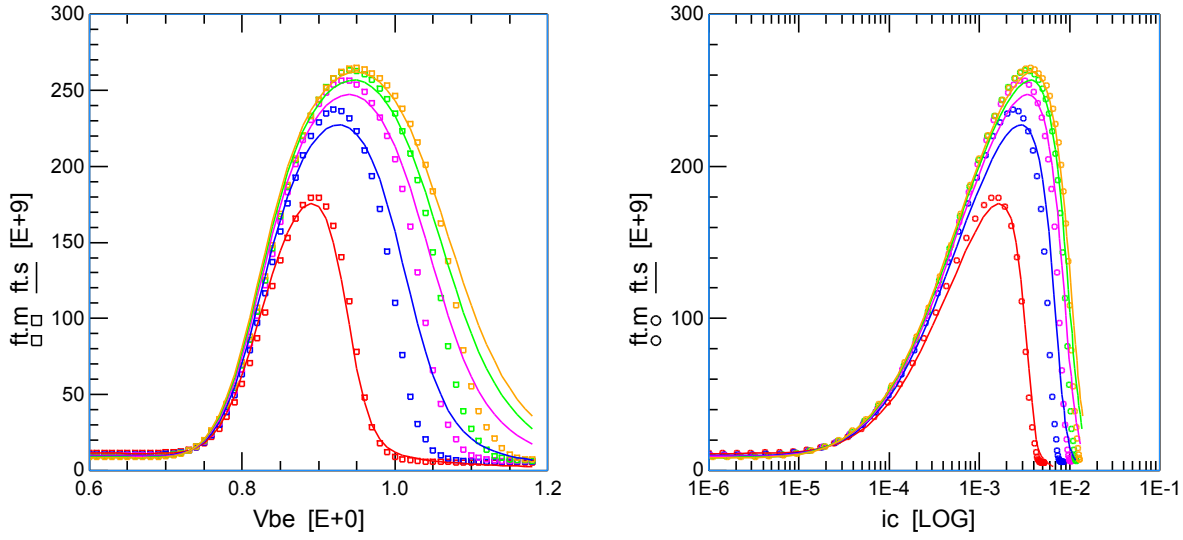

(a) **(b)**

Figure **4.6**: Measurement and simulation of (a) f_T_V_{BE} and (b) f_T_ic curve at different V_{CE}.

Some of the HICUM modeling results are presented in the previous figures. These results prove that a considerable parameter extraction has been performed and the parameter file can be used in the excess phase modeling.

4.2.3. NQS modeling

To observe NQS behavior, high frequency simulation is carried out in the IMEC device structure. This modern device structure admits the simulation to go much beyond the cut off frequency (240GHz) of the transistor. Frequency sweep ac simulation is performed up to 0.5THz and the simulated admittance parameters (Y) are then transferred to ICCAP for further modeling with HICUM. All the NQS parameters are optimized after properly extracting the forward current and transit time parameters and also adjusting base resistance. Next figure (Figure **4.7**) shows the magnitude and phase of h_{21} parameter after NQS parameters (alit, alqf) optimization. Though the simulation is performed beyond f_T, phase of

current gain (h_{21}) at high frequency certainly follows HICUM model and does not show any unexpected behavior.

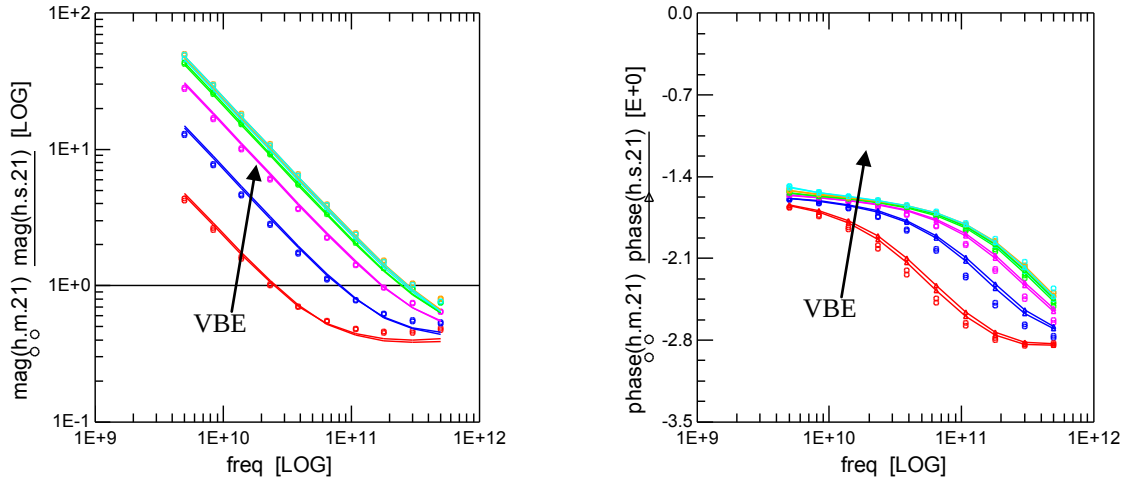

(a) **(b)**

Figure **4.7**: Magnitude and Phase of h_{21} at different V_{BE} (0.75, 0.79, 0.83, 0.87, 0.91, 0.95V) and at V_{CE}= 0.5, 1V

Magnitude and phase variations of Y_{11} and Y_{21} are shown below. Like the current gain, admittance parameters are also well modeled by the HICUM existing formulation.

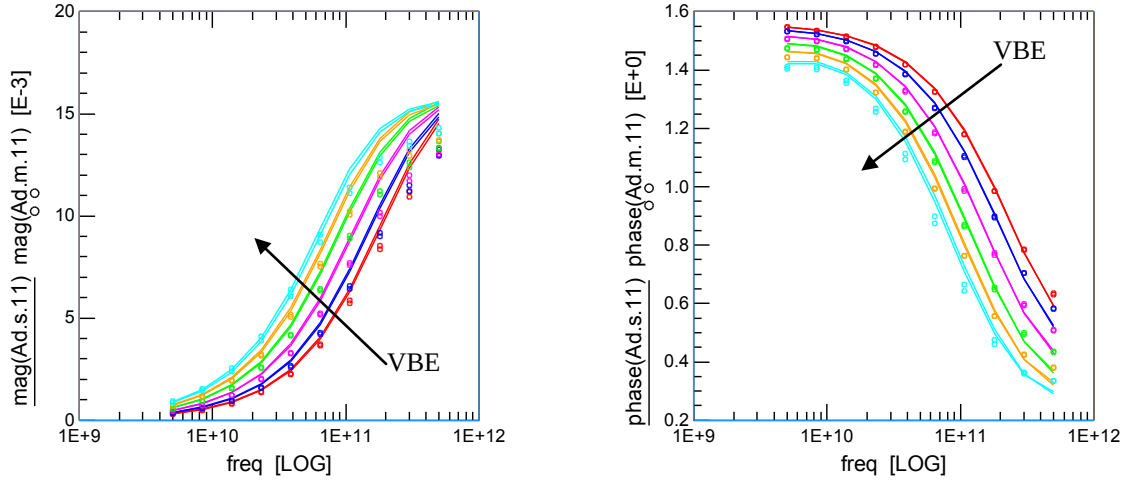

(a) **(b)**

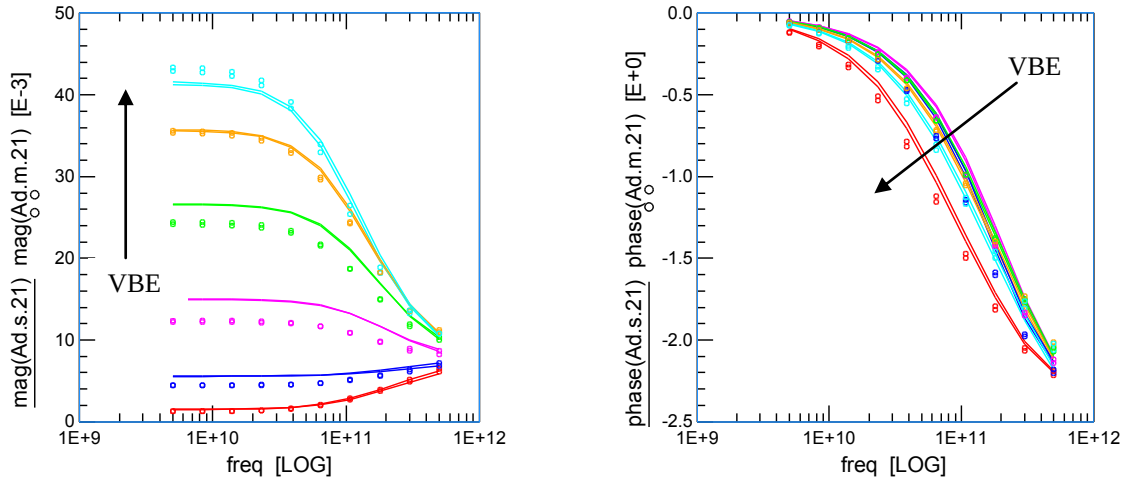

(c) **(d)**

Figure **4.8:** (a, b) Magnitude and phase of Y_{11} at different V_{BE} (0.75, 0.79, 0.83, 0.87, 0.91, 0.95V) and at V_{CE}= 0.5, 1V. (c,d) Magnitude and phase of Y_{21} at different V_{BE} (0.75, 0.79, 0.83, 0.87, 0.91, 0.95V) and at V_{CE}= 0.5, 1V.

4.2.4. Transient simulation in IMEC structure

Up to now, all the NQS results are presented considering only the AC simulation and modeling at high frequencies. The other way to investigate NQS behavior is to perform transient simulation at different frequencies and analyze in time domain. Transient simulation enables one to calculate the time delay of electrical parameters directly from the device. In chapter 1, the theoretical background of small signal operations are discussed and it can be verified from the transient simulations. To investigate transistor operations at high frequency, In the forward active mode a sinusoidal perturbation of 10mV is superimposed to the positive static bias, such that the total base emitter voltage becomes $v_{be}=V_{BE}+10mVsin(\omega t)$. Keeping the base collector junction voltage fixed (V_{BC}=0V), for different bias points (V_{BE}=0.7V, 0.8V, 0.9V, 0.95V) and for different frequency values (f=1KHz, 1MHz, 1GHz, 10GHz, 50GHz, 75GHz, 100GHz, 150GHz, 200GHz) the same device is simulated using the Hydrodynamic equations and using calibrated parameter file. Steps of this process are outlined below.

From the device simulation results, both the base and emitter excess charge are extracted (by integrating the excess carrier concentration over the vertical dimension of the device) and plotted against time.

Base charge:

Excess base charge is plotted against different frequencies considering different bias points (V_{BE}=0.7V, 0.8V, 0.9V, 0.95V). The results are presented below and discussed after.

- At low frequency (1GHz) and moderate injection (0.8V), the variation of excess minority carrier follows the variation of the applied external signal.
- At high frequency (150GHz) and moderate injection (0.8V), a delay is present between the variation of the excess minority carrier and the applied external signal.
- At high frequency (150GHz) and high bias (0.95V), the delay between the excess minority carrier density and the external signal is further enhanced.

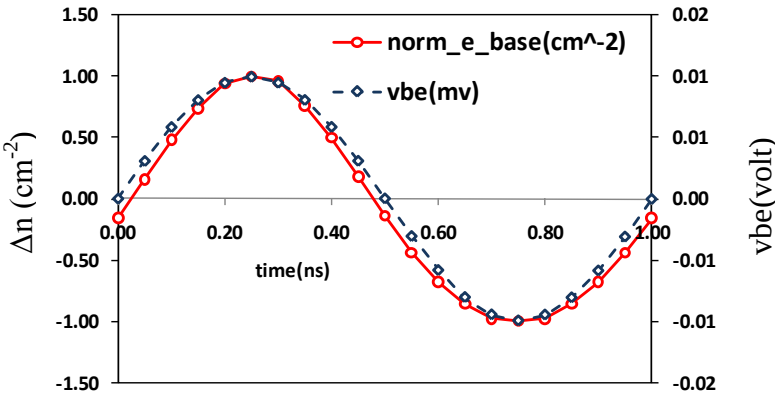

(a)

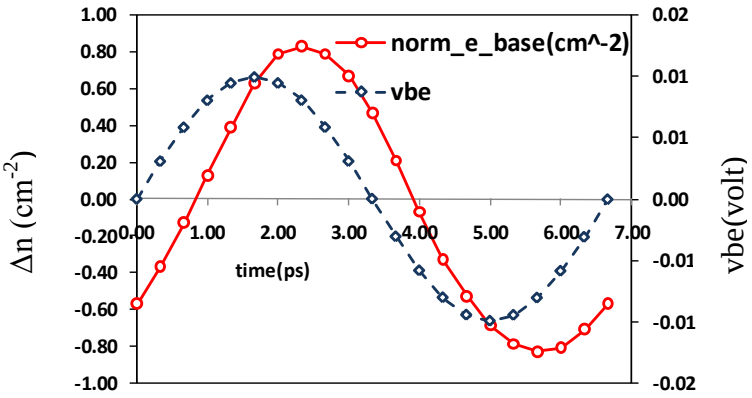

(b)

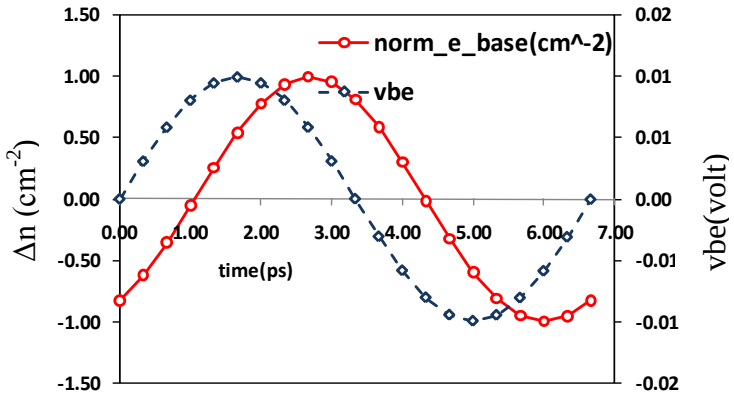

(c)

Figure **4.9**: Variation of excess minority carrier (e) density (red line) inside neutral base over time. Blue graph corresponds to the applied sinusoidal bias variation over time. For (a) V_{BE}=0.8V, f=1 GHz, (b) V_{BE}=0.8V, f=150GHz (c) V_{BE}=0.95V, f=150GHz

Analysing Figure **4.9** it is clear that the accumulated excess charge encounters a delay in high frequency operation. It is also observed that the magnitude of the base charge also varying with frequency.

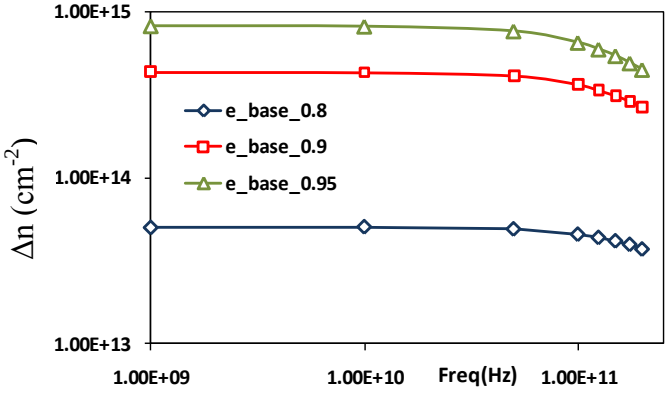

Figure **4.10**: Excess carrier (e) concentration (/cm^{-2}) over frequency in the neutral base for V_{BE} = 0.8V, 0.9V, 0.95V. It shows a gradual decay as frequency increases.

Figure **4.10** shows the frequency dependence of base charge at different base emitter voltage. The charge is constant for a wide range of frequency but at high frequencies (>100GHz) it starts to decrease. The frequency dependence of base charge is not considered inside compact model.

It has been shown that the excess base charge encounters a delay at higher frequencies (Figure **4.9**). To calculate the delay in time domain, a non linear function is fitted over the simulated

data and from the fitting parameter, time delay is calculated. The next figure represents the time delay calculation from a device simulation data,

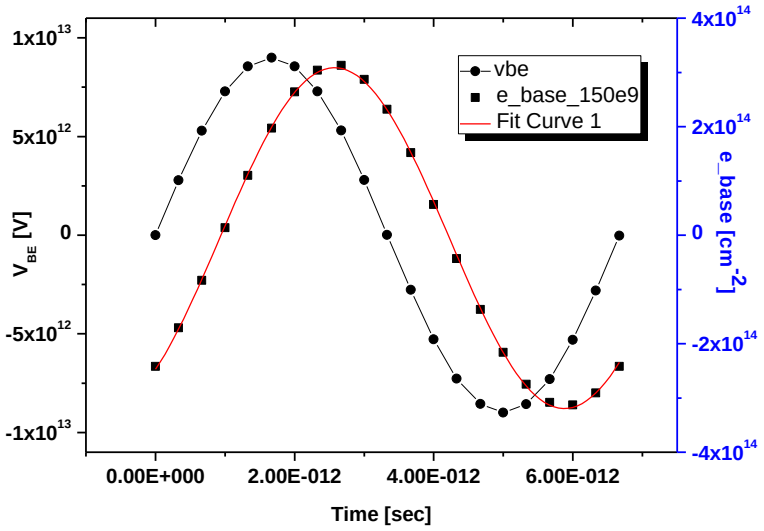

Figure **4.11**: Fitting of excess carrier concentration over time. The fitting function used is of the form, y=y0+a*sin (pi*(x-xc)/W). The parameter xc gives the time delay.

The extracted time delay is plotted over frequency,

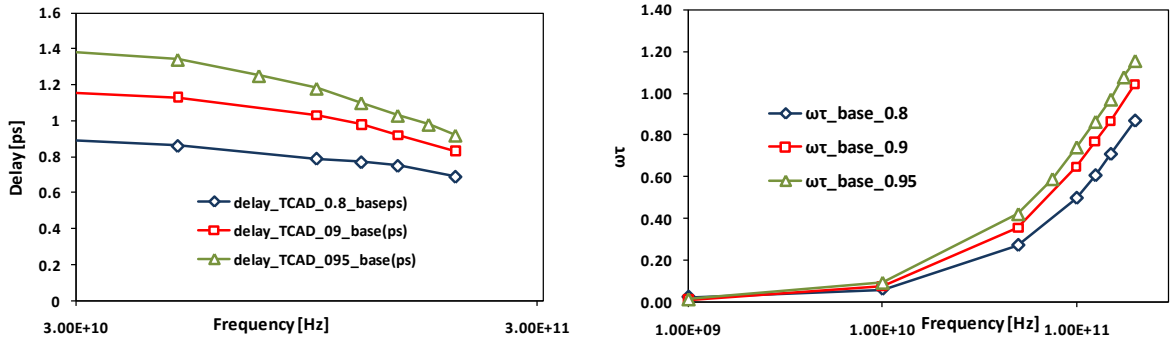

Figure **4.12**: excess charge delay inside base (a) time delay (ps) as a function of frequency; (b) time delay multiplied angular frequency (ωτ) as a function of frequency.

Base charge delay increases as the biasing voltage increase. Also, the phase shift (ωτ) increase as the frequency increases.

From the above analysis, it can be concluded that the base excess charge encounters a delay at higher frequencies. The delay increases as the bias increases and it also depends upon frequency. In the compact model formulation, phase network of excess charge is considered

to model the phase shift of dynamic parameters. The device simulation results hence prove the significance of this type of networks.

In the next part small signal transient results are shown at the neutral emitter side and the excess charge is calculated. The excess emitter charge also shows a comparable time delay for the device. The results for medium and high injection are shown below.

- At low frequency (1GHz) at moderate injection (0.8V), the variation of excess minority carrier follows the variation of the applied external signal.
- At high frequency (200GHz) and moderate injection (0.8V), a delay is present between the variation of the excess minority carrier and the applied external signal.
- At high frequency (200GHz) and high bias (0.95V), the delay between the excess minority carrier density and the external signal is further enhanced.

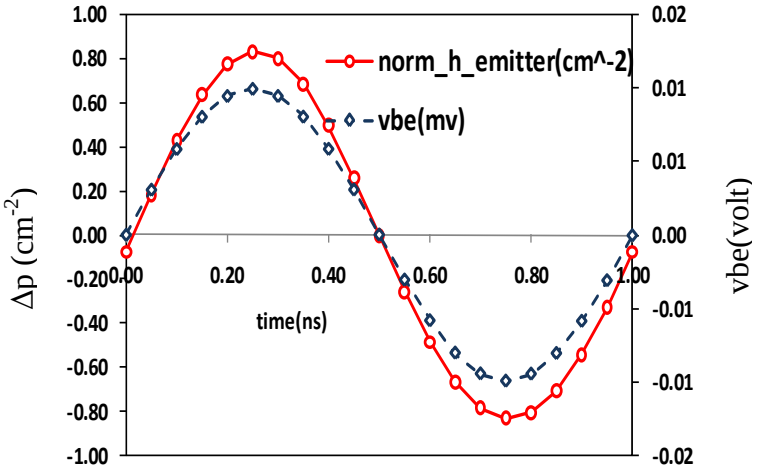

(a)

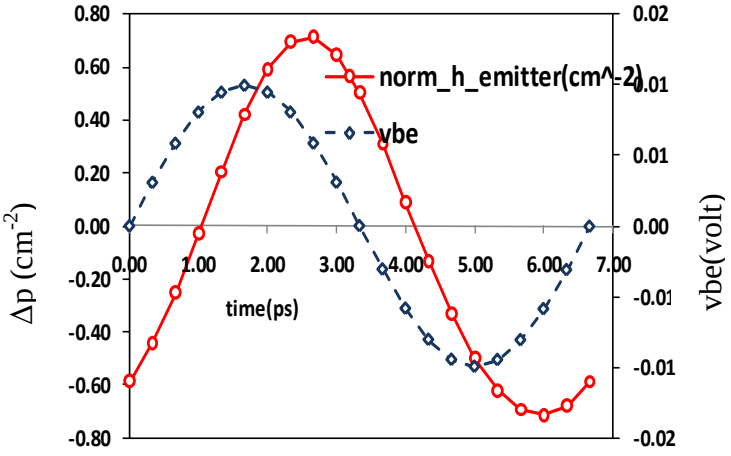

(b)

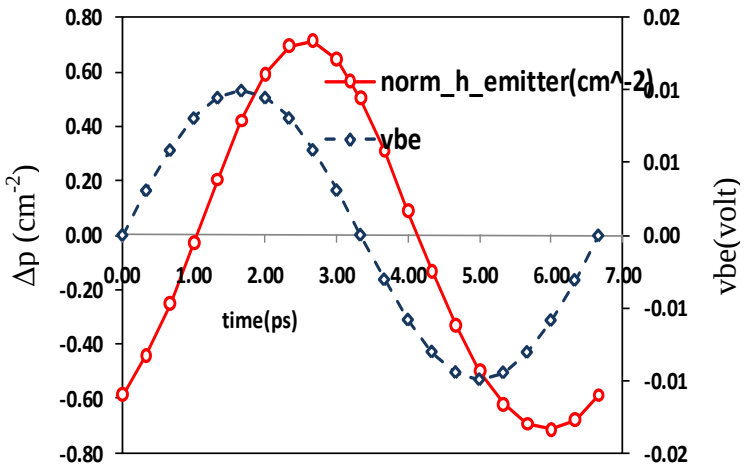

(c)

Figure **4.13**: Variation of excess minority carrier density (red line) over time. Blue graph corresponds to the applied sinusoidal bias variation over time. For (a) V_{BE}=0.8V, f=1 GHz, (b) V_{BE}=0.8V, f=200GHz (c) V_{BE}=0.95V, f=200GHz

The magnitude of excess carrier concentration at emitter side does decay over frequency as it is shown in Figure 4.14 for different bias points.

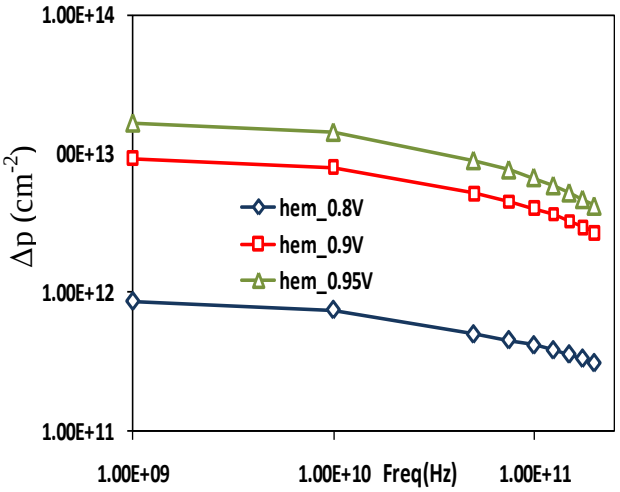

Figure **4.14**: Excess carrier concentration (cm^{-2}) over frequency for V_{BE} = 0.8V, 0.9V, 0.95V. It shows a gradual decay as frequency the increase.

The phase variation of excess charge is important while considering the delay in high frequency. From figure **4.13** it is clear that the delay phase increases at high frequency. This delay is calculated by fitting a sinusoidal function over the excess carrier concentration as presented before (Figure **4.11**)

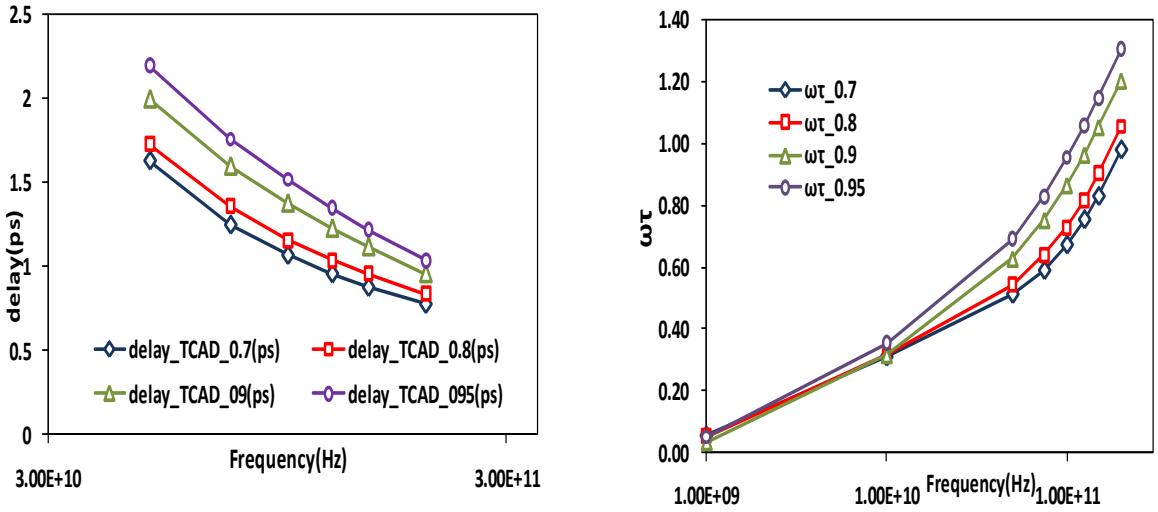

(a) **(b)**

Figure **4.15** calculated charge delay (a) time delay in ps as a function of frequency. (b) phase angle (time delay multiplied by the angular frequency) variation over frequency.

As expected the phase delay at low frequency is negligible and increases as frequency increase. This delayed integrated excess carrier (i.e. minority charge) certainly affects the dynamic behavior at high frequency as well as at high bias. The bias variation is shown in Figure **4.16**.

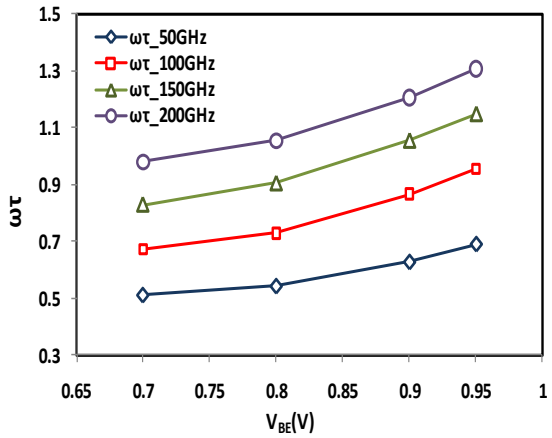

Figure **4.16**: variation of excess phase over bias point.

4.3. SiGe spike mono-emitter

In this part, simulation and modeling results for an npn SiGe spike mono emitter are shown for both DC and high frequency operation. First, the results obtained for a SiGe spike emitter is compared with the conventional HBT. Then parameter extraction and compact modeling with the help of HICUM is performed in the new device. The modeling approach introduces a new recombination time constant inside the existing HICUML2.24 model. Modeling results indicate a good agreement not only in DC characteristics but also in dynamic behavior.

4.3.1. Introduction

The advancement of SiGe HBT over the past decade has enormously increased due to the capability of providing higher cut-off frequency in high-speed application. To achieve higher f_T, transistor dimension is drastically reduced as well as the doping profile is scaled in the neutral base and collector region. The inclusion of Ge inside the base increases the current gain but reduces the open base breakdown voltage (BV_{CEO}). The only way to increase the breakdown voltage without affecting the RF performance is to increase the base current by the band gap engineering in the base or emitter region. One way to increase the base current is the inclusion of a SiGe spike inside the neutral [5][6]. It is reported to increase the base current without affecting the f_T and thus also increase the breakdown voltage. In the next section a SiGe spike mono emitter will be considered and simulation results will be presented for both DC and AC operations.

In the next figure (Figure **4.17**) a diagram is presented to show the position of the SiGe spike inside mono emitter transistors [5].

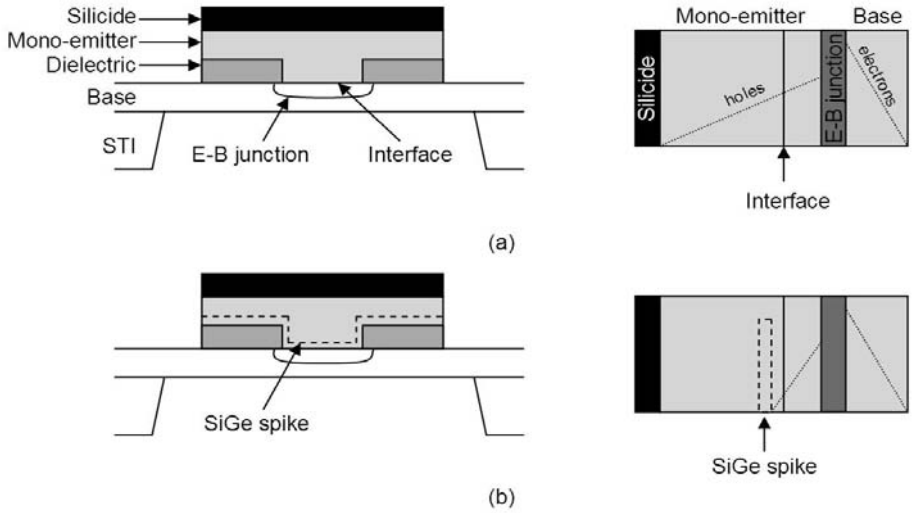

Figure **4.17**: schematic cross section of different emitters and the minority carrier profile inside these emitter (a) emitter without SiGe spike, (b) emitter with SiGe spike.

The next figure shows the fabricated device of mono emitter and mono emitter with SiGe spike in a HBT incorporated with 130nm technology. The width of the spike is 5 nm which is similar to that presented in [5]. To obtain the physical parameters as a function of device dimension, a cut is made at the middle of the internal base region normal to the X axis.

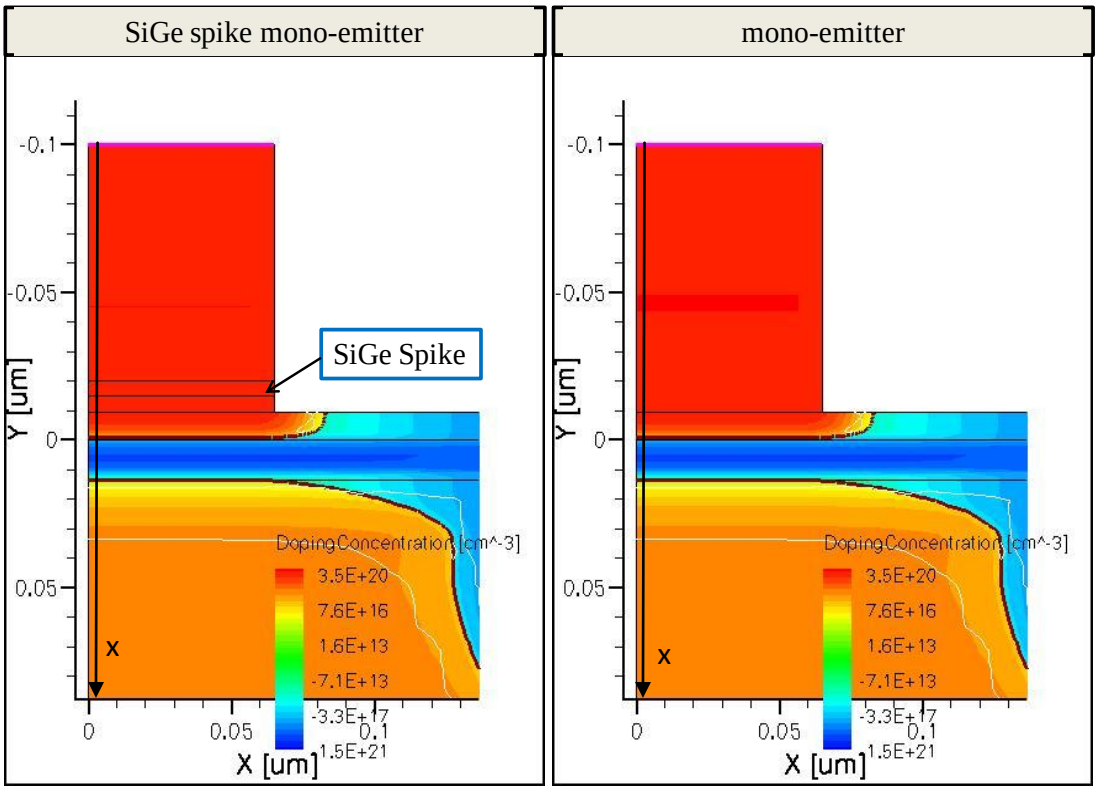

Figure **4.18**: Device structure of SiGe spike mono emitter and emitter without spike. Device structure is showing the device dimension and emitter, internal base and collector region. Arrow indicates the position of the vertical cut.

Doping profile used for both the transistors is the same as before (Figure **4.1**). The only difference is the % of Ge content in the devices. For mono emitter the Ge content in the SiGe base region is about 20%. The Ge content in the SiGe spike is 25% inside the mono emitter which is highly doped with Arsenic. The next figure (Figure **4.19**) shows the x-mole fraction in the base and also in the SiGe spike mono emitter.

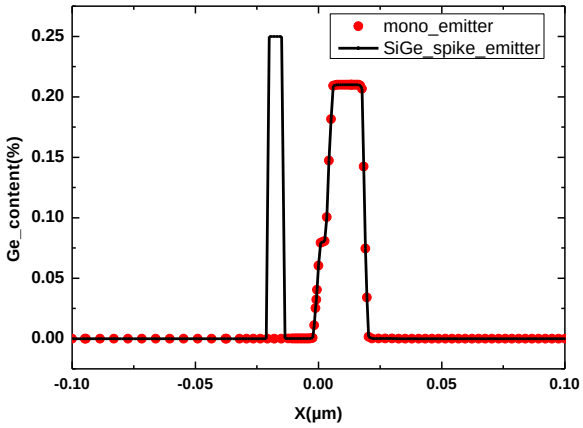

Figure **4.19**: Ge content in the SiGe spike mono emitter device. Showing both the neutral base and emitter region. The horizontal direction in the graph (X) represents the vertical dimension (Y) of the device.

Introducing the SiGe spike inside the emitter region alter the band configuration of normal HBT. In the next figure (Figure **4.20**) a comparison between the conduction and valence bands at zero bias is shown.

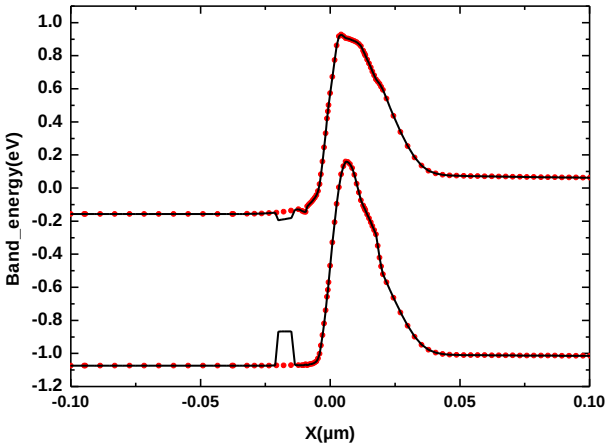

Figure **4.20**: conduction and valence band for mono emitter and SiGe spike mono emitter at V_{BE}=0V. At the position of the spike both the bands show a discontinuity.

The constructed structure is used to perform electrical device simulation. For device simulation, a parameter file is used which had been calibrated for the simple emitter structure. Also, the physical used for the device simulation are the same as used before. The inclusion of SiGe spike inside the mono emitter locally increases the recombination. The total recombination is a summation of SRH recombination, Auger recombination and recombination at the Si SiGe interface. To calibrate the total recombination in the emitter region, a slight modification of the hole recombination lifetime is made. Total recombination rate is then extracted for both mono emitter and SiGe spike mono emitter and is shown in Figure **4.21** . At the position of the spike, there is a certain hill due to sudden increase of recombination.

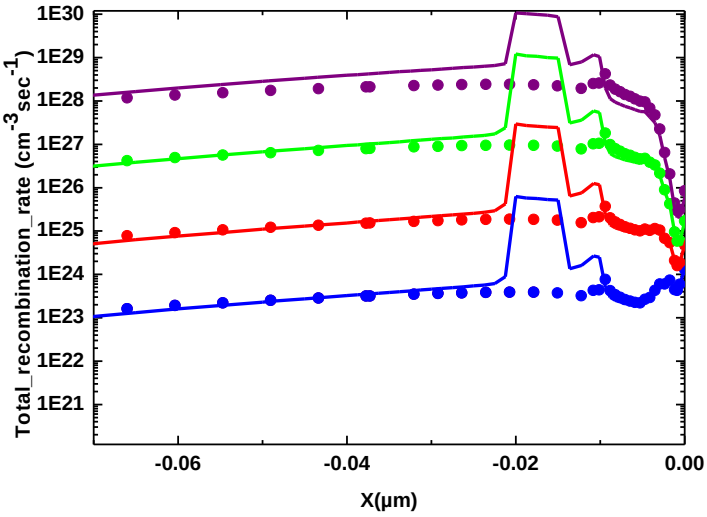

Figure **4.21**: Total recombination rate comparison between mono emitter and SiGe spike mono emitter at different V_{BE} (0.7V, 0.8V, 0.9V, 1V)

This enhanced recombination due to the inclusion of SiGe spike, increases the slope of hole concentration near BE junction and hence base current increases. This can be verified from the hole density profile in the emitter (Figure **4.22**).

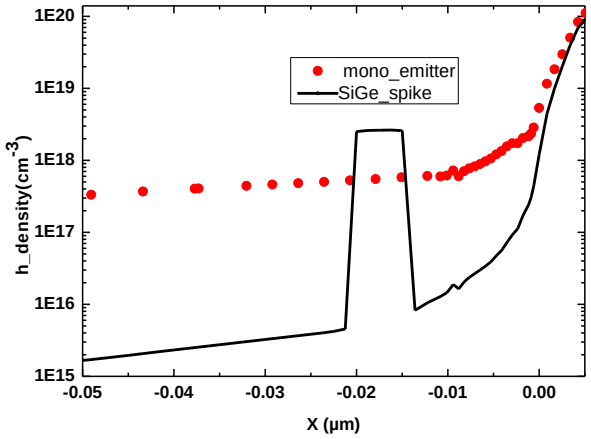

Figure **4.22**: h carrier density in the emitter region at V_{BE}= 0.9V. The increase in the slope of carrier density is clear near Base Emitter junction.

From the basic device simulation results, it is observed that the structure works properly. The next step is to use this structure to perform all the electrical simulations. These simulation results will help to verify that inclusion of a SiGe spike only increases the base current but do not affect the ft characteristics. Also, the effect of this excess charge will be investigated.

4.3.2. Comparison with mono-emitter

Gummel plot: As discussed before, addition of SiGe spike inside emitter region locally increases the recombination and hence it is expected to observe an increase in base current without affecting the collector current. Figure **4.23** represents Gummel plot showing base and collector currents for both SiGe spike emitter and mono emitter transistors. The simulation region covers both the low and high injection region. Figure **4.23** shows a clear increase of base current in SiGe spike emitter at medium bias while the collector current is exactly the same for these two devices.

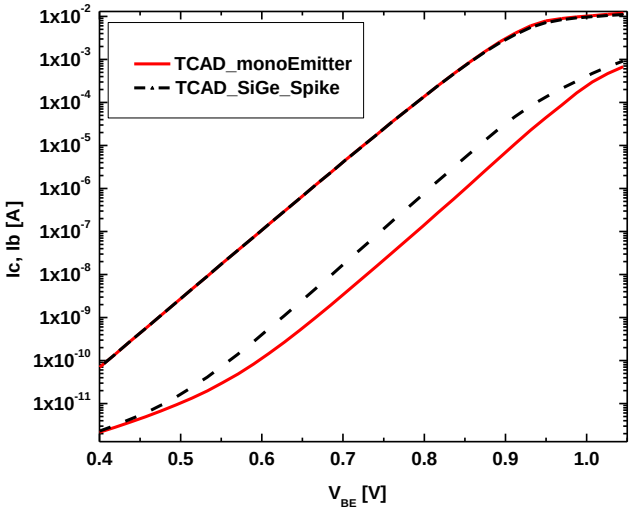

Figure **4.23**: Gummel plot showing Ic and Ib for both SiGe spike and without spike emitter configuration.

Cut off frequency: Though the effect in the base current is evident in the Gummel plot, there is no difference in the dynamic characteristics of the device namely the transit frequency is the same for both the devices. Transit frequency is calculated from the magnitude of h_{21} parameter at a frequency where the slope of h_{21} shows a 20dB/dec roll off. This behavior is expected from the theory and also reported in [5]. The next figure (Figure **4.24**) compares the cut off frequency for both the devices.

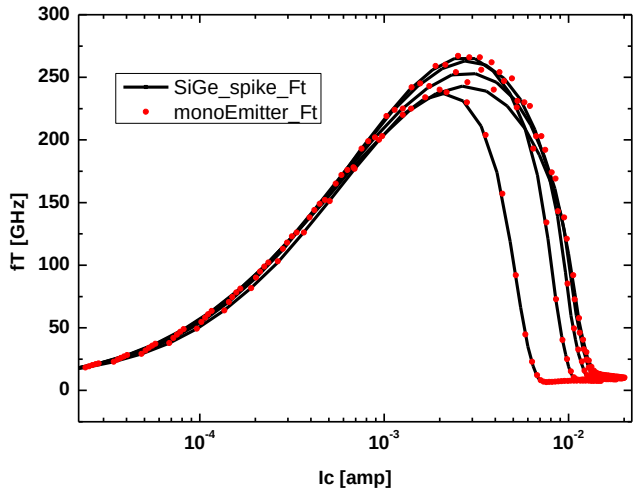

Figure 4.24: Ft Ic plot for two different transistors with and without SiGe spike inside emitter for different V_{CE}.

Current gain: As the magnitude of base current in SiGe spike mono emitter is more than the simple mono emitter, current gain is reduced in the spiked emitter. In the dynamic performance, magnitude of h_{21} presents the current gain. It is compared for the devices with and without SiGe spike inside the emitter. Magnitude of h_{21} is calculated from AC simulation while keeping V_{BC} fixed at 0V and for different V_{BE} = 0.85V and 0.9V.

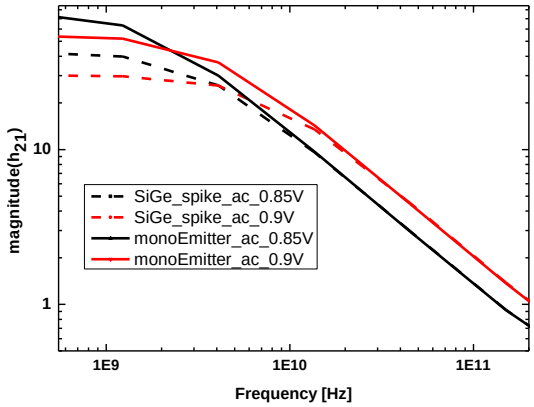

Figure **4.25**: magnitude of h_{21} calculated from AC simulation keeping V_{BC}=0V.

From the figure (Figure **4.25**) it is clearly evident that at higher frequency (>10GHz), there is no difference in the h_{21} magnitude for both the transistors. So, the cut off frequency, which is calculated by multiplying the magnitude of h_{21} with frequency, is the same for spiked and non spiked emitters.

Current gain can also be calculated for different frequencies from the transient analysis and can be compared with the value calculated from the ac simulation. A small signal voltage (10mV) is applied on the DC bias point for the transient simulation. The simulation is performed with a vast range of frequencies and the difference between the magnitudes of maximum and minimum of Ic and Ib currents at a frequency are divided to obtain the small signal current gain (Equation **4.1**).

$$\beta = \left| \frac{Ic(\max) - Ic(\min)}{Ib(\max) - Ib(\min)} \right| \qquad \textbf{4.1}$$

The next figure shows the small signal current gain for a SiGe spike transistor.

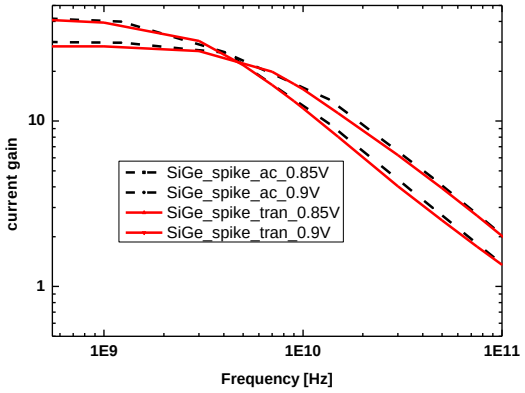

Figure **4.26**: Comparison between current gain calculated from AC and transient simulation in a SiGe spike mono emitter transistor keeping V_{BC}=0V and V_{BE}= 0.85V and 0.90V.

From the Figure 4.26.26, it is clear that transient simulation gives the similar result for small signal current gain in SiGe spike mono emitter transistor. It also indicates that small signal current gain is different for transistors with and without spike at low frequency in normal AC simulation. So, comparing the AC and transient simulations, it can be more strongly concluded that the base current increase certainly decreases the current gain at low frequency.

The accumulated charge not only decrease the magnitude of current gain (h_{21}) but also affects the phase of h_{21} parameter. AC simulation results comparing these two different transistors are shown below

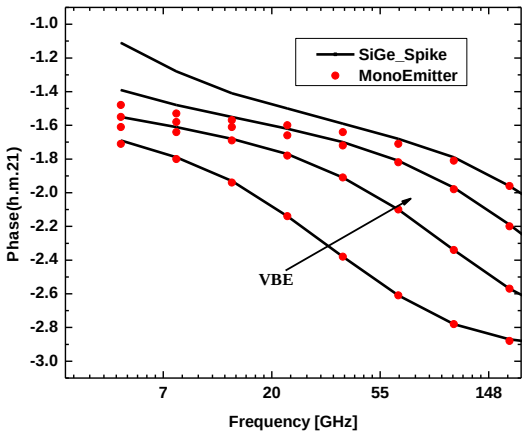

Figure 4.27: Comparison between device simulation results of h_{21} Phase with and without SiGe spike inside emitter. High frequency (200GHz) simulation is performed with a constant V_{CE}= 0.5V and with different V_{BE}= 0.75V, 0.79V, 0.83V, 0.87V. Difference is clear at low frequency.

The sudden increase of h_{21} phase at high bias is evident from the Figure **4.27** . The phase of input admittance (Y_{11}) is also effected due to the inclusion of Ge spike inside Si emitter. It is shown in Figure **4.28**

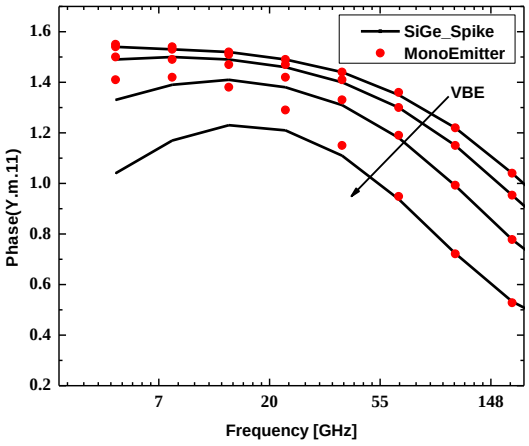

Figure **4.28**: Comparison between device simulation results of Y_{11} Phase with and without SiGe spike inside emitter. High frequency (200GHz) simulation is performed with a constant V_{CE}= 0.5V and with different V_{BE}= 0.75V, 0.79V, 0.83V, 0.87V. Difference is clear at low frequency.

As the SiGe spike inside the emitter locally increases the charge recombination significantly, the impact of this excess charge can not only be seen in the base current but also dominant in h_{21} and Y_{11} phase. From the Figure **4.28** the difference can be observed that at low frequency and at almost medium current range. As the recombination is considered as low frequency phenomena, the effect of excess charge is only at low frequencies and suppressed at higher frequencies

From Figure **4.23** it is clear that collector current is not affected during the process. So, the phase or the magnitude of output admittance (Y_{21}) is same for both the transistors.

4.3.3. Modeling with HICUM

The SiGe spike mono emitter structure is simulated with the calibrated parameter file. Device simulation results with the SiGe spike mono emitter are exported into ICCAP. The simulated results are accepted as measured data and model with HICUM model [7]. To properly extract

all parameters, a step by step procedure is applied which was discussed before (Chapter 3). In the next part, some of the modeling results are discussed.

Gummel plot

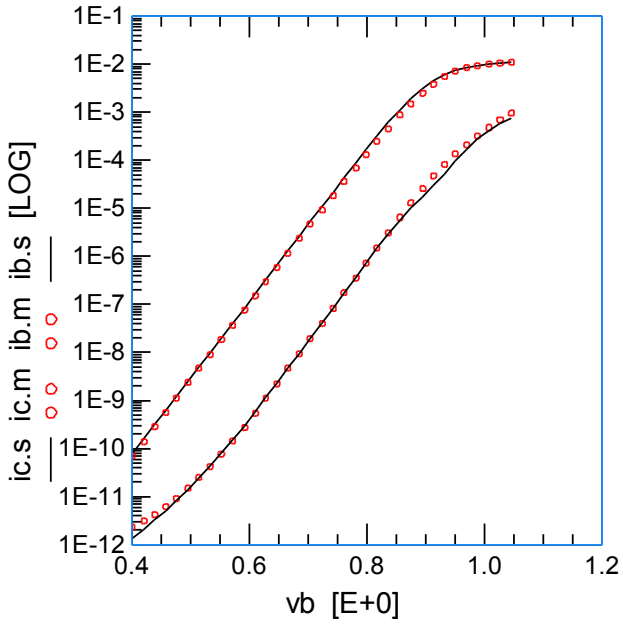

Figure 4.29: Forward Gummel plot at V_{CB}=0V with measurement and simulation.

Figure **4.29** shows Gummel plot for the SiGe spike device. Modeling of transfer current and forward base current is done with the HICUM L2.24 model. Although, the collector current is fitted well the results show that at the medium current range the base current is not fitted properly with the HICUM L2.24 model. In the HICUM model, base current is modeled as a summation of two diode currents and a recombination current. At the low injection range, parameters ireis and mrei model the base current. Over that region ibeis and mbei are the other two parameters to model base current and at high injection a recombination current term (tbhrec) due to the Ge drop in BC sunction in SiGe HBTs, helps modeling the base current. the modeling inaccuracy can be more prominent in the next graph, where ib/exp(V_{BE}/V_T) is plotted,

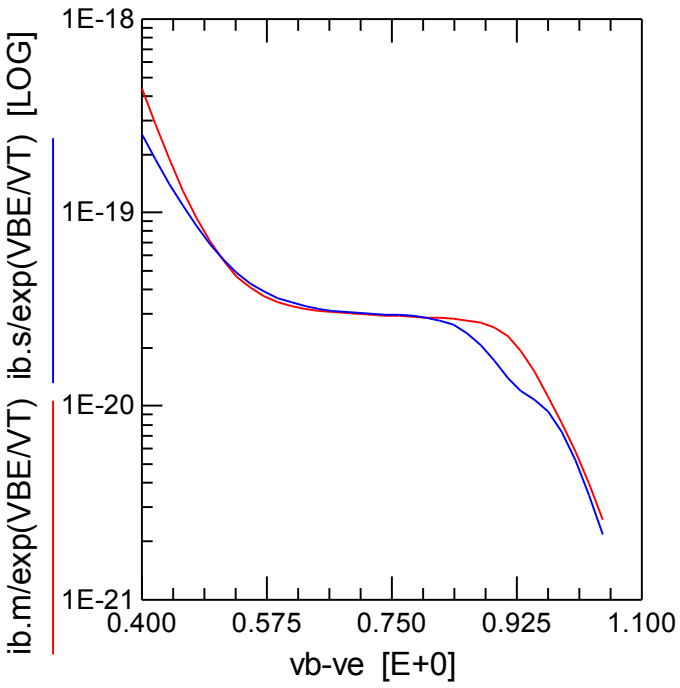

Figure **4.30**: comparison between TCAD simulated and HICUM simulated Ib/exp(V_{BE}/V_T).

From the figures (**4.29** and **4.30**), it can be concluded that an additional parameter is necessary to model the base current increase at medium injection. TCAD device simulation reminds that the sudden increase of base current is basically due to the SiGe spike inside emitter.

Transit frequency:

Dynamic behavior of this transistor is shown in Figure **4.31** where a reasonable fitting is observed in modeling.

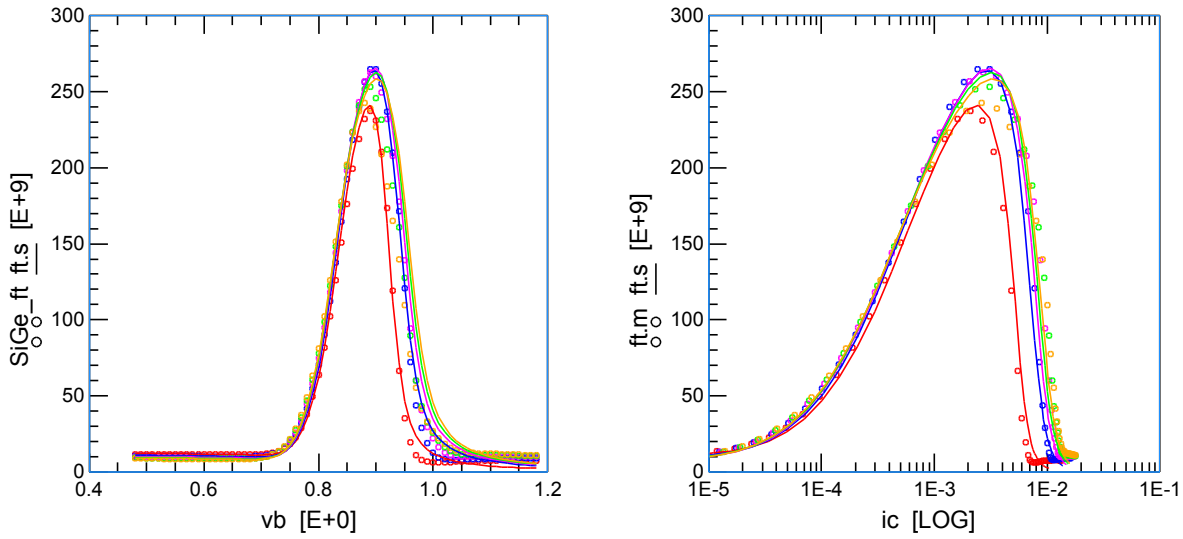

(a) **(b)**

Figure **4.31**: (a) fT vs V_{BE} and (b) fT vs ic plot at different V_{CE}. Measurement is in circle and modeling result in line.

As the cut off frequency is not affected by the Ge spike, the modeling with HICUM provides a good result.

NQS parameters:

After getting required parameters for forward current and transit time and axis resistance, high frequency modeling is done with that parameter set. For the NQS modeling, first h_{21} magnitude and phase is observed after optimizing the NQS parameters (alit and alqf). Next figure shows magnitude and phase of h_{21} parameter in SiGe spike mono emitter.

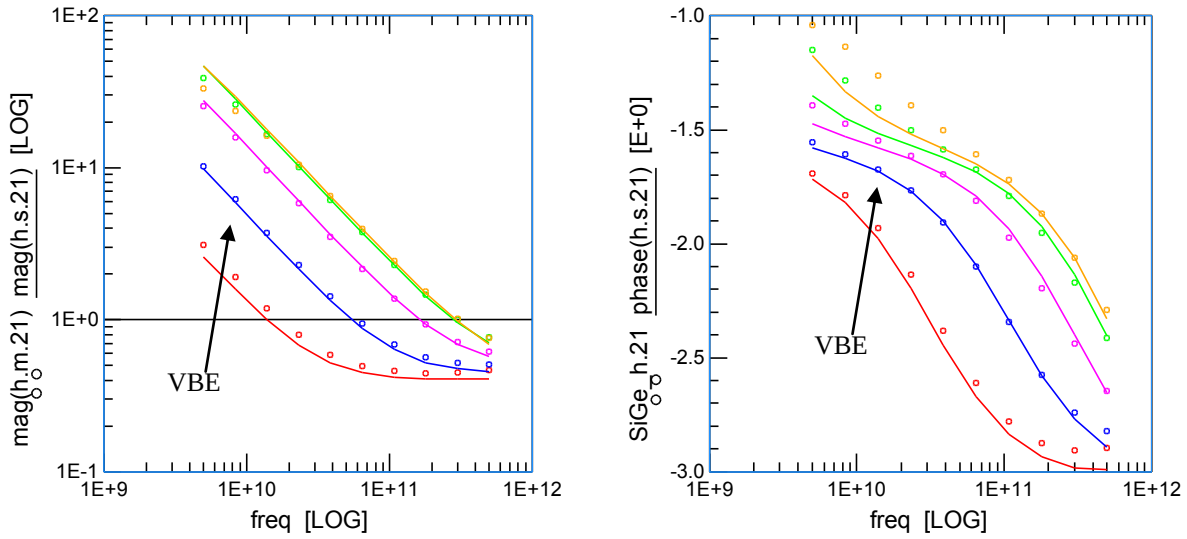

(a) **(b)**

Figure **4.32**: Magnitude and Phase variation of h_{21} parameter at V_{BE}=0.75V, 0.79V, 0.83V, 0.87V, 0.91V at V_{CE}=1V

Magnitude of h_{21} is properly modeled with HICUM (Figure **4.32**). But the phase h_{21}, at high injection, is not properly modeled with the HICUM model. As discussed before, the excess charge accumulated at the emitter side affects the h_{21} phase at low frequency and the modeling becomes inexact with the available HICUM model.

Other dynamic parameters are presented in the next figure,

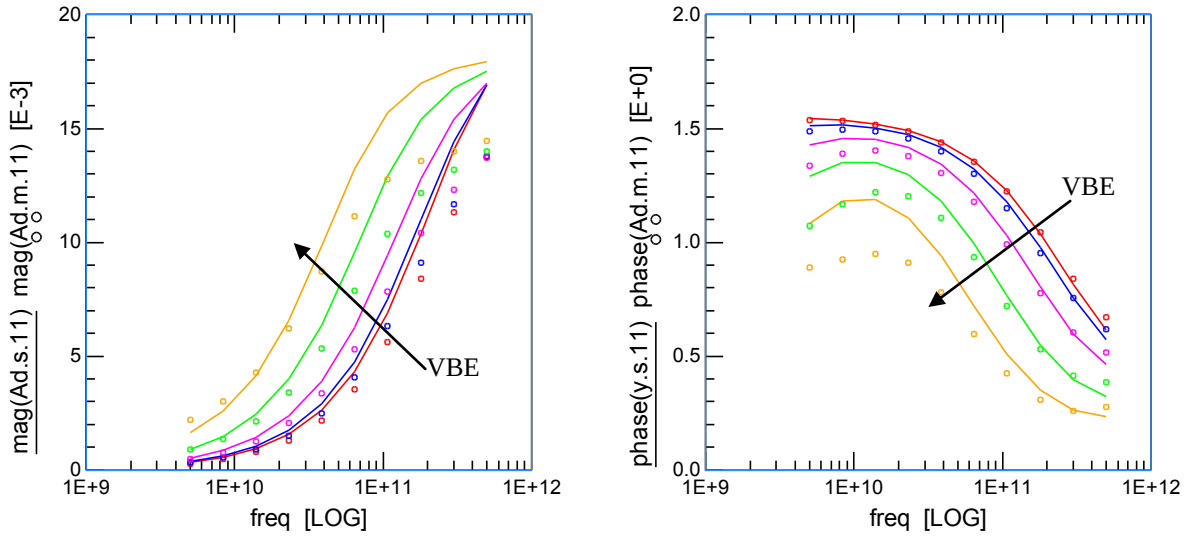

(a) **(b)**

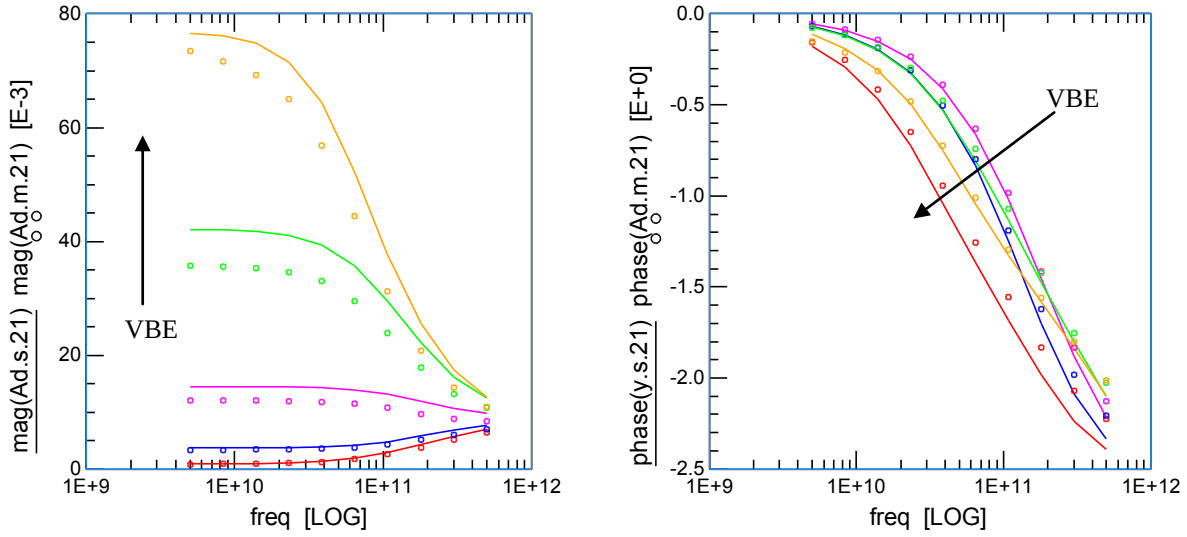

(c) **(d)**

Figure **4.33**: Magnitude and Phase of admittance parameters ((a, b) Y_{11} and (c, d) Y_{21}) at V_{BE}=0.75V, 0.79V, 0.83V, 0.87V, 0.91V and V_{CE}=1V

Again, similar to the h_{21} phase, the phase of input admittance (Figure **4.33**) is not properly modeled at low frequencies. To improve the modeling of SiGe spike mono emitter, certain modification is necessary inside the HICUM model and that is discussed afterwards.

4.3.4. Modeling with improved HICUM

In HICUM model, additional base current at high current density is model by inserting an additional recombination current (I_{Bhrec}) source. The recombination time τ_{berec}, a model parameter, is due to the stored excess minority base charge. The equation in HICUM is [7],

$$I_{Bhrec} = \frac{\Delta Q_{Bf}}{\tau_{bhrec}} \qquad \textbf{4.2}$$

Where, ΔQ_{Bf} is the excess minority charge.

The sudden increase of base current due to excess recombination is difficult to model with the existing HICUM model Therefore; proper modeling of the base current in this new device below I_{CK} requires an additional recombination current which depends upon excess minority

charge stored at emitter side. Remembering excess minority charge at the base-emitter junction is modeled inside HICUM as,

$$\Delta Q_{Ef} = \Delta\tau_{Ef}\frac{i_{Tf}}{1+g_{\tau fE}} \qquad \textbf{4.3}$$

Here, $g_{\tau fE}$ is the HICUM model parameters with i_{Tf} as the transfer current and $\Delta\tau_{Ef}$ denotes the change in the emitter transit time. The excess charge at emitter side (equation **4.3**) undergoes a sudden increase at medium injection and helps increasing the base current. This continues upto high injection where the minority carrier storage due to the Ge drop dominates and the scenario becomes similar to that of mono emitter. The additional parameter needed for modeling is.

$$I_{Berec} = \frac{\Delta Q_{Ef}}{\tau_{berec}} \qquad \textbf{4.4}$$

This controlled current source can be easily implemented parallel to IjBEi inside HICUM model circuit.

Results

Figure **4.34** presents the base current modeled with the conventional HICUM L2V24 model and also with the modified model. As discussed above the sudden increase of the base current is modeled perfectly with the help of additional recombination current.

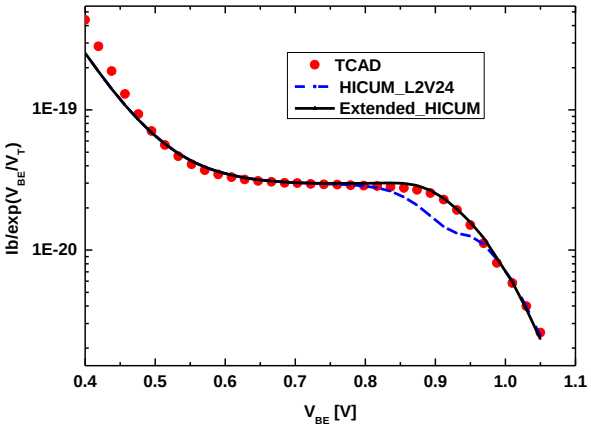

Figure **4.34**: Modeling result of Ib/exp(V_{BE}/VT) with HICUM L2V24 and extended HICUM model.

The additional parameter introduces an additional charge that affects also the HF behavior. In fact, for the high speed application it is also important to correctly model the excess phase shift of dynamic parameters like h_{21} or y_{11}. From the Figure **4.27**, it is evident that the SiGe spiked transistor registers a greater amount of phase delay at moderate injection level and from Figure **4.33** it is clear that the HICUM model is not sufficient to model this excess charge. Next figure presents the modeling result of phase of current gain (h_{21}) with both models. The excess phase circuit used for NQS modeling is considered the same for both models. Again, it is quite clear that the extended model provides better fitting.

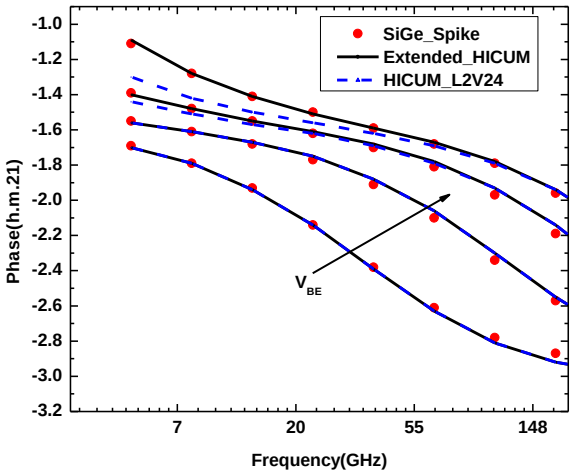

Figure **4.35**: Phase of h_{21} parameter modeled with HICUM and extended HICUM up to high frequency (200GHz) at a constant V_{CE}= 0.5V and with different V_{BE}= 0.75V, 0.79V, 0.83V, 0.87V. Symbols represent the TCAD simulation, dash line HICUM L2V24 model and solid line extended model.

Similarly, for the y_{11} parameter, at low frequency, the phase shift is more for the SiGe spike transistor and modeled satisfactorily by the extended model.

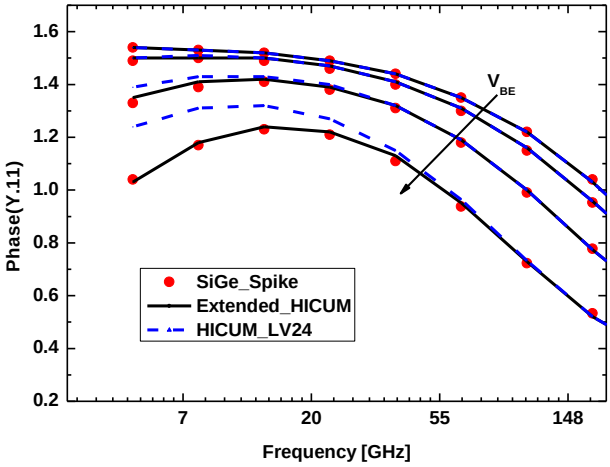

Figure **4.36**: Phase of y_{11} parameter modeled with HICUM and extended HICUM upto high frequency (500GHz) at a constant V_{CE}= 0.5V and with different V_{BE}= 0.75V, 0.79V, 0.83V, 0.87V.

4.4. Conclusion

In this chapter, two different types of devices are considered for TCAD device simulation. The first one is a modern IMEC device with a high cut off frequency dedicated for high frequency operation. To verify NQS effect, both AC and small signal transient operations are considered after calibrating the basic structure. High frequency Device simulation results are modeled with HICUM model. From the transient simulation results, time delays corresponding to the excess charge are calculated and it proves the importance of NQS excess phase circuit. Although, the frequency dependence of accumulated charge is not included inside compact models. Small signal simulations also indicate that the neutral emitter region, which is not so well accounted inside models, introduces a delay quite similar to the neutral base region. It provides a scope for further investigation in this subject. From the dynamic parameters simulation part, high frequency device simulation results are shown for the device. The modeling results with the excess phase network provide a considerable fitting up to very high frequency which in turns proves the significance of the HICUM excess phase circuit.

The second part of this chapter considers a new kind of device which includes a SiGe spike inside emitter. The simulation results show a base current increase compared to the conventional transistor where there is no effect in the transition frequency. The reason behind the current increase is the sudden increase of carrier recombination inside emitter region. Effect of this excess charge is investigated and it is shown that the phase of dynamic parameters such as current gain or input admittance is also affected at low frequency. Modeling of device simulated data is performed with the HICUM model. The modeling results show that there requires an additional current source to model the base current at moderate injection. A recombination time constant, introduced as a parameter inside the HICUM model, relates the excess emitter charge. After that the modeling results show perfect modeling of base current and also the low frequency phase of dynamic parameters with the extended model.

Reference

[1] Hurkx, G.A.M.; Agarwal, P.; Dekker, R.; van der Heijden, E.; Veenstra, H, "RF figures-of-merit for process optimization," *Electron Devices, IEEE Transactions on*, vol. 51.

[2] http://www2.imec.be/content/user/File/leaflet_Cmore/CMORE_bicmos2010.pdf, "CMORE_bicmos2010."

[3] Synopsys, *Sentaurus Device UserGuide*.

[4] http://www.iee.et.tu-dresden.de/iee/eb/hic_new/hic_doc.html, "HICUML2 Documentation."

[5] Choi, L.J.; Van Huylenbroeck, S.; Piontek, A.; Sibaja-Hernandez, A.; Kunnen, E.; Meunier-Beillard, P.; van Noort, W.D.; Hijzen, E.; Decoutere, S, "On the Use of a SiGe Spike in the Emitter to Improve the fTxBVCEO Product of High-Speed SiGe HBTs," *Electron Device Letters, IEEE*, 2007, vol. 24.

[6] Huizing, H.G.A.; Klootwijk, J.H.; Aksen, E.; Slotboom, J.W., "Base current tuning in SiGe HBT's by SiGe in the emitter," *Electron Devices Meeting, 2001. IEDM Technical Digest. International*.

[7] Michael Schroter, Anjan Chakravorty, *Compact Hierarchical Bipolar Transistor Modeling With Hicum*, World Scientific Publishing Company, 2010

General conclusion

Nowadays, when the SiGe HBT has proved their capability to become the building blocks for RF applications, accurate compact modeling of SiGe devices at high frequency has become a crucial step for circuit engineers. Today a modern HBT device can gain a very high (around 500GHz) cut off frequency but the existing models can predict the transistor behavior only upto 60-80GHz range. At that point, the so called Non Quasi Static (NQS) effect is considered very important and requires careful investigation.

In this whole work, one sole question is investigated, what NQS effect is and how one can model this effect. Starting from the beginning, semiconductor physics is analyzed for small signal operation. The whole physical process based on the solution of the transport and the continuity equation in the most important part of a bipolar device- the quasi static base region. The aim is to calculate the admittance parameters for low and high injection condition. Then, there are various approximated models available in the literature. In this work, calculations are made by hand to reach the previously published results. All the previously described models are discussed and compared with each other. This calculation helps to understand the physical mechanism behind the NQS effect and gives correct formulation to implement inside compact model.

By now, calculation is restricted up to the base region, which is considered as the most important part of the bipolar device. Though, the most part of the total transit time comes from the base region, modern semiconductor shows a significant contribution coming from the emitter and base collector junction. Again, in the NQS analysis we are mainly interested on the excess phase shift of dynamic parameters. So, we conclude that the emitter or base collector junction transit time influence the phase behavior without much influencing the magnitude of dynamic parameters. In chapter 1 base collector junction and emitter region are separately investigated. This investigation helps to improve the compact modeling approach.

TACD simulation is an integral part for the semiconductor device research. It not only helps to understand the basic physical models properly but also it can provide useful information to improve the device characteristics. To study the NQS behavior, we need to go up to a very high frequency (more than the cut off). Our most efficient measurement test bench can only provide electrical measurement up to 110GHz, which is far below the transition frequency of modern HBT transistors. At that point, TCAD simulation tool is used to simulate a calibrated HBT structure beyond its cut off frequency. Dynamic parameters are extracted and these simulated data then eventually treated as measurements at very high frequency. After that, a

step by step parameter extraction is performed with a compact bipolar model, HICUM. All the necessary parameters are extracted before proceeding to the high frequency modeling. The modeling results show that the existing HICUM model provide a good fitting of dynamic parameters.

There is another part of the work, to see how the excess phase network in HICUM model works in real measurements. The transistor used here is a modern SiGe HBT with a cut off frequency of 240 GHz. The modeling results show that HICUM provides an overall fitting to the high frequency current gain or the admittance parameters but it can be improved. Then we try to apply the physical understanding of high frequency behavior and proposed a new circuit. In this new excess phase circuit, phase shift due to the BC junction is taken into account. With the improved circuit, more accurate modeling is achieved at very high frequencies.

Last of all, a new kind of device is considered. This HBT device is having a SiGe spike inside the neutral emitter region. The spike acts as a virtual contact and increases the base current significantly but does not affect the AC behavior of the transistor. This device is constructed with a modification of previously used HBT device. The TCAD device simulation results show an improvement in base current which lead to a high collector to emitter breakdown voltage. While comparing SiGe spike emitter HBT with the conventional one, input admittance and current gain show some ambiguity at low frequency. This is due to the excess charge formed inside the neutral emitter region. Similarly, in the HICUM modeling of SiGe spike transistor, we observe that another recombination term is necessary to model the excess base current. Including an ideal current source in the HICUM model circuit, modeling results show significant improvement in base current and also in the low frequency admittance parameters.

With all the analysis, it is shown that high frequency characteristics of HBT has become an important topic for modeling engineers. The available compact models provide a global fitting of dynamic parameters but to apply in high frequency circuits, exact fitting is necessary. The difficulty is to implement complex models inside the model code and convergence issues are also there. Nevertheless, this work provides NQS analysis in both physical and compact modeling point of view. It can be treated as a starting point of high frequency analysis for modern day HBT devices.

LIST OF PUBLICATIONS

International Conferences

[1] A. Bhattacharyya, C. Maneux, S. Fregonese, T. Zimmer, “Modeling of SiGe spike mono emitter HBT with HICUM in static and dynamic operations”, BCTM 2011, October 9-11, Georgia, USA (Accepted)

European Workshops

[2] A. Bhattacharyya, C. Maneux, S. Fregonese, T. Zimmer, “Non quasi-static effects modeling in compact transistor models”, Spring MOS-AK GSA workshop, April 7-8, 2011, Paris, France

[3] A. Bhattacharyya, C. Maneux, S. Fregonese, T. Zimmer, “NQS modeling with HiCuM: What works, what doesn't”, 24th BipAk, May 6, 2011, Munich, Germany

[4] A. Bhattacharyya, C. Maneux, S. Fregonese, T. Zimmer, “SiGe spike mono emitter HBT modeling with HICUM”, European HICUM Workshop, June 28-29, 2011, Bordeaux France (Accepted)

MEDEA^{+} SIAM project presentations

[5] A. Bhattacharyya, C. Maneux, S. Fregonese, T. Zimmer, “NQS effects in SiGe HBTs”, Web conference, June 23rd, 2009

[6] N. Derrier, D. Gloria, D. Céli, A. Bhattacharyya, T. Zimmer, MEDEA+ SIAM conference, March 1, 2011, Crolles, France

Abstract

Modern high speed (RF) transistors encounter certain delay while operated at high frequency or under fast transient condition. This effect is named as Non Quasi Static (NQS) effect. In the current work, NQS effect is analyzed in a concise manner so that it can be readily implemented in a compact model using the VerilogA description language. The basic physics behind this effect is investigated in small signal domain and the results are compared with the published work. In popular bipolar model HICUM lateral and vertical NQS are examined separately and uses the same model for both transient and AC operation which requires an additional minimum phase type sub circuit. Compact modeling with HICUM model is performed in both measurement and device simulated data. At last, an improved excess phase circuit is proposed to model the NQS effect.

Key words
Computer Aided Design (CAD), Bipolar transistor, SiGe HBT, Compact modeling, HICUM model, Parameters extraction.

Résumé

Les transistors rapides actuels présentent un retard lorsqu'ils fonctionnent à très hautes fréquences ou en régime transitoire rapide. Cet effet est appelé effet non quasi-statique (NQS). Dans cette thèse, l'effet NQS est analysé de manière concise de façon à être directement implanté dans les modèles de composant pour les bibliothèques de circuit en utilisant le langage standard VerilogA. Les mécanismes physiques à la base de l'effet NQS sont évalués dans le domaine de fonctionnement petit signal et les résultats sont comparés aux travaux déjà publiés. S'agissant du modèle standard bipolaire HICUM, les effets NQS latéraux et verticaux sont examinés séparément à partir du même modèle, en régime de fonctionnement transitoire et fréquentiel grâce à un sous-circuit dédié au calcul de la phase du signal. A partir de ce sous-circuit, la modélisation compacte avec HICUM est comparée aux données issues de mesures et issues de simulation amont. Enfin, un nouveau sous-circuit calculant l'excès de phase est proposé pour prendre mieux en compte les effets non quasi-statiques dans les transistors bipolaires.

Mots-clefs
Conception assistée par ordinateur (CAO), Transistor bipolaire, TBH SiGe, Modélisation compacte, Modèle HICUM, Extraction des paramètres.